ASPECTS OF EMBRYOGENESIS IN *Brassica napus* L. cv. Regent: A LIGHT AND ELECTRON MICROSCOPIC INVESTIGATION FROM ANTHESIS TO THE QUADRANT STAGE OF PROEMBRYO DEVELOPMENT

by

André G. Dufresne

A thesis
submitted in partial fulfillment
of the requirements for the degree of
Masters in Science in the Department of Botany
The University of Manitoba
August, 1992

National Library
of Canada

Acquisitions and
Bibliographic Services Branch

395 Wellington Street
Ottawa, Ontario
K1A 0N4

Bibliothèque nationale
du Canada

Direction des acquisitions et
des services bibliographiques

395, rue Wellington
Ottawa (Ontario)
K1A 0N4

Your file *Votre référence*

Our file *Notre référence*

The author has granted an irrevocable non-exclusive licence allowing the National Library of Canada to reproduce, loan, distribute or sell copies of his/her thesis by any means and in any form or format, making this thesis available to interested persons.

L'auteur a accordé une licence irrévocable et non exclusive permettant à la Bibliothèque nationale du Canada de reproduire, prêter, distribuer ou vendre des copies de sa thèse de quelque manière et sous quelque forme que ce soit pour mettre des exemplaires de cette thèse à la disposition des personnes intéressées.

The author retains ownership of the copyright in his/her thesis. Neither the thesis nor substantial extracts from it may be printed or otherwise reproduced without his/her permission.

L'auteur conserve la propriété du droit d'auteur qui protège sa thèse. Ni la thèse ni des extraits substantiels de celle-ci ne doivent être imprimés ou autrement reproduits sans son autorisation.

ISBN 0-315-77908-X

Canada

ASPECTS OF EMBRYOGENESIS IN *Brassica napus* cv. REGENT: A LIGHT AND ELECTRON MICROSCOPIC INVESTIGATION FROM ANTHESIS TO THE QUADRANT STAGE OF PROEMBRYO DEVELOPMENT

BY

ANDRE G. DUFRESNE

A Thesis submitted to the Faculty of Graduate Studies of the University of Manitoba in partial fulfillment of the requirements for the degree of

MASTER OF SCIENCE

© 1992

Permission has been granted to the LIBRARY OF THE UNIVERSITY OF MANITOBA to lend or sell copies of this thesis, to the NATIONAL LIBRARY OF CANADA to microfilm this thesis and to lend or sell copies of the film, and UNIVERSITY MICROFILMS to publish an abstract of this thesis.

The author reserves other publication rights, and neither the thesis nor extensive extracts from it may be printed or otherwise reproduced without the author's permission.

Table of Contents

PAGE

List of figures

PAGE

List of Abbreviations

a	Antipodal
ABB	Aniline blue-black
Bb	Basal body
ca	Apical cell
Cb	Cytoplasmic band
cb, ci	Basal cell
cc	Central cell
Ch	Chalaza
cII	Crushed inner integument
CpC	Companion cell
Cu	Cuticle
D	Dictyosome
DER	Dilated endoplasmic reticulum
DNPH	2,4 dinitrophenyl hydrazine
dS	Degenerate synergid
E	Egg
EN	Endosperm nuclei
ER	Endoplasmic reticulum
Fa	Filiform apparatus
FF	Forming face
FNE	Free nuclear endosperm
Fu	Funiculus
GA	Gibberellic acid
h	Hypophysis initial
HBO	Super pressure mercury lamp (50 W)
II	Inner integument
k, f	Suspensor cells
KFeCN	Potassium Ferricyanide
kV	Kilovolts
L	Lipids
LM	Light microscopy
m	Mitochodrion
Mb	Microbodies
*m*C	Middle cell
MF	Maturing face
MG	Megagametophyte
mi	Micropyle
mL	Middle lamella
N	Nucleus
nP	Nucellar proliferation tissue
NU	Nucellus
Nu	Nucleolus
OI	Outer integument

O_sO_4	Osmium tetroxide
Ov	Ovules
PA	Periodic acid
PA-TCH-SP	Periodic acid-Thiocarbohydrazide-silver proteinate (Thiery test)
PAS	Periodic acid-Schiffs Reaction
Pb	Lead citrate
Pd	Plasmodesmata
PE	Proembryo
Ph	Phloem
Pipes	Piperazine-N,N'-bis[2-ethane-sulfonic acid]
Pl	Plastid
PM	Paramural body
Pm	Plasma membrane
pN	Polar nuclei
Po_4	Phosphate
pS	Persistant synergid
Pt	Pollen tube
Ra	Raphe
Re	Replum
RER	Rough endoplasmic reticulum
S	Synergid
Sh	Synergid hook
SP	Silver proteinate
St	Starch
Stm	Sieve tube member
TCH	Thiocarbohydrazide
TEM	Transmission Electron Microscopy
Tv	Transition vesicles
UA/Pb	Uranyl acetate-lead citrate
UV	Ultraviolet
v	Vacuole
Vs	Vesicles
Wp	Wall projection
X	Xylem
Z	Zygote
Zh	Zygote hook

Acknowledgements

I wish to gratefully acknowledge my supervisor, Dr. M. J. Sumner for his constructive criticism and review of the manuscript. I would also like to thank the other members of the advisory committee, Dr. J. Chong, Dr. W. Remphrey and Dr. L. VanCaeseele.

I wish to thank the graduate students, academic and support staff from the department of Botany for their support and **patience** over the duration of the thesis. I am particularly indebted to Mr. G. Burgess who gave freely of his time to teach me the basic techniques of electron microscopy and providing me with a constant supply of optimism. A special thanks to Ms. C. Hotz, and Mr. E. Groot for their friendship, encouragement, and **countless** hours of discussion over the past years, good luck to you both.

I wish also to thank Dr. J. Stewart for providing me with the opportunity to achieve my goal.

Finally, I wish to acknowledge my wife, Cécile, for her patience, help, understanding and support. Thank you.

Abstract

Aspects of *Brassica napus* L. cv. Regent (Canola-Rapeseed) proembryo development were studied from the egg to the globular quadrant stage of embryo development using light, fluorescence and electron microscopy. The proembryo follows the classical Onograd type of development. Fertilization occurs approximately 11 hours after pollination with an initial slight reduction in zygote size, the reorganization of zygote cell polarity, the reduction of insoluble carbohydrate reserves, followed by the ampuliform elongation of the zygote. During apical zygote elongation, the cell increases its vacuolation and demonstrates a β D-glucan gradient with a reduced amount at the distal end of the zygote cell wall. After fertilization, cell wall projections become evident in the micropyle region of the zygote, adjacent to the synergid cells and the central cell wall projections. The zygote cytoplasm adjacent to the wall projections contains accumulations of mitochondria and dictyosomes.

The first cell division producing the apical proembryo cell occurs 96 hours after pollination and after 120 hours the proembryo consists of 8 cells. In contrast to the zygote cell, the proembryo cell wall shows an even β D-glucan distribution throughout. The cells of the suspensor are highly vacuolated and are similar in cytoplasmic content. During early embryogenesis, the basal suspensor cell continuously elongates up to the quadrant stage of development. All the cells of the proembryo are linked by plasmodesmata; however, unlike the egg cell, no plasmodesmata were observed between the proembryo and synergid cells. After pollination, one of the two synergid cells shows degenerative symptoms. After

fertilization, the degenerative synergid contains remnants of pollen cell wall material and polysaccharide spheres identified in the pollen tube cytoplasm. The second synergid cell remains viable until ampuliform zygote elongation, 22 hours after pollination.

The integument cells of the seed are not connected to the megagametophyte by plasmodesmata. Upon fertilization, inner integument layers, adjacent to the micropyle region of the megagametophyte, show a reduction of PAS-positive insoluble carbohydrate; however, as the seed matures, insoluble carbohydrate accumulates in the basal body region of the seed.

Seed vasculature was observed as an extensive "net-like" arrangement in the raphe region of the seed.

Aberrant ovules, with poorly developed sporophytic (integuments) or gametophytic (embryo sac) identities,were occasionally observed during the course of this study.

1.0 Introduction

In the 1980's, Canola contributed a higher return to the farm economy per acre than cereal crops and accounted for 65-70% of Canada's oilseed production. Since Canola is important for the Western Canadian farm economy, interest in improving Canola's agronomic values (percent oil content, oil type, plant vigor, and disease resistance) has become important (Ag Canada 1991). To further understand how agronomic values can be improved during seed development, I propose to focus my attention on early seed ontogeny of *Brassica napus* L. cv. Regent with the intention of increasing the pool of knowledge used by Canola breeders.

The anatomical description of crucifer megagametophyte ontogeny and embryogenesis has been the subject of many scientific investigations. Studies by Sumner (1986, 1992) and Sumner and VanCaeseele (1988, 1989, 1990) have shown the ultrastructural development of the *Brassica campestris* megagametophyte prior to and immediately following fertilization. Details of crucifer embryogenesis have been well documented by Schulz and Jensen (1968a,b,c, 1969, 1971, 1973, 1974) in *Capsella bursa pastoris* and by Mansfield *et al.* (1991a,b) in *Arabidopsis thaliana* .

Using light microscopy, Tykarska described the embryonic stages of different cultivars of *Brassica napus* L. and in subsequent publications showed developmental changes within the embryo (Tykarska 1976, 1979, 1980, 1982, 1987a,b). Tykarska's publications proved an excellent source of information about *Brassica napus* cultivars; however, little ultrastructural detail was provided. In the literature uncertainty exists about the development and function of the multicellular suspensor unit, the fate of

the synergids and central cell, and the importance of the integument and vascular tissues for the survival of the *Brassica napus* seed.

The purpose of this investigation is to:

1. Describe morphological and cytological changes during embryogenesis of *Brassica napus* L. cv. Regent from the egg to the early globular stage of development.

2. Describe the chemical nature of the proembryo, synergid cells, central cell and integument cells using light, fluorescence and electron microscope techniques.

3. Examine possible routes of nutrient mobilization and uptake during the early stages of embryogenesis.

2.0 Literature Review

2.1 The Ovule

The ovule primordium develops as a result of several periclinal and anticlinal cell divisions in the dermal or sub-epidermal layers of the placental wall (Willemse and Went 1984). In angiosperms, the most common type of ovule formed is the anatropous type, whereby the innermost portion of the ovule is the nucellus or megasporangium. The nucellus is described by Esau (1976) as a core of sporogenous parenchyma cells where megasporogenesis and megagametogenesis take place.

The mature nucellus is covered by one or two distinct integument cell layers. The integument layers initially developed from the base of the chalazal nucellus and eventually covered the nucellus at the opposing pole forming a passage called the micropyle. The integument has two important functions. First, following fertilization, it provides protection for the developing embryo by forming a seed coat, and secondly it is thought to be involved in assimilate translocation and storage for the developing nucellus and future embryo (Maheshwari 1950, Hendrix 1990).

The ovule is attached to the placental wall by a stalk-like funiculus. It is vascularized and is involved in assimilate movement towards the developing embryo (Corner 1976, Mogensen 1981, Brady and Combs 1988).

2.2 Megagametophyte

Research on megagametophyte development has been documented in many different species including *Gossypium* (Jensen 1963, 1964, 1965a-c), *Petunia* (Went 1970a,b), *Capsella* (Schulz and Jensen 1968a,b, 1973), *Helianthus* (Newcomb 1973ab, Yan *et al.* 1991), *Aquilegia* (Fougère-Rifot 1975, 1978), *Stipa* (Maze and Lin 1975), *Paspalum* (Chao 1977), *Spinacia* (Wilms 1981a,b), *Jasione* (Berger and Erdelskà 1973), *Plumbago* (Russell

1989, Huang *et al.* 1990), *Oryza* (Jones and Rost 1989), *Glysine* (Folsom and Cass 1989), *Papaver* (Cass and Fabi 1990), and *Brassica campestris* (Sumner 1986, Sumner and Van Caeseele 1988, 1989, 1990).

In most angiosperms, the normal or polygonum haploid megagametophyte is made up of eight nuclei and seven-cells. The egg apparatus, located at the micropylar pole of the megagametophyte, is a three haploid cell structure made up of two synergids and one egg cell. The three cells of the egg apparatus are approximately the same length (Maheshwari 1950). The egg cell protrudes inwards towards the central cell; however, it does not extend to the base of the megagametophyte at the micropyle pole. The two synergid cells are located in the extreme micropylar portion of the megagametophyte, adjacent to the inner integument micropyle, and share common cell walls with the egg and central cell.

The central cell contains two fused or partially fused nuclei prior to fertilization. It occupies the large central area within the megagametophyte, sharing common walls with the antipodals, egg, synergid cells, and lateral integument cells (Willemse and Went 1984).

In most cases, the smallest and least understood cells of the megagametophyte are the three haploid antipodal cells. These antipodals are located at the chalazal pole of the megagametophyte and are in contact with the central cell, inner integument and nucellus (Willemse and Went 1984).

2.3 The Synergids

Many authors have commented on the roles of synergid cells; however, conclusive evidence demonstrating chemotropic properties or mechanisms of nutrient translocation have not been shown. In most species, both fusiform synergids touch one another and have thickened walls forming a structure known as the filiform apparatus (FA) at the micropylar pole of the megagametophyte. In *Plumbago* (Russell 1989), the FA is directly associated with the egg cell and appears to be similar in structure and function to the synergid FA cell complex of most species. Russell and Mao (1990) speculate that the FA is linked to synergid degeneration in *Linum*. In *Linum,* the synergids with the smallest FA at the time of pollination are first to demonstrate degenerative symptoms. Jensen (1965a,b) suggests that the synergid FA in cotton is aiding in the transfer of nutrients into the synergid cells for the developing egg cell. Gunning and Pate (1969) indicate that the FA has similar structural characteristics as transfer cells and may have similar role or function. The most significant similarity to the transfer cells is the finger-like nature of the FA increasing its absorptive surface area with the synergid cells. This nutrient transfer theory seems possible; however, in *Jasione,* this is not possible since the presence of a cuticle over the micropyle would prevent any absorption at that particular end of the megagametophyte (Berger and Erdelskà 1973).

Because of the constant success the pollen tube exhibits in identifying the micropyle and eventually the megagametophyte, researchers have considered the secretory activity of the synergids as part of the chemotropic theory for pollen tube growth. Histochemical analysis by Malik and Vermoni (1975) has revealed the presence of cytochrome

oxidase, succinate dehydrogenase, acid phosphatase, adenosine triphosphatase, phosphorylase, alkaline phosphatase and lipases in the synergids of *Zephiranthes* and *Lagenaria*.. In *Spinacia*, Wilms (1981a,b) observed the dissolution of the middle lamellae near the synergid FA as the ovule became receptive. This suggests that enzyme secretion by the synergids occurs in anticipation of fertilization. In *Paspalum*, enzymes may be secreted from the synergids for the dissolution of integument cells, resulting in a PAS-positive reaction at the micropyle (Chao 1971). Bruun and Olesen (1988, 1989) have also observed PAS-positive substances in the micropyle of sugar beet. These two authors suggested that the PAS-positive substances and the degenerating synergid are involved in the guidance of the pollen tube through the micropyle. Brewbaker and Kwack (1964), Jensen (1965a), Chaubal and Reger (1990) suggested that deposits rich in calcium in the synergid cells may have a chemotropic effect. Chaubal and Reger (1990) speculate that the high calcium gradient may arrest pollen tube growth in the synergid, causing it to rupture and release its content near the egg cell.

Other observations possibly linked to pollen tube receptivity is synergid cell degeneration; however, the timing of synergid degeneration varies between species and the cause is not understood. Symptoms of the synergid degeneration process include a decreased cell volume, the collapse of vacuoles and a loss of the plasma membrane integrity. In *Zea* (Diball 1968), *Quercus* (Mogensen 1972), *Spinacia* (Wilms 1980a,b), *Linum* (Russell and Mao 1990) and *Helianthus* (Yan *et al.* 1991) pollination has been shown to trigger synergid degeneration . *Petunia* (Went 1970a) and *Capsella* (Schulz and Jensen 1968a) synergids remain intact until the pollen tube has penetrated one of the synergids, after which the penetrated

synergid begins to exhibit similar degeneration symptoms as those triggered by pollination. In *Brassica campestris, Hordium* and *Glysine,* synergid degeneration occurs prior to pollen tube penetration into the synergid; however, there is no conclusive evidence to show that pollination causes synergid degeneration (Sumner and VanCaeseele 1989, Dute *et al* 1989, Engell 1989). In sugar beet, synergid degeneration has been shown to occur in unpollinated plants (Bruun 1987). In peanut, one or both synergid cells may degenerate before anthesis. In rice, one synergid begins to degenerate soon after anthesis (Dong and Yang 1990, Xi 1991). The onset of synergid degeneration may be attributed to normal megagametophyte development.

Once the pollen tube enters the synergid cytoplasm, it grows a short distance within the synergid. Jensen and Fisher (1968) reported pollen tube growth within a synergid showing degenerative symptoms which may trigger pollen tube discharge. In *Gossypium,* discharge takes place at a subterminal pore located on the side of the pollen tube, oriented towards the egg cell (Jensen and Fisher 1968). In *Petunia* and *Brassica campestris,* the tip of the pollen tube bursts open releasing its contents into the synergid (Went 1970b, Sumner 1992). Pollen tube content released into the synergid includes the two sperm cells, the vegetative nucleus and PAS-positive spheres found in the pollen tube cytoplasm (Schulz and Jensen 1968a, Went 1970b, Jensen and Fisher 1968). The role of the PAS-positive polysaccharide spheres released into the synergid from the pollen tube is not understood (Sumner 1986).

In most mature angiosperm megagametophytes, the synergid and egg cells are separated by two plasma membranes and in some circumstances a cell wall. Went (1970a) and Jensen (1972) speculate that

the lack of cell wall material between synergids and the egg at the chalazal pole of the egg apparatus, allows the synergids to play an essential role in the process of gamete fusion. The fusion theory proposed by Went (1970a) and Jensen (1972) begins when one sperm cell contacts the plasma membrane of the egg or central cell. This contact triggers the formation of plasma membrane bridges that enlarge, providing a pathway for the sperm nucleus and possibly some sperm cytoplasm (Russell 1980, 1983). In *Capsella*, a PAS-positive cell wall is present between the synergids, egg and central cell; however, a pore in the synergid cell wall was observed near the tip of the pollen tube by which Schulz and Jensen (1968a) speculate a sperm cell may enter. Sumner and VanCaeseele (1989) have reported PAS and PA-TCH-SP-positive amorphous material at the chalazal end of the synergid and egg cells of *Brassica campestris* which were not shown to affect gamete fusion. These observations indicate that cell walls between the synergid and the egg do not necessarily hinder gamete fusion (Jensen 1972). Russell *et al.* (1990) diagrammatically reviews five different gametic fusion models based on barley, cotton, spinach, *Populus* and *Plumbago*. The differences in models with respect to the mechanism of fusion and the cells involved in the process are shown.

Synergids show a complex cytoplasmic organization. Common features of the synergid cytoplasm are the presence of a large number of mitochondria and dictyosomes, extensive arrays of endoplasmic reticulum and an abundance of ribosomes. In *Petunia*, (Went 1970a) the mitochondria are dispersed evenly throughout the cytoplasm; however, in *Capsella* (Schulz and Jensen 1968a) most organelles are generally concentrated at the micropyle pole of the synergid. Newcomb (1973a,b) reported dictyosomes, numerous vesicles and dilated endoplasmic

reticulum to be more abundant in *Helianthus* during FA formation. In *Capsella* (Schulz and Jensen 1968a) and *Spinacia* (Wilms 1981a), dictyosomes are observed even after FA formation is complete. In most species, plastids are present in the synergids near the FA (Mogensen and Suthar 1979), but they are less abundant and smaller in size in other taxa, such as *Petunia* (Went 1970a). Schulz and Jensen (1968a) have indicated that the synergid FA has two structural phases: a dense staining core consisting of a tightly packed mass of microfibrils and a peripheral zone of loosely packed microfibrils in a transluscent matrix. Huang *et al.* (1990) have shown a similar FA arrangement in *Plumbago*. The two microfibril regions contain β1-4 linked glucans; however, the loosely packed region also reacted positively when tested immunologically for microtubules (Huang *et al.* 1990) Not all synergid FA have two separate structural phases. In *Petunia* and *Torenia*, the FA is relatively homogeneous in nature with *Petunia* containing loosely organized cellulosic microfibrils embedded in a pectic matrix (Went 1970a). In *Capsella*, the FA gives a strong PAS-positive reaction for carbohydrates, and a negative reaction for nucleic acids and proteins (Schulz and Jensen 1968a). Sumner and VanCaeseele (1989) suggest that the PAS- and PA-TCH-SP-positive FA matrix contains α 1-4 polyuronides and β 1-4 glucan.

2.4 Egg Cell

The egg cell shares common walls with cells of the inner integument, synergids and the central cell. Like the synergids, the egg cell wall is thickest at the micropyle pole and gradually thins towards the chalazal region, where portions of the egg cell is mostly delimited by plasma membrane (Sumner 1989, Dong and Yang 1990, Yan *et al.* 1991, Mansfield *et al.* 1991a). In *Capsella*, a thin irregular PAS-positive cell wall

material at the chalazal region was identified by Schulz and Jensen (1968b). In *Plumbago*, the FA is part of the egg cell and assumes the partial function of the synergid cells in their absence (Cass 1972a,b, Cass and Karas 1974, Russell 1989).

In most species the egg cell demonstrates strong polarity prior to fertilization. It has a single large vacuole which occupies two thirds of the micropylar region. The chalazal region of the egg cell normally contains most of the cytoplasm, the egg nucleus and small vacuoles (Mansfield *et al.* 1991a). In *Stipa*, vacuoles are smaller and exhibit a random distribution throughout the cytoplasm in the cell (Maze and Lin 1975). Although the egg cell polarity is similar in many species, cytoplasmic ultrastructure varies greatly. In *Petunia*, endoplasmic reticulum is scarce; polysomes, mitochondria, plastids and dictyosomes are few (Went 1970b). In *Zea mays*, dictyosomes and endoplasmic reticulum are few, but many mitochondria and plastids are found (Diboll and Larson 1966). In *Spinacia*, large amounts of starch containing plastids accumulate at the chalazal pole and mitochondria at the micropyle pole. (Wilms 1981a). In*Helianthus* is, the egg cell is rich in ribosomes, polysomes, mitochondria and plastids, but contains little endoplasmic reticulum, and few dictyosomes and vacuoles (Yan *et al.* 1991).

The ultrastructure of the egg cell in *Plumbago* is specific, yet it maintains a certain amount of polarity. The egg cell cytoplasm is divided by a large centrally located vacuole. Cytoplasm located at the micropyle contains a large amount of mitochondria and dictyosomes while cytoplasm located at the chalazal pole contains some mitochondria, plastids, polysomes and conspicuous rough endoplasmic reticulum (Cass 1972b, Cass and Karas 1974).

2.5 Antipodal Cells

The antipodal cells show much variation and are the least understood among all the cells of the megagametophyte. In most cases the antipodal cells are located at the chalazal pole of the megagametophyte. They are in direct contact with the central cell, thus raising questions about nutrient mobilization. Schulz and Jensen (1971) describe the antipodals in *Capsella* as small and inactive, surrounded by a cell wall of uniform thickness containing plasmodesmata. This has also been reported in *Helianthus* (Newcomb 1973a) and *Jasione* (Berger and Erdelskà 1973). Observations in *Helianthus* and *Spinacia* by Newcomb (1973a) and Wilms (1981a) show nucellar cell wall projections, like those described by Gunning and Pate (1969), bordering the antipodal cell wall. Along with plasmodesmata the cell wall projections could possibly be providing a pathway by which nutrients are mobilized and moved from the nucellus to the central cell via the antipodals (Bhojwani and Bhatnagar 1986).

The antipodals may also be involved in secretion of substances. Histochemical tests on *Zephyranthus* and *Lagenarea* have indicated the presence of peroxidases, cytochrome oxidases and lipase in the highly metabolic antipodals (Malik and Vermani 1975). Yu and Chao (1979) observed an increase in RNA, protein and the transformation of lipids from solid to a liquid state, within the antipodal cells of *Paspalum* during megagametophyte maturation.

The cytoplasm of the antipodals normally contain many organelles such as mitochondria, dictyosomes, plastids, ribosomes and endoplasmic reticulum with parallel and partly concentric cisterns. In most cases the antipodals usually degenerate before or during fertilization, but in some species they may persist throughout embryo and endosperm

development. The number of antipodals may vary depending on species. In some grasses they can proliferate into multicellular tissue consisting of up to 100 cells. In such species antipodals may develop with more than one nucleus (Maze *et al.* 1970). In *Helianthus,* only two antipodals are present (Newcomb 1973a). Little information is available concerning the antipodal ultrastructure, histochemistry and development.

2.6 Central Cell

The central cell is the mother cell of the future developing endosperm. The central cell occupies the largest portion of the megagametophyte. It is in contact with the egg apparatus and the antipodals at the micropyle pole and the chalazal pole, respectively. In most species, two polar nuclei are located at the micropyle end of the central cell near the egg apparatus prior to fertilization. At maturity, the *Brassica campestris* central cell shows little vacuolation, and most of the cytoplasm and organelles accumulate near the egg apparatus (Sumner and VanCaeseele 1989). The central cell contains numerous mitochondria, rough endoplasmic reticulum and dictyosomes (Willemse and Went 1984). Although plastids can be found the number and ultrastructure is variable. Starch containing plastids are usually present in the mature central cell of *Gossypium* (Jensen 1964), *Capsella* (Schulz and Jensen 1973), *Nicotiana* (Mogensen and Suthar 1979), *Spinacia* (Wilms 1981a) and *Arabidopsis* (Mansfield 1991a), but are not observed in *Helianthus* (Newcomb 1973a).

The ultrastructure of central cell nuclear fusion was first described by Jensen (1964) using *Gossypium* and more recently by Sumner and VanCaeseele (1990) in *Brassica campestris* . Jensen (1964) described the nuclear envelope as continuous and connected by cisternae of

endoplasmic reticulum. Nuclear fusion occurs when the outer and inner nuclear membranes of the polar nuclei fuse together; small connections or bridges are formed which gradually enlarge and coalesce (Sumner and VanCaeseele 1990). The actual timing of fusion varies among taxa. Yan *et al.* (1991) have shown fusion completed in *Helianthus* three days prior to anthesis. In *Capsella* and *Arabidopsis* (Schulz and Jensen 1973, Mansfield *et al.* 1991a) fusion completed before fertilization. Fusion in *Spinacia* (Wilms 1981a) and *Brassica campestris* (Sumner and VanCaeseele 1990) begins at megagametophyte maturity, and is completed after fertilization. In *Populus deltoides,* Russell *et al.* (1990) showed fusion occuring after fertilization.

In *Capsella* (Schulz and Jensen 1973), *Spinacia* (Wilms 1981a), *Brassica campestris* (Sumner and VanCaeseele 1989, 1990), *Helianthus* (Yan *et al.* 1991) and *Orysa* (Dong and Yang 1990), lateral central cell wall projections are observed at the micropyle pole as the megagametophyte matures. In *Capsella* (Schulz and Jensen 1971) and *Helianthus* (Newcomb and Steeves 1971, Newcomb 1973a,b) similar projections are observed at the chalazal pole. In *Jasione,* cell wall projections are discontinuous with the cuticle that surrounds the megagametophyte (Berger and Erdelskà 1973). The central cell wall projections are thought to increase the surface area of the plasma membrane and this may have a role in nutrient mobilization (Sumner and VanCaeseele 1990).

2.7 Zygote Development

Zygote formation occurs once the sperm and egg gametes are fused (Esau 1976). Once fertilized, the zygote shows a characteristic polarization. The micropylar pole is vacuolated while the chalazal pole contains most of the cytoplasm, including the nucleus.

Cytological changes occur soon after fertilization in many species. Early investigations show zygote and embryo ultrastructure in *Gossypium* (Jensen 1968a,b), *Capsella* (Schulz and Jensen 1968b,c) and *Epidendrum* (Cocucci and Jensen 1969). In *Jasione montana*, an oil droplet forms at the micropylar end of the zygote, and disappears as the zygote matures (Natesh and Rau 1984). Twenty-four hours after fertilization, endoplasmic reticulum, ribosomes, plastids and mitochondria cluster near the nucleus at the chalazal pole of the zygote cell (Natesh and Rau 1984). Relocation of organelles in zygotes of other plants have been observed. In *Papaver nudicaule* (Olson and Cass 1981) and *Zea mays* (Lammeren 1981) changes in polarity occurs. In the unfertilized egg cytoplasm, ribosomes occur freely or associated with endoplasmic reticulum. After fertilization, ribosomes aggregate into polysomes in *Capsella* (Schulz and Jensen 1968b) and *Epidendrum* (Cocucci and Jensen 1969). In cotton, the cytoplasm contains starch, endoplasmic reticulum and polysomes (Jensen 1963, 1968a,b). Nateh and Rau (1984) suggested that a high metabolic activity is present due to the increase in numbers of mitochondria and plastids after fertilization. These authors reported an increased number of organelles which may have originated from the sperm cell cytoplasm. Sperm organelles differ in size and shape from those in the egg and central cell of *Plumbago* (Russell 1980); however, studies indicating survival and multiplication of these organelles after fertilization are lacking.

In species such as *Capsella* (Schulz and Jensen 1968b), *Epidendrum* (Cocucci and Jensen 1969), *Plumbago* (Cass and Karas 1974), *Papaver* (Olson and Cass 1981), *Brassica campestris* (Sumner 1986) and *Helianthus* (Yan *et al.* 1991) complete, partial or no cell wall exists prior to fertilization. In Cotton a complete wall surrounds the egg cell 36 hours after

fertilization (Jensen 1968a). In *Nicotiana*, wall synthesis requires 40 to 50 hours (Mogensen and Suthor 1979). In *Quercus*, a new discontinuous wall was found, and eventually surrounds the cell (Mogensen 1972). After fertilization, the zygote in *Helianthus* begins to divide prior to completing cell wall formation (Yan *et al.* 1991). During cell wall formation, an increase in metabolic activity was suspected. Mogensen and Suthor (1979) observed in the penetrated synergid a large number of polysaccharide spheres, which are thought to be the building blocks of the new cell wall of the zygote. Increased numbers of dictyosomes and endoplasmic reticulum after fertilization are believed to be involved in the wall formation process (Cocucci and Jensen 1969, Mogensen and Suthor 1979, Yan *et al.* 1991).

In *Hordeum*, *Quercus* and *Epidendrum* the zygote remains the same size (Norstog 1972, Singh and Mogensen 1975, Cocucci and Jensen 1969). In some taxa such as *Gossypium* (Pollock and Jensen 1964, Jensen 1968a), and *Nicotiana tabacum* (Mogensen and Suthor 1979) the zygote decreases in volume after fertilization. The most dramatic volume changes occur in *Gossypium* zygote which decreases its volume by half, 8 to 10 hours after fertilization. In *Datura stromanium*, *Cypripedum insigne* and *Jasione montana*, an increase in zygote volume occurs prior to cell division (Natesh and Rau 1984). Schulz and Jensen (1968b) have shown in *Capsella*. a restoration of zygote volume after a temporary shrinkage In most circumstances, it is not clear why the zygote changes in volume prior to cell division, or what mechanism triggers this volume change.

2.8 Early Embryo Development

Descriptions of early embryo ontogeny began in the 1920's and resulted in a complex system, developed by embryologists Souèges and

Schnarf, for describing and naming embrygenic types (Natesh and Rau 1984). The five types found in dicots were initially termed the Cruciferen, Astereen, Salanaceen, Chenapadiaceen and Coryophyllaceen embryogenic types. Maheshwari (1950) redefined the five types as Crucifer, Asterad, Solanad, Chenapadiad and Caryaphyllad. Johansen (1950) added a sixth type to the list, the Piperad, and he changed the name of the Crucifer type to the Onagrad type which is currently in use today. Johansen (1950) also recorded variations in each type and suggested schematic representation of each type presently known as the Schnarf and Johansen system of classification (Natesh and Rau 1984). Differences in ontogenic groupings reflect the amount of cellular material that is actually involved in the production of the embryo proper and the position of the first cell wall formed in the apical portions of the two-celled proembryo.

Variations such as sequence, timing of cell division and the orientation of cell wall formation during proembryonic stages are different in most angiosperm taxa and even within the same species (Natesh and Rau 1984). Many species in the crucifer family have been studied and show the typical Onagrad embryonic ontogeny (Schulz and Jensen 1968a,b, Tykarska 1976, 1979, 1980, Mansfield *et al.* 1991a,b). Onagrad taxa investigations demonstrate many similarities in the early stages of differentiation as shown diagrammatically in figure A. Initially the zygote divides horizontally, producing the basal suspensor cell and the apical cell of a two-celled proembryo. The apical portion of the proembryo divides vertically producing a dyad apex. Through a series of horizontal divisions the suspensor develops into a peg-like structure supporting the apical portion of the proembryo. As the suspensor divides, the apical cell

undergoes vertical and oblique divisions producing a tetrad, quadrant and octant proembryo arrangement not shown in figure A.

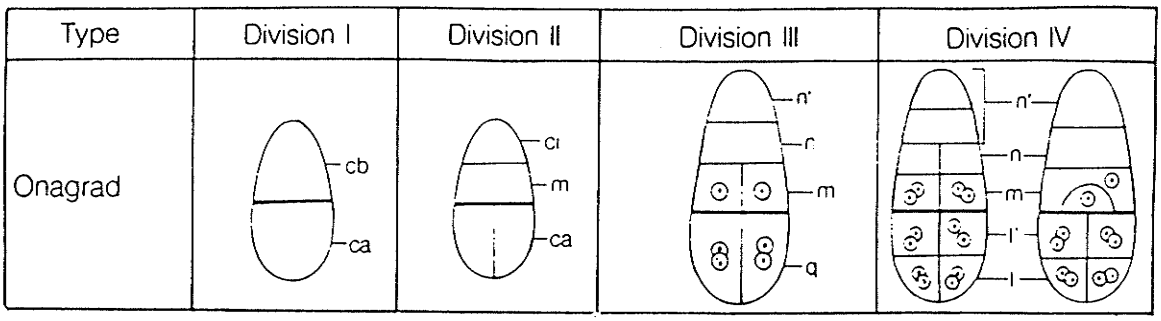

Fig. A. Schematic representation of the Onagrad embryonogy; based on Schnarf (1929) and Johansen's (1950) system of classification (from Natesh and Rau 1984).

Figure B is a diagramatic representation by Tykarska (1976, 1979) of early proembryo development in *Brassica napus* . The labelling system for the cells of the proembryo, employed of Tykarska, will be used in this thesis.

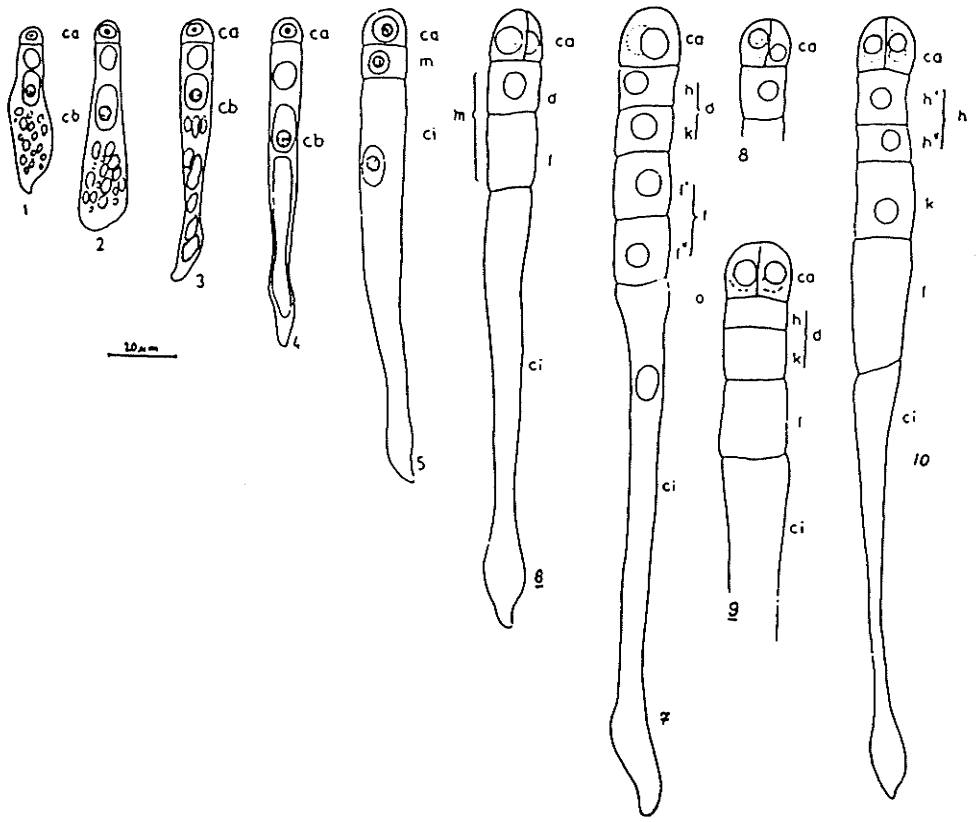

Fig. B. Diagramatic representation of the first division of the zygote (1-5) and the formation of the quadrants (6-10) in *Brassica napus* (from Tykarska 1976).

The Onagrad description of embryo ontogeny shows the apical cell giving rise to the majority of the embryo proper. Vertical and transverse divisions, in the apical portion of the proembryo, produces the embryo proper which at the globular stage consists of an upper and lower octant cell arrangement. The upper octant gives rise to the apical meristem epicotyl and cotyledons and the lower octant gives rise to the hypocotyl. Periclinal divisions in the globular embryo produces the protoderm which becomes evident soon after (Tykarska 1976, 1979). The rapidly developing

apical cell region may also be referred to as the embryonal mass (Esau 1976). The basal portion of the proembryo next to the embryonal mass, contributes to the formation of the hypophyseal region. This region is important as it is the upper most region of the suspensor, in close proximity to the embryo proper. The hypophyseal region eventually gives rise to the root and the root cap in angiosperms (Tykarska 1976, 1979). At maturity, the embryo development changes from a radial to a bilateral symmetry and begins to exhibit the typical heart-shape characteristic of the dicotyledons (Schulz and Jensen 1968b). Growth of the cotyledons continues, with periclinal and anticlinal divisions occuring below the protodermal cell layer. At this stage, the embryo becomes green, as stacked thylakoids become present in the plastids of the *Capsella* embryo (Schulz and Jensen 1968b). As the hypocotyl and cotyledons grow, they assume a torpedo shape. Eventually the embryo bends and the cotyledons reach the chalazal pole of the megagametophyte (Esau 1976).

The suspensor in the developing proembryo has two major roles. First, it is an organ which absorbs nutrients from the somatic tissue of the seed and transports them to the developing embryo. Secondly, it is a source of important nutrients and growth regulators for the developing embryo (Bohdanowicz 1987, Dute *et al.* 1989, Folsom and Cass 1986, Nagl 1974, Nagl 1990, Schulz and Jensen 1969, Tykarska 1976, Yeung and Clutter 1979, Yeung and Sussex 1979, Yeung 1980).

In most angiosperms, the cellular activity in the suspensor occurs during early basal cell development. As the basal cell increases in cytoplasmic volume, it becomes enrich in mitochondria, dictyosomes, rough endoplasmic reticulum, lipids, proteins, insoluble polysaccharides and RNA. Early in the basal cell development the nucleus is often located

chalazally. Later the nucleus migrates micropetally as the basal cell prepares to divide. The young suspensor cell in *Capsella* (Schulz and Jensen 1969), *Alisma* (Bohdanowicz 1990), *Glycine* (Dute *et al.* 1989) and *Brassica* (Tykarska 1976, 1979) has a distinctly PAS-positive thin cell wall. As the proembryo matures, the suspensor increases in size, cell number and metabolic activity. In many cases, the micropyle wall of the maturing basal cell form PAS-positive ingrowths and there is a notable increase in RNA, rough endoplasmic reticulum, mitochondria and dictyosomes distributed throughout the cell (Yeung and Clutter 1979). There is also a marked reduction in the quantity of lipids and insoluble polysaccharides during this stage of development (Schulz and Jensen 1968, Tykarska 1982, 1987). Schulz and Jensen (1968b) have shown dictyosomes dispersed throughout the suspensor cells with the highest concentration located in the basal cell . The ultrastructure of plastids varies in different areas of the suspensor and the developing embryo proper. In some cases plastids exhibit ultrastructural changes later in embryo development. In *Alisma*, large plastids have been observed in the basal cell and, may have a specific role in embryo development (Bohdanowicz 1990). Yeung and Clutter (1979) and Gartner and Nagl (1980) presume the plastids in *Phaseolus* are the site of synthesis of substances which may control embryo development.

Certain organelles adjacent the cell wall and a complex series of convoluted projections at the cell surface are characteristic of the transfer type cells described by Gunning and Pate (1969) and Pate and Gunning (1972). These transfer type cells are involved in a short distance apoplastic type of translocation; however, the plasmodesmata between suspensor cells allows nutrient flow towards the embryo proper symplastically

(Mansfield *et al.*1991b). Mitochondria and endoplasmic reticulum are found throughout the cytoplasm of the transfer cells, but their numbers are higher near the plasma membranes of the cell wall ingrowths (Davis *et al.* 1990). Bohdanowicz (1990) noted endoplasmic reticulum cisternae often run from the area of micropyle wall ingrowths to the chalazal end of the basal cell. Other authors have also noted the presence of endoplasmic reticulum near wall ingrowths and speculate that the cisternae may play an important role in intracellular transport of various substances (Schulz and Jensen 1969, Yeung and Clutter 1979, Bohdanowicz 1990).

In *Capsella* (Schulz and Jensen 1969), *Helianthus* (Newcomb 1973b) and *Stellaria* (Newcomb and Fowke 1974), the cell walls between the suspensor cells have numerous plasmodesmata, but no such interconnections exist between the suspensor and the central cell, with the exception of sugar beet (Bruun 1987). Plasmodesmata have been observed between the basal suspensor cell and synergids in sugar beet. In most angiosperms, plasmodesmata interconnecting the megagametophyte with the integumentary and nucellar tissues are not observed after fertilization (Mansfield *et al.* 1991b). Yeung (1980) demonstrated that the suspensor of *Phaseolus coccineus* as is a site for nutrient uptake in a C-14 sucrose solution to developing embryos in vitro. Similar results were obtained by Brady and Combs (1988) using the Prussian Blue technique on developing whole plants.

Rough endoplasmic reticulum is associated with the production of proteineaceous material in the basal cell of the suspensor, and may have a secretory function (Bohdanowicz 1990). Some authors indicate that the suspensor may control the output of certain hormones or may be the site of hormone production (Picciarelli *et al.* 1984). Gibberellic acid (GA)-like

compounds detected in *Cyisus laburnum* at the globular and heart stage of embryo development are suspected to influence growth (Picciarelli *et al.* 1991). Cionini *et al.* (1976) demonstrated that GA-like compounds are important for embryogenesis. They removed the suspensor of a young *Phasiolus coccineus* embryo which resulted in reduced embryo development. The embryo devoid of suspensor was then treated in vitro with a solution of GA and normal development resumed. A dramatic decrease in the concentration of the GA occurs in the suspensor at the cotyledonary stage in embryo development (Alpi *et al.* 1975). Brady and Combs (1988) have also successfully replaced a partially damaged suspensor using GA. This indicates GA is needed for normal embryonic development. Auxins have also been detected in higher levels in the suspensor than the embryo proper of *Tropaeolum majus* (Przybyllock and Nagl 1977). Lorenzi *et al.* (1978) observed high levels of biologically active cytokinins in the suspensor of *Phaseolus* in the heart-shaped embryo. At the same stage the embryo proper contains little cytokinins. However, when the embryo reaches the mid-cotyledonary stage, the concentration of cytokinins is lower in the suspensor and higher in the embryo proper.

In some cultivars of *Brassica napus*, 14 cell suspensor units have been observed (Tykarska 1976, 1979). Mansfield *et al.* (1991b) has shown 7 to 9 celled suspensors in *Arabidopsis* . Thompson (1933) describes the suspensor in *Brassica oleracea* as having 10 to 12 cells. Suspensor growth rates vary depending on the stage of development. Simoncioli's (1974) observed that in *Diplotaxis* a suspensor, at the octant stage, demonstrated a rapid growth rate between the globular and the heart-shaped stages of development. This rapid growth of the suspensor during the early stages of embryogenesis have also been reported in *Phaseolus* by Yeung and

Clutter (1979). In *Brassica napus*, the suspensor divides and elongates rapidly through the globular stage of embryo development. Once the hypophysis cell is formed, suspensor elongation is reduced; however, the ability of the suspensor cells to divide is maintained (Tykarska 1976). Once the embryo proper differentiates into a mature embryo, the suspensor begins to degenerate. It is not known what regulates suspensor growth. Using an *Arabidopsis* embryo-lethal mutant, Marsden and Meinke (1985) showed that the suspensor unit was interacting late in the development of the embryo proper.

3.0 Materials and Methods

3.1 Plant Material

All fresh plant material was maintained in the controlled environment of a growth chamber in order to better observe plant development optimizing selective emasculation and harvest of desired plants. Plants of *Brassica Napus* L. cv. Regent (Canola-Rapeseed), a self-compatible species, were maintained in a growth chamber (Controlled Environments Ltd., Model E 15) under Sylvania Lifeline cool white fluorescent tubes and incandescent bulbs (Sylvania 60 watt) at a radiance of $200W/m^2$.

At the seedling stage, the plants were maintained in a shortday 8 hours photoperiod for a period of four weeks until the rosette stage of development. After the four week period, the photoperiod was increased to 16 hours to induce bolting and subsequent inflorescence formation (Orr 1978). The temperature inside the growth chamber varied between a day temperature of 22°C and a night temperature of 18°C.

3.1.1 Pollination

Pre-anthesis flowers were selected in all cases for pollination. Using forceps, the flowers were opened to expose the pistils. Pollen from dehiscing anthers was deposited directly onto the receptive pistil to complete pollination. To ensure no possible self incompatibility, flowers from different *Brassica Napus* L. cv. Regent plants were used. The flowers were collected after various post pollination periods (Fig 3).

3.1.2 Ovule Collection

The ovules were harvested at various post-pollination periods ranging from time zero (pollination) to 120 hours. The procedure consisted of removing the entire flower at the stem. With the aid of a

stereo microscope (Olympus SZH zoom), an incision was made along the marginal seam of the pistil with a fine glass microprobe to reveal the locule containing the suspended anatropous ovules attached to the parietal type placenta by the funiculus. Before the ovules were removed from the ovary, a buffered fixative was splashed into the locule.

The external morphology of recently fertilized ovules was very similar to that of the unfertilized ovules. Since no method exists to determine fertilization prior to sectioning, potentially fertilized ovules were discriminated from unfertilized ovules using modified techniques developed by Olson and Cass (1981) to determine ovule/pollen tube association. Desired ovules were placed in a well slide and stained with 0.05% Aniline Blue (CI 42755, Polyscience) in 0.025M phosphate buffer (PO_4) pH 6.8 and viewed with an epifluorescence microscope.

Aniline Blue contains a fluorochrome that binds to β 1-3 glucans and will fluoresce blue-white when excited under ultraviolet light (O'Brien and McCully 1981). Fluorescing β 1-3 glucans located in the pollen tube cell wall identifie the pollen tubes and this technique has been used to observe the penetration of the pollen tube into the micropyle region of the ovule (Sumner 1986). Pollen tube penetration; however, does not confirm fertilization.

3.2 Light Microscopy

A Nikon Optiphot compound microscope was used for brightfield microscopy. Differential interference contrast light microscope observations were made using a Leitz Ortholplan compound microscope. Photomicrographs were recorded on 35 mm Plus-X 125 ASA film (Black/White) or 35 mm Ektachrome 160 professional film (Colour slides). All light micrographs were recorded using a Nikon Microflex AFX

photomicrographic attachment. Black and white positive prints were made using a Simmon-Omega enlarger and recorded on Ilford multigrade II medium grade paper.

3.2.1 Fixation, Dehydration, Infiltration and Embedding

Ovules/seeds were fixed in 3% glutaraldehyde in 0.025M PO_4 buffer (pH 6.8) for 2 hours at room temperature followed by 24 hours at 4°C. Some samples were also post-fixed in 2% osmium tetroxide (OSO_4) in 0.025M PO_4 for 4 hours.

After fixation, samples were dehydrated in an ascending series of ethanol/water washes 30%, 50%, 70%, 85%, 95%, 2 x 100%, 20 minutes each, followed by an ascending series of propylene oxyde/ethanol washes 50%, 75%, 2 x 100% for 30 minutes each.

The samples were infiltrated with a mixture of propylene oxide and Spurr's epoxy resin (Spurr 1969) in proportions of 3:1, 1:1, 2 hours each, and 1:3 for 48 hours followed by 3 days of 100% epoxy resin changed daily. Constant rotation of the tissues in small specimen vials was maintained during the infiltration process. Infiltrated samples were placed in aluminum weighing boats (Fisher brand) and embedded using fresh epoxy resin. Once the samples have been properly positioned, polymerization was effected by placing the boat in the oven at 70°C for 24 hours.

To obtain the desired ovule orientation, square cubes containing the embedded ovule were cut out of the polymerized Spurr epoxy discs and mounted to a blank epoxy beam capsule with 5-minute epoxy (Lepage's). The block was then rough trimmed using a Dremel grinder and fine trimmed using a double edged razor blade.

Sections for light microscopy were obtained using a Sorvall Porter Blum JB4 microtome with a glass knife equiped with a water trough

(Fisher 1968). Sections 0.75-1.5 μm in thickness were floated onto water and removed from the knife boat using glass microprobes and transferred to drops of filtered water on a gelatin-coated slide. All slides in this study were coated with 0.5% gelatin adhesive (Jensen 1962), unless otherwise indicated. Coated slides were placed on a slide warmer (75°C) to dry and flatten the sections and to ensure proper section adhesion to the slide.

3.2.2 Fresh Sectioning

Fresh sections of *Brassica napus* seeds were obtained using a freezing stage (Bailey Instruments). The seeds were positioned in a gelatin embedding compound (Tissue Tek. Ames Co.) on the freezing stage until the tissue embedding compound was frozen (2 minutes). Ten μm sections were removed using a steel (American Optics) knife and discarded. Once the desired region of the seed was located, the frozen tissue was thawed from gelatin embedding compound and carefully rinsed in 0.025M PO_4 buffer (pH 6.8) to remove the gelatin. The tissue was then placed in a depression slide, stained with aniline blue or calcofluor and viewed using ultraviolet illumination. Materials and methods used for staining fresh tissue are described in the section "Fluorescence Microscopy".

3.2.3 Staining Epoxy Embedded Tissue

3.2.3.1 Crystal Violet

Some epoxy sections were stained on a slide warmer (75°C) with 2% ethanolic crystal violet (C.I. 42555, Fisher) in 0.05M ammonium oxalate buffer (pH 6.7) (Gerhardt *et al.* 1981) for 0.5-1.0 minutes. The sections were rinsed with warm filtered water to remove the excess stain and then dried with filtered compressed air. Overstained sections were washed for extended periods of time (30 minutes) in warm filtered water. Excellent

results were obtained when using crystal violet for routine examinations. (Sumner 1986).

3.2.3.2 Aniline Blue-Black

Aniline blue-black, an anionic dye, was used to localize protein. Sections were stained in 1% aniline blue-black (C.I.20470, Polyscience) in 7% acetic acid for 15 minutes at 60 °C. The sections were briefly rinsed in 7% acetic acid to remove excess stain then mounted in glycerol containing 5% acetic acid. The cytosol of healthy cells stained light blue while that of degenerating cells, presumably rich in hydrolytic proteins, stained dark blue. Mitochondria, plastids, and regions of nuclei stained light to dark blue.

3.2.3.3 Periodic Acid Schiff Reaction (PAS)

According to Jensen (1962), the PAS reaction is the most important histochemical technique available for the localization and identification of insoluble carbohydrates. The chemical basis of the reaction is that periodic acid (PA) will cleave carbon-carbon bonds where these carbon atoms have vicinal hydroxyl groups (1, 2 glycol) or adjacent hydroxyl and amino groups to form aldehydes. These aldehyde groups are then allowed to react with Schiff's reagent, a colourless reagent, which gives a red to purple colour when combined with aldehydes. This reaction is termed PAS-positive. Compounds are PAS-negative when the hydroxyl groups are not attached to the vicinal carbon atoms. This occurs when the glycol group is substituted with a sulfate in the case of sulfated polysaccharides or with phosphate in the case of nucleic acids. This is also the case when one of the vicinal carbons is involved in linkages such as a β 1–3 glucans (i.e. callose). Polysaccharides such as cellulose, hemicellulose, pectic

compounds, oligosaccharide side chains of glycoproteins and starch should all be PAS-positive. Certain carbohydrates, such as the cellulose in the cell walls, produce a PAS-negative reaction. O'Brien and McCully (1981) speculated that stearic hindrance may block the available vicinal glycol groups. A PAS-positive reaction of cellulose in the cell walls only occurs after extended oxidation in PA (1-24 hours) (O'Brien and McCully 1981). Certain non-carbohydrate compounds will also exhibit a PAS-positive reaction. This includes polypeptides containing amino acids such as serine, threonine and hydroxylysine, which have adjacent hydroxyl amino groups, and certain lipids. Lignin will also give a positive reaction with Schiff's reagent without prior PA treatment (O'Brien and McCully, 1981). Since Schiff's reagent reacts with any free aldehydes such as that of aldehyde fixing agents, an aldehyde blocking agent (2,4 dinitrophenyl hydrazine (DNPH) or Schiff's reagent) is used prior to PA oxidation as a control treatment.

For the control treatment, slides bearing the sections were submerged in a 5% DNPH in 15% acetic acid for 15 minutes and washed in warm filtered water for 10 minutes to block any endogenous aldehyde sites. Sections were oxidized in a 1% aqueous PA solution for 30 minutes, followed by a 15 minutes wash in filtered water. The sections were then transferred to modified Schiff's reagent (Fisher 1968) for 40 minutes then washed for 10 minutes in filtered water and dried with filtered air. The sections were viewed either directly or after counter staining with crystal violet or aniline blue-black.

3.3 Fluorescence Microscopy

Several organic compounds present in plant material will exhibit primary autofluorescence. Such examples are phenolic compounds (lignins) and chlorophyll. Most organic components (carbohydrates), however, will not produce primary fluorescence, therefore, secondary fluorescence must be induced. This is done by using fluorescent dyes (fluorochromes). Many fluorochromes will bind directly to macromolecules in the same way as orthochromatic and metachromatic dyes, but the major advantage of fluorochromes over conventional dyes is greater detection sensitivity with the fluorescence microscope technique (O'Brien and McCully 1981).

Prior to staining with fluorochromes, the epoxy resin was removed from the sectioned material using a method modified from Lane and Europa (1965). This provides access for fluorochrome to tissue and removes autofluorescence caused by the epoxy resin. The mounted sections were submerged in a saturated solution of potassium hydroxide in 95% ethanol for 3 minutes followed by three successive changes in 95% ethanol and a 5-minute wash in filtered water.

In all cases, stained sections were viewed by a Nikon Optiphot compound microscope fitted with a Nikon "EF" episcopic (epi-) fluorescence attachment. Illumination was provided by a 50 watt high pressure mercury vapor (HBO) bulb and the desired wavelength of light was selected using various barrier and excitation filters. To obtain ultraviolet (UV) illumination, a UV excitation filter (330-380 nm) and a barrier filter transmitting above 420 nm were used. To obtain blue illumination, a blue (B) excitation filter (410-485 nm) and a barrier filter transmitting above 515nm were used. For observations using green

illumination, a green (G) excitation filter (535-550 nm) and a barrier filter transmitting above 580 nm were used. All photomicrographs were taken using the same Nikon photographic materials and methods described in "Brightfield Microscopy".

3.3.1 Calcofluor

Calcofluor White M2R is one of the most fluorescent compounds available in microscopy for plant cell walls (Fulcher and Wong 1980). O'Brien and McCully (1981) also used calcofluor to stain cell walls of algae and fungi. The mechanism of how calcofluor binds to plant cell walls is not completely understood. Some authors speculate that the dye binds to the glucan components of the cell walls (O'Brien and McCully 1981, Fulcher and Wong 1980).

Sections were stained in a 1% aqueous solution of Calcofluor white MR2 (C.I. 40622, Polyscience) for 5 minutes, followed by a brief rinse in filtered water. The sections were dried with filtered air, mounted in 70% sucrose, and viewed under UV illumination. Stained cell walls will exhibit a blue-white fluorescence.

3.3.2 Aniline-Blue

Aniline blue is a fluorochrome thought to be specific for β 1,3 glucans (callose) (O'Brien and McCully 1981); however, some authors question its specificity (Fulcher and Wong 1980). Callose is a cell wall polysaccharide that cannot be located using the Periodic Acid Schiff's (PAS) procedure since the vicinal hydroxyl groups are not available due to the 1,3 linkage at the polymers. Smith and McCully (1978) have shown that the aniline blue specificity for callose may be increased by prior treatment of the tissue with toluidine blue, which blocks acid and sulfate

polysaccharides and with the PAS procedure, which blocks polysaccharides with vincinal hydroxyl groups (O'Brien and McCully 1981).

Fresh and sectioned material were stained for 5 minutes in a 0.05% aniline blue (C.I. 42755, Polyscience) in 0.01M PO4 buffer (pH 6.8) then mounted in the buffered stain and viewed with UV or B illumination. Under UV excitation, stained callose within the cell walls exhibits a blue-white yellow fluorescence.

3.4 Transmission Electron Microscopy (TEM)

Transmission Electron Microscopy observations were carried out using a Hitachi H-7000 TEM and electrons were excelerated at operating voltages from 65 to 100 kilovolts (kV). Electron images were recorded on Ilford and Kodak EM quality 8.3 x 10.2 cm sheet film. Negatives were developed using Kodak D-19 developer and photomicrographs were printed on Ilford multigrade II medium grade paper using a Simmon-Omega (model automega D3) point source photographic enlarger.

3.4.1 Fixation, Dehydration, Infiltration and Embedding

Material and methods used for tissue preparation with TEM was previously described in the above section for light microscopy. Ultrathin sections for TEM were obtained with a Reichert OM-U2 and a Reichert Ultracut microtomes using a Dupont diamond knife. Ultrathin sections were mounted on uncoated 75/300 mesh and Hex 200 mesh nickel grids.

3.4.2 Staining Epoxy Embedded Tissue for TEM

3.4.2.1 Uranyl Acetate (UA)/Lead Citrate (Pb)

Uranyl acetate and lead citrate are the most commonly used heavy metal stains for electron microscopy (Hayat 1970,1975). Although UA/Pb staining provides excellent specimen contrast, these stains have no histochemical value.

Nickel grids supporting sections were submerged in a saturated solution of UA in 50% methanol for 25 minutes in a dark environment. The sections were then washed in 50% aqueous methanol followed by filtered distilled water 30 minutes each. The grids were then blotted dry and transferred to the Pb stain for 10 minutes in a saturated nitrogen gas environment (Reynold 1963). The grids were then washed for 30 minutes in degassed, filtered, distilled water, air dried and observed.

3.4.2.2 Periodic Acid-Thiocarbohydrazide-Silver Proteinate (PA-TCH-SP)

PA-TCH-SP is a modified PAS technique developed by Thiery (1967) to detect polysaccharide. The modified PAS technique, using silver metheamine or silver proteinate following thiocarbohydrazide treatment, provides good contrast and resolution for the ultrastructural localization of polysaccharides. The PA-TCH-SP technique, used PA to selectively oxidize vicinal glycol or glycol amino groups to aldehydes. The aldehydes were then condensed using thiocarbohydrazide, producing thiocarbohydrozones. The silver proteinate staining resulted in reduced silver deposits over PAS-positive polysaccharide sites within tissues (Thiery 1967). As with the PAS technique for light microscopy the PA-TCH-SP technique requires controls (aldehyde blocks). The control treatments involved the omission of periodic acid, thiocarbohydrazide or silver proteinate.

Sections on nickel grids were submerged for 30 minutes in 1% aqueous PA and maintained in a high humidity chamber. Sections were then washed 3 times in filtered distilled water 10 minutes each. The sections were transferred to a 0.2% thiocarbohydrazide (TCH) in 20% aqueous acetic acid for 4 hours in a high humidity chamber. Sections were then rinsed in successive 10%, 5%, 1% rinses in aqueous acetic acid 20

minutes each. The sections were then submerged in a 1% aqueous silver proteinate (SP) for 30 min in a high humidity dark chamber, followed by 3 successive rinses in filtered distilled water for 1 hour each.

3.4.2.3 Osmium Tetroxide and Potassium Ferricyanide (OsFeCN)

The OsFeCN post-fixation procedure was used to stain the endoplamic reticulum (ER) and the nuclear envelope. The initial use of this procedure in plant ultrastructure was by Hepler (1980) in an effort to observe the distribution of ER in dividing cells of barley.

The removal of calcium chloride from the fixatives or the addition of phosphate buffer, which would precipitate the calcium, abolishes the selective staining of the ER and nuclear envelope (Hepler 1981); therefore, a cacodylate buffer was used in this study.

Ovules were fixed in 3% gluteraldehyde in 0.025M cacodylate buffer (pH 6.8) with 5 mM calcium chloride for 2 hours at room temperature followed by 24 hours at 4°C in the same fixative. Following a wash in 0.025M cacodylate buffer (pH 6.8) with 5 mM calcium chloride, the ovules were post-fixed in a mixture of 2% osmium tetroxide and 0.8% potassium ferricyanide in 0.025M cacodylate buffer with 5 mM calcium chloride for 4 hours at room temperature. The methods of dehydration, infiltration, embedding, orientation, sectioning and staining have been described above in section 3.4 under TEM.

4.0 Observations

4.1 The Flower

The inflorescence of *Brassica napus* is a raceme . Each yellow flower (Fig. 3) is bisexual and actinomorphic with a calyx of four separate sepals and a corolla of four separate petals. The stamens have a tetradynamous configuration, with four of them being long and two short. The gynoecium is composed of two united carpels with parietal placentation divided by a replum. The mature fruit is a silique and contains approximately 22 to 25 seeds (Smith 1977). Figure 3 shows flower morphology of *Brassica napus* over time. The length of the pistil in flower A (time 0; anthesis) is 8 mm. Flowers B to E show post-anthesis flower morphology at time periods 24, 48, 72 and 96 hours, respectively, with a maximum pistil length of 22 mm at 96 hours.

4.2 The Mature Ovule

The anatropous ovule of *Brassica napus* is attached to the replum of the ovary by a stalk-like funiculus (Figs 2, 8). After anthesis, the ovule shows four distinct structural zones; the megagametophyte, the raphe, the nucellus, and the integuments (Figs 4, 14). The integuments consist of an inner and an outer integument which vary in the number of cell layers depending on the location in the ovule. The megagametophyte is composed of seven cells: three antipodal cells, one central cell with two polar nuclei, an egg and two synergid cells (Fig 4). The egg and two synergid cells are positioned in a triangular arrangement at the micropyle end of the ovule (Figs 15, 17, 18, 20).

4.2.1 Inner Integument

The inner integument surrounds the megagametophyte and varies in thickness. The inner integument has 2 to 3 cell layers at the micropyle

and has 5 to 12 cell layers at the chalazal pole of the ovule (Fig 4). At anthesis, the micropyle portion of the megagametophyte is surrounded by slightly vacuolated rectangular inner integument cells. Eight to ten hours after anthesis, the integument cells nearest the megagametophyte appear to be crushed by the expanding megagametophyte and have a densely stained cytoplasm with crystal violet and thick layers of calcofluor-positive cell wall material (Figs 15, 16). At this stage of the development, most of the PAS-positive starch grains were found in the micropyle inner integument (Figs 5, 15, 18). Later during embryogenesis, starch reserves in the inner integument at the micropyle are decreased, especially at the cell layer next to the megagametophyte (Figs 46, 47, 49). The inner integument of the basal body is composed of 8 to 12 layers of highly vacuolated parenchyma cells, which remain constant throughout early embryogenesis (Figs 4, 5, 59). After anthesis, the cells of the basal body nearest the micropyle contain most of the PAS-positive starch grains. During embryogenesis, when starch accumulations in the inner integument at the micropyle are depleted, the number of PAS-positive starch grains increased in the vacuolated cells of the basal body at the crotch of the curved megagametophyte (Fig 59). The inner integument adjacent to the chalazal nucellar proliferation tissue is 5 to 7 cell layers in thickness and shows little vacuolation or starch accumulation. The remaining inner integument distal to the micropyle is 8 to 12 layers in thickness (Figs 4, 59). The 5 to 8 cell layers of cells, adjacent to the outer integument, have a cuboidal appearance; however, the remaining cell layers adjacent the megagametophyte are oval and more vacuolated making it difficult to accurately count cell layers. The oval cells of this inner integument layer become more vacuolated during early embryogenesis; however, the PAS-

positive starch accumulation remains similar (Fig 59). Plasmadesmata are present in the inner and outer integument cells; however, no plasmodesmata are observed between the inner and outer integument or between the inner integument and the megagametophyte.

4.2.2 Outer Integument

The outer layer of the outer integument forms the distal most portion of the micropyle. The outer integument is 3 to 4 celled layer thick and is covering most of the ovule from maturity to the early embryo development stage (Figs 4, 14, 59). The highly vacuolated cells of the outer integument cells, at the micropyle pole of the ovule, has more PAS-positive starch grain accumulations (Figs 5, 47, 59) than the outer integument cells of the raphe region (Fig. 59). These starch reserves are present from anthesis to early embryogenesis. A single vascular trace of xylem and phloem runs from the replum of the ovary to the raphe region of the ovule (Fig. 8). The raphe (Fig. 4) is a region of tissue located between the aniline blue positive chalazal proliferation tissue and the funiculus where calcofluor-positive cell walls of the xylem (Fig.9) and the aniline blue positive sieve plates of the phloem elements are visible (Figs 8, 10). Once the vascular traces enter the ovule, they branch out laterally at the base of outer integument layer forming a vascular network extending from the basal body to the chalaza (Figs 8, 10). The vacuolate sieve tube members are associated with electron opaque companion cells (Fig. 12) and are mainly distributed in the lateral chalazal tissues of the ovule (Fig 11) with a cluster of sieve tube elements in the micropylar region of the ovule near the raphe (Fig. 59). Figure 14 is a diagramatic interpretation of the pattern of vasculature of the ovule.

4.2.3 Antipodals

Since the focus of this study relates mainly to developmental aspects of the embryo, no antipodal data were obtained. Antipodals were not observed in any developmental stages after anthesis, confirming antipodals are ephemeral.

4.2.4 Central Cell

At anthesis, the pre-fertilized central cell has a heterogeneous cytoplasm which extends from the egg apparatus to the chalazal end of the megagametophyte. Small vacuoles are dispersed throughout the central cell with the highest concentration at the chalazal pole (not shown).

Wall projections are shown associated with the longitudinal walls of the central cell and the inner integument and appear to pocket the micropylar portion of the megagametophyte (Figs. 17, 20). The wall projections extend from the mid-region of the central cell equal to the polar nuclei to the synergids near the synergid hook region. Using brightfield microscopy, the wall projections are hardly visible (Fig. 15); however, when stained with calcofluor and viewed under UV illumination, the wall projections appear as a pale blue haze surrounding the megagametophyte (Figs 17, 19, 20). Ultrastructurally, the central cell cytoplasm is maintained by a plasma membrane which contacts the evenly distributed convoluted central cell wall projections (Fig. 21). The electron-transparent convoluted wall projections have a fibrillar appearing matrix with some electron-opaque deposits (Figs 21, 22). Few dictyosomes are shown near the central cell wall projections. Mitochondria and endoplasmic reticulum are located throughout; however, some small strands of endoplasmic reticulum and most M&M-shaped mitochondria

with prominent tubular cristae are located near the synergid cells adjacent the wall projections (Figs 21, 22).

The two polar nuclei are adjacent to each other and are located centrally at the micropyle of the central cell next to the egg apparatus (fig. 4). The nuclei are mostly ovoid with a few invaginations and contain large nucleoli. Fusion is not complete since a small amount of cytoplasm can be seen between the two polar nuclei (Figs 15, 17, 18, 20). Small amounts of PAS-positive spheres and orthochromatic plastids are shown throughout the central cell; however, most are perinuclear.

4.2.5 Egg Cell

The cone-shaped egg cell is approximately 97 μm in length at maturity and shares common boundaries with the central cell, synergids and the megagametophyte wall adjacent to the inner integument (Figs 18, 20). The egg cell is attached to the megagametophyte wall approximately 34 μm from the micropyle up to were the central cell extends creating the egg hook region (Figs 18, 19, 20, 81). The distance between the hook region of the egg and the chalazal apex of the egg is approximately 63 μm. Of the three cells of the egg apparatus, the egg cell extends chalazally beyond the synergid cells. The wall between the egg and the synergids appears to be electron-transparent and contains plasmodesmata (Fig 25). In cross-section, the egg and synergid common cell wall and the egg-central cell common wall show expanded areas occupied by intermittent electron-opaque inclusions while the narrow areas show a thin layer of fibrillar cell wall material between plasma membranes (Figs 22, 26, 27). The wall between the central cell and the egg cell is electron transparent (Figs 22, 27). In the egg apparatus, the egg cell shows a definite reduction in cell wall material at the chalazal pole of the cell. Cell wall glucans present in the

egg cell walls were detected with calcofluor and UV illumination at the micropyle; however, no reaction occured at the chalazal pole (Figs 16, 19). At anthesis, the egg cell shows polarization. The chalazal (1/3) of the egg cell is occupied by the nucleus and the majority of the egg cytoplasm. The micropyle (2/3) contains a large vacuole and some cytoplasm near the cell walls (Figs. 18, 20). Plastids with electron-opaque stroma and electron-transparent areas believed to be starch, are mainly perinuclear at the chalazal end of the cell (Figs. 26, 27). Mitochondria with well-developed cristae are more numerous than the plastids and are found both in the perinuclear (Fig. 27) and micropylar regions adjacent the common wall between the egg and synergid (Fig. 25). Few lipid bodies have been observed at the chalazal end of the egg cell. Dictyosomes composed of 5 to 7 flattened cisternae are present in the egg cell; however, most are found near the cell wall (Figs. 25, 27).

4.2.6 Synergid Cells

The cone-shaped synergid cells appear more ovoid than the adjacent egg cell and are approximately 105 μm in length at maturity (Figs 4, 15, 18). Both synergid cells are located at the extreme micropyle end of the megagametophyte next to the inner integument (Figs 4, 15, 17). From the micropyle, the synergid cell wall adjacent the megagametophyte extends chalazally until the synergid comes adjacent the central cell forming the synergid hook region (Fig. 20). Cell walls exist between the two synergids, the egg and central cell (Figs 22, 23, 25). The common cell wall between the synergid cells is more prominent at the micropyle where it becomes continuous with the filiform apparatus (Figs 15, 17). The synergid cell wall adjacent to the megagametophyte shows a similar pattern; it is thicker at the micropyle and thinner towards the chalaza (Fig

19). At anthesis, the synergid cell has many small irregular shaped vacuoles distributed evenly throughout the cell (Figs 15, 18, 22). Circular to ovoid mitochondria with well-defined tubular cristae and rough endoplasmic reticulum are present, with some strands of endoplasmic reticulum pressed along the synergid plasma membrane of the synergid-central cell wall (Figs 22, 23). Dictyosomes composed of 5 to 6 flattened cisternae show small spherical transition vesicles at the forming face and vesicles of various sizes actively being produced at the maturing face (Figs. 22, 23, 25). The centrally located nucleus has an electron-dense nucleolus and is surrounded by mitochondria, plastids and smooth endoplasmic reticulum. A unique feature of the synergid cells is the filiform apparatus which is located at the micropyle pole of the cell (Fig 4). The filiform apparatus has finger-like projections extending into the cytoplasm of the synergid cell (Figs 17, 19). At anthesis, the filiform apparatus stains orthochromaticly with crystal violet (Fig. 15); and is intensely stained by calcofluor for presence of β 1-4 glucans (Figs 6, 16, 19). When stained with UA/Pb, the filiform apparatus has an electron-opaque area in the centre of the projections and electron-transparent areas at the margins of the projections (Fig 32).

Synergid orientation with respect to the funiculus was not determined in this study.

4.3 The Fertilized Ovule

4.3.1 Pollen Tube Migration

The stigmatic surface of the style (Fig 3) is composed of highly vacuolated papillae cells which provides the proper environment for pollen germination. Below the stigmatic surface, the style is composed of highly vacuolated rectangular parenchyma cells flanked by vascular tissue

distibuted up to the replum (not shown). At anthesis, the stigmatic surface was pollinated with the pollen of several donor flowers. Five hours after pollination, pollen resting on the stigmatic surface produced a pollen tube which grows between the lateral walls of the papillae cells (Fig 1). Ten hours after pollination, the pollen tubes have elongated between the core cells of the style (Fig 2) eventually entering the non-cellular environment of the ovule loculi. In the loculi, the pollen tube follows along the replum surface until it encounters the stalk-like funiculus of a mature ovule which is positioned parallel to the longitudinal axis of the ovary with the micropyle directed towards the stigma. The pollen tubes contact the ovule near the funiculus, eventually entering the ovule at the micropyle (Fig. 6). Several pollen tubes may be associated with a single ovule, but only a single pollen tube is successful in entering the ovule at the micropyle. Once in the ovule (Fig 6), the pollen tube grows between the micropyle integument cells (Fig 7) towards the filiform apparatus (Figs 32, 33). Since it was impossible to determine the exact time of fertilization, stages of megagametophyte penetration and the process of double fertilization were not observed in this study.

After fertilization, the megagametophyte has a central cell with free nuclear endosperm, a persistent and a degenerating synergid cell, and a zygote cell with a centrally located nucleus (Figs 34, 36).

4.3.2 Central Cell

After double fertilization, a free nuclear endosperm is present near the developing zygote cell (Figs 30, 35, 45, 46). Chloroplasts with well-developed thylakoids and large starch granules are present in the micropyle region of the central cell often perinuclear to the developing free nuclear endosperm (Figs 78, 79, 86). During early zygote development

prior to ampuliform zygote elongation, the PAS-positive starch in the central cell becomes depleted; however, as the zygote matures, starch reappears and becomes more prevalent in the micropyle region of the central cell (Figs 30, 34, 36, 79). The zygote is flanked laterally by the central cell which contains many mitochondria with well-developed tubular cristae adjacent the cell wall projections (Figs 33, 36, 39, 81). The central cell wall projections adjacent the megagametophyte wall appear hazy at the micropyle pole and become reduced towards the chalazal pole of the zygote cell (Figs 31, 34, 35, 36, 48). Central cell wall projections cut obliquely, adjacent the micropyle end of the persistent synergid cell show a web-like appearance as the synergid cytoplasm appears to be invaginated by the central cell wall (Fig 36). The central cell shows a few lipid bodies and small fragments of endoplasmic reticulum (Figs 43, 44). The central cell adjacent to the degenerate synergid is separated by its plasma membrane and thin cell wall (Fig 38). At the chalazal pole of the persistent synergid cell, the central cell plasma membrane and the common cell wall are not present (Figs 36, 39). After fertilization, the central cell which surrounds most of the developing zygote, becomes highly vacuolated in the micropylar and mid chalazal region. Enlarged vacuoles are shown positioned at the chalazal tip of the zygote cell (Figs 28, 29, 30, 35).

4.3.3 Early Zygote Development

After fertilization, the large pre-fertilized micropylar egg vacuole has disappeared (Figs 34, 36). The nucleus is located in central position and the zygote has assumed an ovoid shape. No observations of very early fertilization events were documented; however, the zygote shows a reduction in size with respect to the egg subsequent to fertilization. At this

stage of development, the zygote cell cytoplasm shows an irregular shaped nucleus surrounded by a distinct nuclear membrane. The nucleus appears as densely stained as the zygote cytoplasm with UA/Pb; however, the nucleolus is more electron-opaque. In many circumstances two nucleoli are present in the nucleus (Fig. 29). Plastids containing starch, and mitochondria with well-developed tubular cristae, and many small vacuoles show a predominant perinuclear and micropylar distribution (Figs. 41, 42). The chalazal tip of the developing zygote shows less cytoplasm and larger numbers of vacuoles than at the micropyle (Fig. 36). Lipid bodies show an increase in size and number and are distributed throughout. Dictyosomes, mostly at the micropyle end of the zygote, show little active vesicle production (Fig. 41). Short strands of endoplasmic reticulum throughout the zygote are associated with ribosomes and are shown lining the plasma membrane.

Later in development, the zygote shows the initiation of an ampuliform chalazal tip (Figs 28-31, 35). Figures 28-29 show the zygote initiating the ampuliform tip extending from the filiform apparatus to a large central cell vacuole at the chalazal tip. At this stage of zygote development ultrastructure is similar to the previous ovoid stage; however, as the zygote matures PAS-positive perinuclear starch grains shown earlier become reduced and are relocated towards the ampuliform chalazal tip (Fig 30).

The electron-transparent lateral cell wall of the zygote is thin at the chalazal pole and thick at the micropyle (Fig 36). The electron-opaque middle lamella shown in the centre of the lateral zygote cell wall has a granular appearance when stained with UA/PB. The ampuliform zygote cell stained positive in the micropyle and lateral cell walls with calcofluor

and PAS; however, a progressively weaker fluorescent reaction occured from the mid-chalazal region to the chalazal tip (Figs 30, 31).

4.3.4 Degenerate Synergid

After fertilization, the degenerate synergid stains orthochromatic with crystal violet and a size reduction occurs at the chalazal end of the cell (not shown). The degenerate synergid shows a strong affinity for aniline blue-black and a pale uniform staining reaction with the PAS (not shown). The integument cells which form the micropyle opening leading to the synergid cells remain intact after fertilization has occurred. The inner integument cells show a cytoplasm containing mitochondria, amyloplasts with starch grains, and endoplasmic reticulum adjacent the plasma membrane. The pollen tube passes through the micropylar opening first contacting the synergid filiform apparatus (Figs 6, 28). The thick walled pollen tube grows through the synergid filiform apparatus and always appears in the cytoplasm of the degenerating synergid cell (Figs 32, 33). The pollen tube shown in the degenerate synergid cytoplasm has a thinner cell wall than the pollen tube at the micropyle of the filiform apparatus (Figs 29, 36, 37). The cytoplasm of the pollen tube in the micropyle near the filiform apparatus contains some flocculent material continuous with the pollen tube cell wall (Fig. 32) and small spherical particles with electron-transparent borders surrounding a fine granular electron-opaque core (Fig 37). It is impossible to predict if organelles in the vicinity of the pollen tube originated from the pollen tube cytoplasm; however, organelles in the degenerate synergid resemble those in the persistent synergid cytoplasm. Not present in the persistent synergid, however, are the numerous spherical particles shown in the degenerate synergid. These spherical particles are similar in appearance to those

described earlier in the pollen tube cytoplasm (Fig 37). In the degenerate synergid a cone-shaped zone of spherical discharge particles extends to the chalazal end of the degenerate synergid cell (Fig 36).

Ultrastructurally, the degenerate synergid cytoplasm has a granular appearance; however, closer observations indicate a loss in organelle integrity. The starch containing plastids and several smaller sized mitochondria shows a non-continuous electron-opaque membrane (Figs. 36, 37). The degenerate synergid cell nucleus shows the loss of nuclear membrane and there is an absence of endoplasmic reticulum and dictyosomes. At 22 hours after fertilization the degenerate synergid shows no evidence of a plasma membrane (Figs 36, 37, 38).

The calcofluor-positive synergid filiform apparatus shows finger-like projections deep into the degenerate and persistent synergid cell cytoplasm. After fertilization, the synergid common cell wall and the degenerate synergid-zygote common cell wall thickens; however, the lateral cell wall of the degenerate synergid cell shows a less intense fluorescence than the lateral walls of the zygote cell which fluoresces brightly (Fig 31). The common cell wall between the central cell and synergid also thickens and shows a similar calcofluor-positive fluorescence.

4.3.5 Persistent Synergid

Following fertilization, the persistent synergid remains intact (Fig 36) and does not appear to undergo any volume changes. The persistent synergid stains similarly to the zygote cell with UA/Pb; however, it stains negatively with aniline blue-black and PAS stains. The calcofluor-positive synergid filiform apparatus extends deep inside the cytoplasm of both synergid cells and consists of an electron-opaque core and is surrounded by

an outer electron-transparent margin when stained with UA/Pb (Figs 32, 36). The persistent synergid contains few vacuoles with the largest located at the micropyle adjacent to the cell wall. The synergid contains mitochondria, dictyosomes and plastids containing no starch distributed throughout (Figs. 39, 40). The persistent synergid contains some dilated endoplasmic reticulum, and small electron-opaque vesicles absent from the degenerate synergid. The synergid also contains a few electron-opaque lipid bodies similar in size and number to those in the zygote cell (Fig 36).

The synergid cell is separated from the central cell by a thin irregular electron-transparent cell wall (Figs 36, 39). The lateral synergid cell wall extends chalazally from the micropyle terminating in the mid to upper chalazal region of the synergid cell. Since the chalazal end of the synergid cell lacks a cell wall, the cytoplasmic composition of the central and synergid cells in this region show similar mitochondrial, lipid, endoplasmic reticulum, and vacuole distribution. The central cell wall projections adjacent the persistent synergid cell at the micropyle are extensive and have a granular appearance similar to the filiform apparatus (Fig 39).

4.4 Advanced Zygote and Embryo Formation

4.4.1 Late Zygote Development

The ampuliform apex of the zygote is present 22 hours after anthesis (Figs 28, 29). Twenty six hours after initial ampuliform elongation is observed, the zygote cell begins to show a more extensive elongation of the chalazal portion of the zygote (Figs 30, 31, 35).

Forty eight hours after pollination, the elongated basal cell is 58 μm in length. The chalazal and middle regions are narrow (13 μm) in comparison to the micropylar end of the cell (22 μm) (Fig 45). Stained

with crystal violet, the ampuliform zygote cytoplasm reveals a peppered appearance, contains a few vacuoles at the micropyle end and also shows reduced chalazal PAS-positive starch grains (Figs 45, 46). The zygote cell wall stains PAS-positive with the most intense reaction at the micropyle end of the cell. Perinuclear PAS-positive starch spheres of the pre-ampuliform stage of development are not shown in the cytoplasm near the mid-micropylar located zygote nucleus.

Seventy two hours after pollination, the zygote is 235 μm in length (Figs 47, 49). The elongated zygote extends deep into the free nuclear endosperm. The longitudinal section throughout the zygote reveals a large portion of the darkly stained aniline blue-black positive zygote cytoplasm and nucleus located at the chalazal apex of the cell. The chalazal end of the remaining zygote cytoplasm extends to the micropyle along the lateral walls as a thin layer, staining lightly with aniline blue-black. Cytoplasmic strands extend across the large zygote cell vacuole (Fig 47). Except for the PAS-positive starch grains in the integument cells, very few starch grains are evident in the zygote cell. The chalazal tip of the zygote shows little vacuolation; however, a large vacuole appears to be forming adjacent to the narrowest portion of the nucleus (Fig 47).

The zygote cell wall does not stain as intensely as the walls ot the integument cells with calcofluor (Fig 48). The micropyle base of the zygote cell has a hazy appearance and the lateral walls show uniform fluorescence between both ends of the zygote. The cell wall becomes thin at the chalazal tip of the zygote and shows a pale fluorescent reaction with calcofluor. The central cell wall extending along the zygote lateral walls becomes wider and hazy at the micropyle next to the synergid cells.

4.4.2 Embryo Formation

The first zygote cell division occured 96 hours after anthesis. The resulting non-symmetrical division produced a two-celled proembryo (Figs 50-53, 57). The first cell division is transverse and occurs at the chalazal portion of the basal cell (*cb*), producing a small semi-circular apical cell (*ca*). From this point the *ca* cell will give rise to the future embryo proper and the *cb* cell will give rise to the suspensor unit.

The apical *ca* cell shows no vacuolation and has a very dark staining nucleolus within the nucleus and shows small orthochromatic perinuclear bodies when stained with crystal violet (Fig 50). The *cb* cell nucleus located in the chalazal region of the cell does not stain as intensely as the *ca* cell of figure 80, nor does it contain the dark staining perinuclear bodies in the cytoplasm. In contrast to the apical cell, the chalazal portion of the *cb* cell above the nucleus shows a few large vacuoles and the micropyle portion below the nucleus occupied by several large vacuoles (Fig 51). At this stage of development the *cb* cell accounts for most of the total two-celled embryo length.

The *cb* cell is surrounded on both lateral walls by the free nuclear endosperm. The micropyle portion of the basal cell shows lightly stained cytoplasm with crystal violet and is vacuolated (Figs 51, 52). Stained with calcofluor, the megagametophyte shows an abundance of fluorescent central cell wall projections at the micropyle adjacent the *cb* cell. The *cb* cell wall at the micropyle tip fluoresces intensely and shows cell wall projections distributed from the mid-micropyle to the micropyle tip of the *cb* cell (Fig 53).

4.4.3 Three-Celled Proembryo

The next cell division is transverse resulting in an unequal and differential division of the *cb* cell. The chalazal portion of the *cb* cell divides and produces the middle cell (*mC*). The reduced *cb* cell is now termed the *ci* cell. After the *mC* cell is produced, subsequent proembryo division does not occur at the expense of the *ci* cell (Figs 54, 58).

Ninety six hours after anthesis, the *mC* cell is 23 µm long and is the same width as the chalazal end of the *ci* cell (Figs 60, 61). The cytoplasm of the *mC* cell is slightly vacuolated at both ends of the cell. The centrally located nucleus of the *mC* cell shows dark staining perinuclear bodies in the cell cytoplasm (Fig 55).

The elongated *ci* cell is 361 µm long and has an enlarged base (Fig 60). The elongated *ci* cell contains large vacuoles which are transcended by a band of cytoplasm containing the mid-chalazal nucleus. The nucleus of figure 56 shows two densely stained nucleoli. Most of the *cb* cell cytoplasm is located adjacent the lateral walls in the *ci* cell. The thickness of the basal cell walls is uniform and wall projections are not shown at the chalazal end of the cell; however, the micropyle end of the cell shows distinct wall projections extending 40 µm from the micropyle tip (Fig 60). Stained with calcofluor, the walls at the enlarged micropyle end of the *ci* cell fluoresces more intensely than the lateral walls. Cell walls of the *mC* cell shows similar fluorescence when stained with calcofluor (Fig 64).

The nucleolus of the apical cell stains orthochromaticly with crystal violet. The cytoplasm contains few vacuoles and has densely stained bodies and plastids. The *ca* cell and the*mC* cell are similar in size, vacuolation and cytoplasmic distribution at this stage of development (Figs 54, 55, 60). There was no significant amounts of PAS-positive starch

in any of the cells of the developing proembryo 96 hours after pollination (Fig 59).

4.4.4 Four-Celled Proembryo

The first division of the apical cell occurs in a vertical plane, producing two sister cells of approximately the same size (Figs 62, 63). At this stage the bulbous apical cells have a width of 16 μm across the center of the cell and a height of 11 μm. The cytoplasm of the apical sister cells stain intensely with aniline blue-black (Fig. 65) and each has a centrally located nucleus, mitochondria (Fig 71) and dictyosomes. As the proembryo matures, the apical cells show a more globular appearance (Fig 71). Both *ca* apical sister cells are surrounded by cell walls that are electron-transparent. Bridged by plasmodesmata, the common *ca* cell wall is thinner than the lateral cell walls (Figs 62, 66, 71). Plasmodesmata are also shown in the horizontal wall separating the first suspensor cell (*mC*) and the apical sister cells (not shown) and the *mC* and basal *ci* suspensor cell (Fig 74).

When the proembryo has reached the two-celled apex stage of development, the *mC* has elongated 13 μm in comparison to a proembryo with the single *ca* apical cell. The *mC* cell has two large vacuoles on either side of a centrally located nucleus. The nucleus is surrounded by mitochondria and plastids (Figs 71, 72). Cytoplasmic composition adjacent the lateral *mC* cell wall includes ribosomes, endoplasmic reticulum, active dictyosomes producing vesicles and mitochondria. The common electron-transparent *mC* cell wall and central cell shows a dark staining middle lamella (Figs 72, 73).

After the two-celled apex has formed and prior to quadrant apex formation, the suspensor unit continues to divide producing 3 to 4 cells. The *mC* cell of the suspensor unit divides producing the *d* and *f* cells.

Figure 84 shows the cytoplasm of a suspensor cell *d* 84 hours after pollination. It has a centrally located nucleus surrounded by perinuclear horseshoe-shaped plastids with no distinct starch grains. The cytoplasm is peppered with ribosomes and shows mitochondria, active dictyosomes producing vesicles and short strands of endoplasmic reticulum distributed throughout the cell (Figs 83, 84, 85). The *d* suspensor cell walls have a densely stained middle lamella bordered by electron-transparent margins. Plasmodesmata are present in the walls between the apical sister cells and the *f* suspensor cell (Figs 83, 87). Some areas of the *d* cell shows paramural bodies projecting from the plasma membrane into the cell wall adjacent the free nuclear endosperm (Figs 86, 89).

The *f* suspensor cell in cross-section has a circular appearance with cytoplasmic strands extending through a large central vacuole. The dark staining cytoplasm reveals a dense community of organelles such as mitochondria, active dictyosomes, plastids with no starch and dense staining ribosomes (Figs 88, 90, 91, 93, 96). The electron-transparent cell wall around the circumference of the *f* cell shows uniform thickness. The active dictyosomes distributed throughout the thin layer of *f* cell cytoplasm shows maturing vesicles migrating towards the tonoplast (Fig. 98) and the plasma membrane of the cell (Figs. 90, 92). Electron micrographs showing plasmodesmata through the common cell wall of the *f* and *ci* suspensor cells are shown (Fig 97).

Located in the mid-chalazal region of the *ci* cell, the centrally located nucleus is surrounded by perinuclear plastids devoid of starch and

mitochondria with few tubular cristae (Fig 75). Active dictyosomes near the *ci* cell wall are composed of 3 to 4 individual golgi cisternae with semi-transparent vesicles being released from the maturing face. Mitochondria and a few strands of rough endoplasmic reticulum are shown adjacent the plasma membrane in the *ci* cell (Figs 75, 76, 77, 80-82). The highly vacuolated *ci* cell cytoplasm stained lightly with aniline blue-black (Fig 65) and is less electron opaque compared to the cytoplasm of the other suspensor cells and the central cell. In cross-section the common *ci* and central cell wall shows an electron-dense matrix near the undulating plasma membrane and electron-transparent margins (Fig 81).

When the four-celled proembryo was stained with calcofluor and viewed under UV light, the most intense fluorescence occured at the enlarged micropyle end of the *ci* cell. The intensity of fluoresence in the outer longitudinal walls of the *ci*, *mC* and *ca* cells is similar; however, the inner horizontal *mC* cell walls and the longitudinal wall between the apical sister cells shows a reduced fluorescence (Fig 66).

4.4.5 Quadrant Formation

Once the apical sister cells have an enlarged bulbous appearance, both cells will subsequently divide in a vertical direction producing the quadrant apex (Figs 69, 70). The globular apex cells which form the embryo proper, show little vacuolation; however, the suspensor unit which includes the *h*, *k* and *f* cells show a higher degree of vacuolation and cytoplasmic bands (Fig 70). When stained with calcofluor 120 hours after pollination, the fluorescent cell walls of the quadrant embryo proper are similar in thickness. The cell wall between the apical cells and the hypophysis initial (*h*) stains more intensely with crystal violet than the cell walls of the apical cells (not shown).

Division of both apical sister cells in the quadrant apex is not always synchronized. The unsynchronized division often results in the production of a three-celled apex which eventually becomes four-celled (Figs 68, 69). It is impossible; however, to detect if the unsynchronized division is caused by the accelerated division of a single apical cell or the retardation of an apical cell since no precise information can be shown from a static investigation.

The *ci* cell of the suspensor cell shows extensive vacuolation with most of the lightly stained cytoplasm lining the cell walls (Figs 96, 101). The nucleus is shown in the mid-chalazal portion of the *ci* cell and contains a dark staining nucleolus (Fig 99). Wall projections are shown concentrated in the micropyle tip of the *ci* cell (Figs 81, 82).

As the quadrant apex matures, the outer apical cell walls increase in size; however, the cell walls of the apical cell central axis shows less wall development (Figs 68, 69). Outer cell wall growth causes the apex to adopt a globular appearance. This causes the *h* suspensor cell adjacent the embryo proper to invaginate the globular apex of the quadrant embryo proper.

At this stage of development the suspensor unit usually consists of three to four cells; however, the suspensor may have reached this number of cells prior to the quadrant initiation.

4.4.6 Synergids, Central Cell and Integuments during Proembryo Development

When ampuliform zygote elongation occurs, both synergids show degenerative symptoms (Figs 28, 29). A longitudinal section through the micropyle of the megagametophyte 72 h after pollination shows an elongated *cb* cell and two densely stained synergid cells (Fig 47). In seeds

older than 96h after anthesis no evidence of the dark staining cytoplasm region is shown; however, the micropyle calcofluor-positive synergid cell filiform apparatus remains evident even in older seeds. The enlarged *cb* cell appears to have crushed the chalazal end of the synergid cells leaving the more resilient synergid filiform apparatus (Fig 60).

During zygote development, free nuclear endosperm nuclei continue dividing and are distributed throughout the enlarging megagametophyte central cell. The free nuclear endosperm nuclei are distributed adjacent the elongating proembryo (Figs 62, 63, 95), in the thin parietal cytoplasm adjacent the lateral central cell wall (Fig. 57) and in the extreme chalaza of the central cell adjacent the nucellar proliferation tissue (Fig. 67). In the globular stages of formation, the elongating proembryo is thrusted into the central cell cytoplasm. Near the globular tip of the proembryo, the central cell is largely vacuolated providing a space for the elongating embryo. Ultrastructurally, the central cell cytoplasm shows both amyloplasts with few thylakoids and chloroplasts which have well-developed thylakoids and a dark staining stroma (Figs 78, 79, 86, 89). The cytoplasm is peppered with ribosomes and shows short strands of rough endoplasmic reticulum and dilated endoplasmic reticulum throughout. Mitochondria are shown throughout; however, increased numbers are shown adjacent the free nuclear endosperm nuclei (Fig 95) and adjacent to the central cell wall projections (Figs 36, 38, 39, 94). Vesicles adjacent central cell wall projections are similar to those actively produced by dictyosomes (Figs 43, 44). A plasma membrane follows the contours of the thick electron-transparent cental cell wall.

Adjacent to the central cell wall a dark electron-opaque layer suspected to be cuticular in nature surrounds the megagametophyte in a

semi-continuous fashion (Fig 100). The cell walls of the inner integument are shown adjacent the dark cuticular layer with a thick layer of cell wall material suspected to be crushed inner integument cells (Figs 101, 105).

The inner integument cell walls are similar to those described in early stages of development. Sectioned in the proper plane, microtubules are present adjacent to the cell wall. Plasmadesmata are also present. (Fig 104). The inner integument shows a distinct reduction in starch grains, relative to the pre-fertilization development of the ovule. Ultrastructurally, the integument cells are peppered with ribosomes, plastids with starch and thylakoids, mitochondria with well-developed tubular cristae, small lipid bodies and dictyosomes producing vesicles (Figs 101, 102, 103). Starch grains and the cell walls of the inner integument cells react positively with PA-TCH-SP (Figs 108, 109). The cytoplasm of integument cells shows short strands of rough endoplasmic reticulum; however, the inner integument cell layer adjacent the megagametophyte shows dilated endoplasmic reticulum containing electron-opaque inclusions in a "honey comb" orientation when cut in cross-section (Figs 105, 106). When sectioned longitudinally, the dilated endoplasmic reticulum shows the same outer membrane with ribosomes adhered to it; however, the small electron-opaque spheres appear as striated inclusions (Figs 105, 107).

4.5 Aberrant Ovules

4.5.1 Underdeveloped Ovule

Occasionally a poorly developed or abortive ovule was sectioned during the course of this study. A poorly developed ovule is easily recognized when the megagametophyte is sectioned longitudinally. The egg apparatus of such an ovule has intact synergid cells (Fig. 110) and

filiform apparatus (Fig 112). The chalazal portion of the megagametophyte contains vacuolated nucellar cells (Fig 110). The megagametophyte is surrounded by an under-developed inner integument cell layer made up of 1 to 2 cell layers. The outer integument appears to have developed normally (Fig 110). Because the inner integument does not cover the micropyle portion of the megagametophyte, this allows the synergid cells to protrude into the micropyle opening. Both the inner and outer integument cell layers show typical starch distribution at the micropyle 22 hours after anthesis (Fig 111). Because the poorly developed inner integument cell layer of the ovule is reduced, the underdeveloped ovule is smaller in size relative to the normally developed ovule of the same age. In young underdeveloped ovules, the synergid cells appear healthy; however, the fate of the synergid cells is unknown since no underdeveloped ovules older than 22 hours after anthesis have been observed.

4.5.2 Ovules Without Megagametophytes

The second type of aberrant ovule showed a lack of megagametophyte development. The aberrant ovule, collected 10.5 hours after anthesis, shows similar external morphology as a normally developed ovule, making it more difficult to detect (Fig. 113). Sectioned longitudinally, the ovule appears to show normal integument development. Starch accumulation and distribution in the integument cells is similar to normal ovules of the same age. In the aberrant ovule a functional megagametophyte is absent. The region normally occupied by megagametophyte is composed of micropylar nucellus typically lined by a single layer of nucellar epidermis. A similar aberrant ovule, collected 96 hours after anthesis is shown in figure 114. The integument layers in this

ovule show normal development and enlargement and are similar to those in a fertile post-anthesis ovule (Fig. 59). However, starch distributions are altered. The reduction of starch in the micropylar integuments is similar to that of viable seeds at the same time after pollination; however, the large starch accumulation normally shown in the inner integument basal body portion of the ovule is not evident.

Figure Descriptions

Figure 1 Epifluorescence light micrograph of the stigmatic surface 5 hours after pollination. The fresh tissue was strained with aniline blue and viewed using blue light resulting in green autofluorescence from the stigmatic tissues and bright yellow fluorescence from the pollen tubes (arrows). Pollen resting on the stigmatic surface produces a pollen tube which grows between the cells of the pistil. Aniline blue Scale bar = 24.40 μm

Figure 2 Epifluorescence light micrograph of ovules (Ov) attached to the replum (Re) of an ovary 15 hours after pollination. The fresh tissue was stained with aniline blue and viewed using blue light. The pollen tubes (Pt) show callose walls and cell plugs (arrow heads) which fluoresce yellow in contrast with the red autofluorescent chlorophyll. Mature ovules are distributed parallel to the longitudinal axis of the ovary. The pollen tube grows along the replum surface and contacts the ovule near the funiculus. Aniline blue. Scale bar = 150.00 μm

Figure 3 Light macrograph showing the morphology of the flower of *Brassica napus* over time. Flower A represents pistil length at time 0 (anthesis) at 8 mm. Flowers B to E represent the development over time periods 24, 48, 72 and 96 hours respectively (postanthesis) with a maximum pistil length of 22 mm at 96 hours. Ruler = mm

Figure 4 Diagram showing the longitudinal overview of an ovule at anthesis. The egg apparatus consists of two synergids (S), each with a filiform apparatus (Fa), and the egg (E). The central portion of the megagametophyte is occupied by the central cell which includes two polar nuclei (pN). At the chalazal pole of the megagametophyte, the three antipodals (a), nucellus (NU) and nucellar proliferation tissue (nP) are shown. Vascular tissue (arrow heads) in the raphe (Ra) portion of the ovule terminates at the chalazal pole of the nucellus. The megagametophyte is enclosed by the inner integument (II) and outer integument (OI). Scale bar = 100 μm

Figure 5 Light micrograph showing an ovule 10.5 hours after pollination. The central cell (cc) in the megagametophyte is vacuolated. The inner (II) and outer (OI) integuments at the micropyle (mi) has accumulations of intensely magenta stained insoluble starch (arrows). At this stage a small amount of starch grains are located in the inner integument basal body (Bb). The area with the least amount of starch is the chalazal (Ch) pole of the ovule. PAS. Scale bar = 39.34 μm.

4

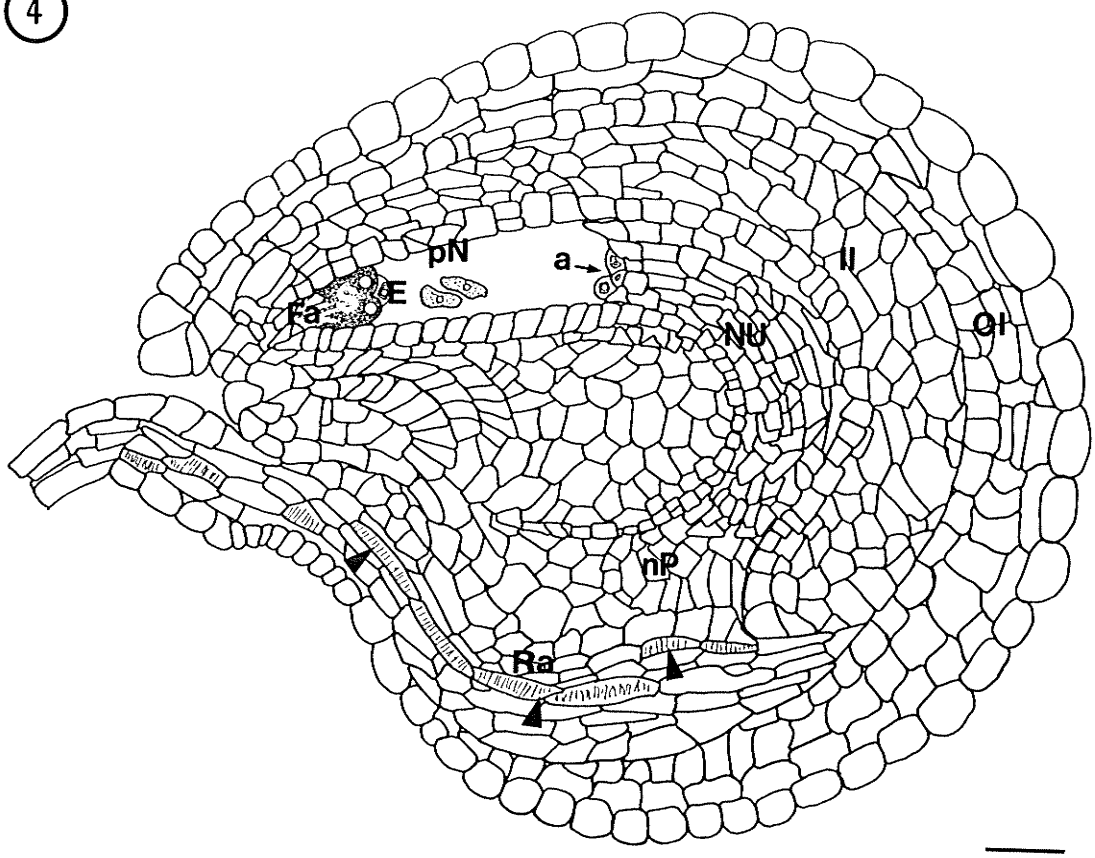

5

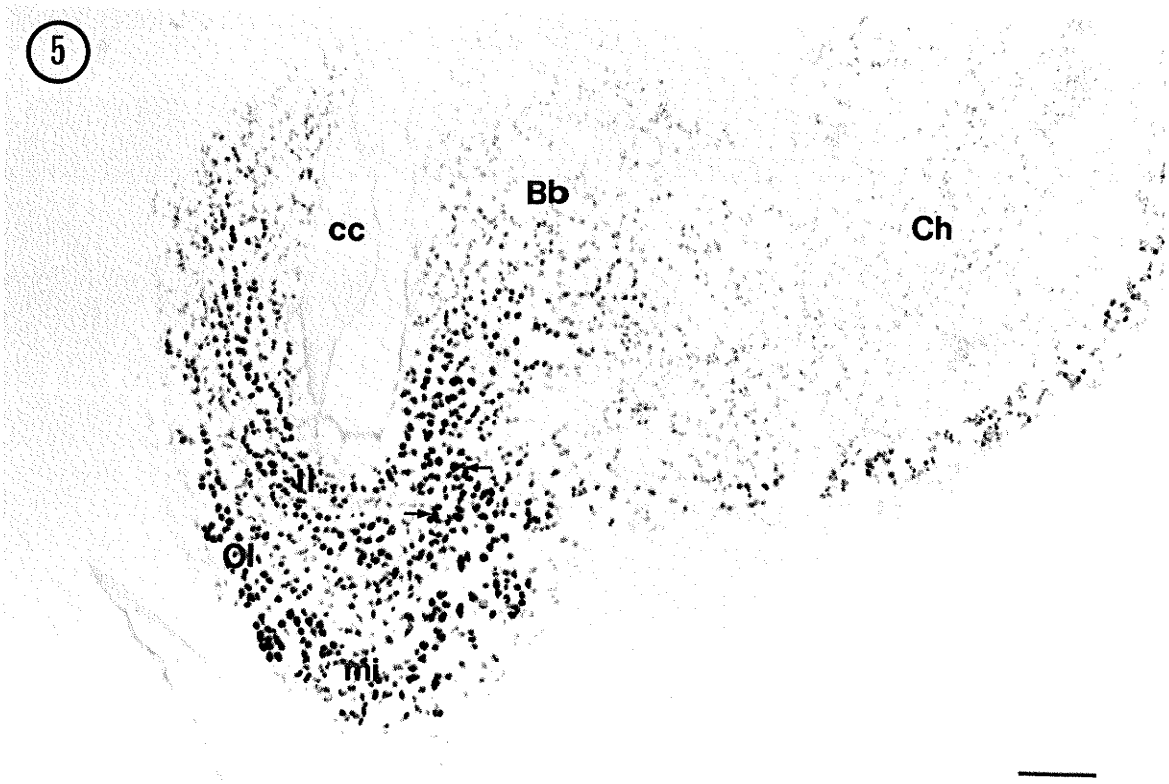

Figure 6 Light micrograph of the micropyle region of a seed 48 hours after pollination. A pollen tube (Pt) entered the ovule at the micropyle near the synergid filiform apparatus (Fa). Crystal violet. Scale bar = 12.68 μm.

Figure 7 Epifluorescence light micrograph of the micropyle region 15 hours after pollination. The cross section was stained with calcofluor and viewed under UV light. The inner integument (II) and outer integument (OI) cell wall fluoresce bright blue as do the thick pollen tube cell wall (Pt) located between the integument cells in the micropyle. Calcofluor. Scale bar = 11.61 μm.

Figure 8 Epifluorescence light micrograph showing an ovule 24 hours after anthesis. The fresh section was stained with aniline blue and observed under UV light. The ovule is attached to the replum (Re) by the funiculus (Fu) which shows xylem (X) tracheary elements and phloem sieve tubes (Ph) with brightly fluorescing disc-like sieve plates (arrows). The micropyle (mi) region shows no significant staining, but the chalazal proliferation tissue (nP) stains aniline blue positive. Aniline blue. Scale bar = 88.50 μm.

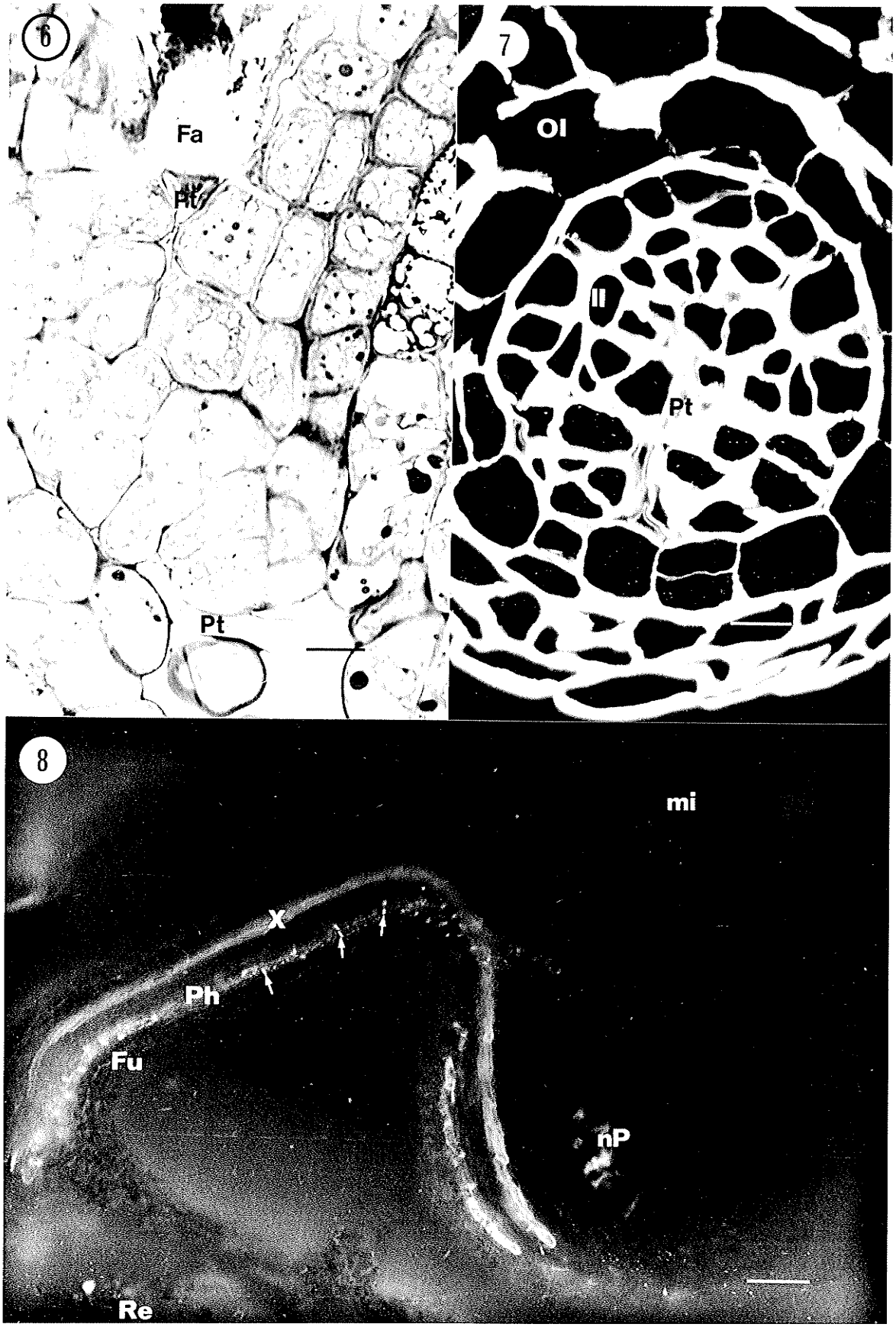
6
Fa
Pt
Pt
7
Ol
II
Pt
8
mi
X
Ph
Fu
nP
Re

Figure 9 Epifluorescence light micrograph of xylem (X) tissue in the developing ovule. The section was stained with calcofluor and viewed under UV light. Xylem tracheary elements show secondary wall helical thickenings (arrows) which fluoresce light blue. Calcofluor. Scale bar = 11.61 μm.

Figure 10 Epifluorescence light micrograph of an ovule 18 hours after anthesis. The fresh section was stained with aniline blue and viewed under UV light. A vascular bundle from the funiculus (Fu) branches and forms net-like distribution of vascular tissue at the chalazal pole of the ovule. Sieve tubes, with fluorescent sieve plates (arrows), occupy the lateral aspects ovule chalaza while the autofluorescent xylem tracheary elements (X) are in a more central position. Aniline blue. Scale bar = 88.50 μm.

Figure 11 Light micrograph of an oblique section through the chalaza of an ovule showing the distribution of vascular tissues. The main vascular bundle is in the raphe (Ra). Xylem tracheary element (X) occupy the central chalazal region while the phloem sieve tube members (arrows) with densely staining companion cells are distributed in a circular pattern along the lateral chalazal regions of the ovule. Crystal violet. Scale bar = 41.15 μm.


9
X
X


10
FU
X

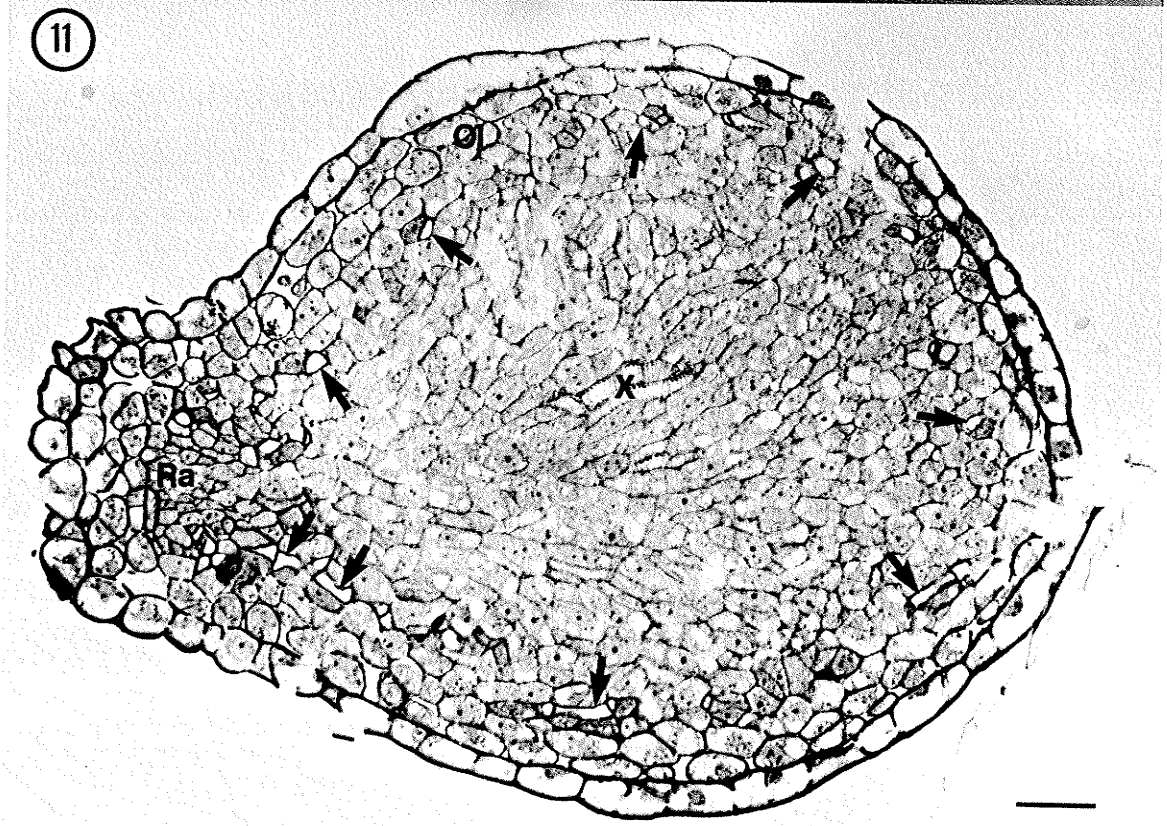
11
Ra
X

Figure 12 Electron micrograph of a cross section of phloem from the chalaza of an ovule showing sieve tube member (stm) and two companion cells (CpC). UA/Pb. Scale bar = 1.1 μm.

Figure 13 Diagrammatic interpretation of the developing ovule and early seed in cruciferae (*Lunaria annua*) according to Corner (1976). From these diagrams the vasculature (hatched lines) is described as a main vascular bundle with only slight branching in older stages of development. A,B x 25; C x 8.

12

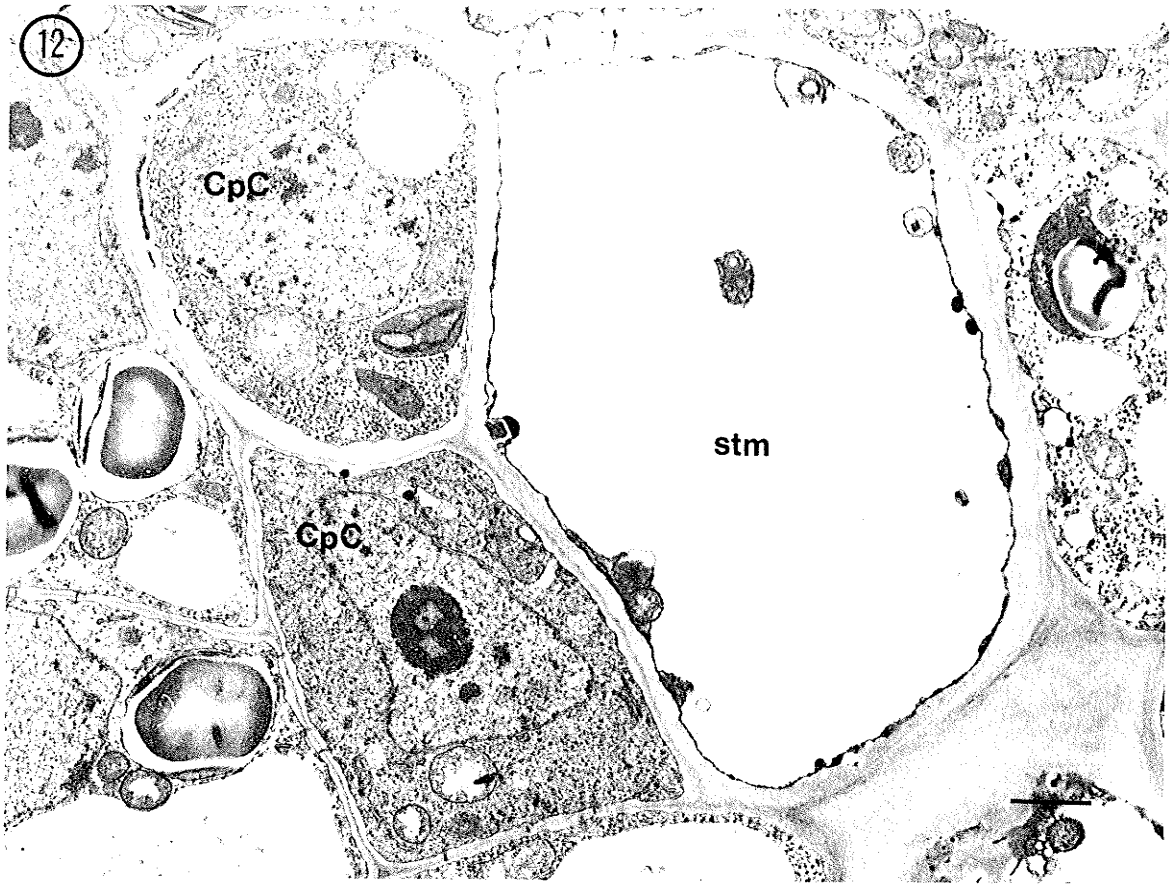

13

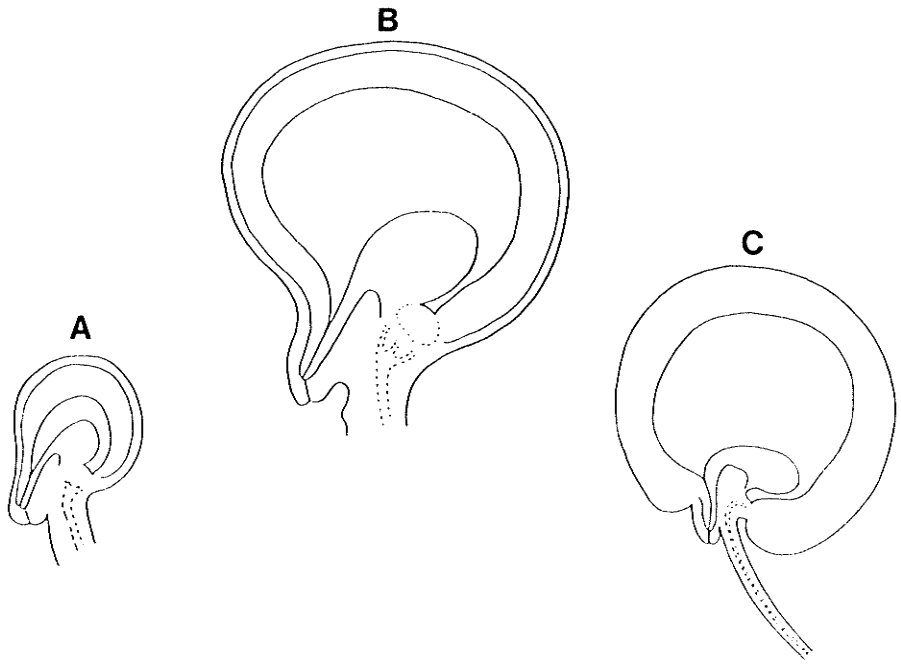

Figure 14 Diagrammatic representation showing longitudinal and cross sections at various planes (*a-f*) in the early developing ovule of *Brassica napus*. The hatched lines represent vascular tissues. The diagram also shows the inner integument (II), outer integument (OI) and megagametophyte (MG). x 77

14

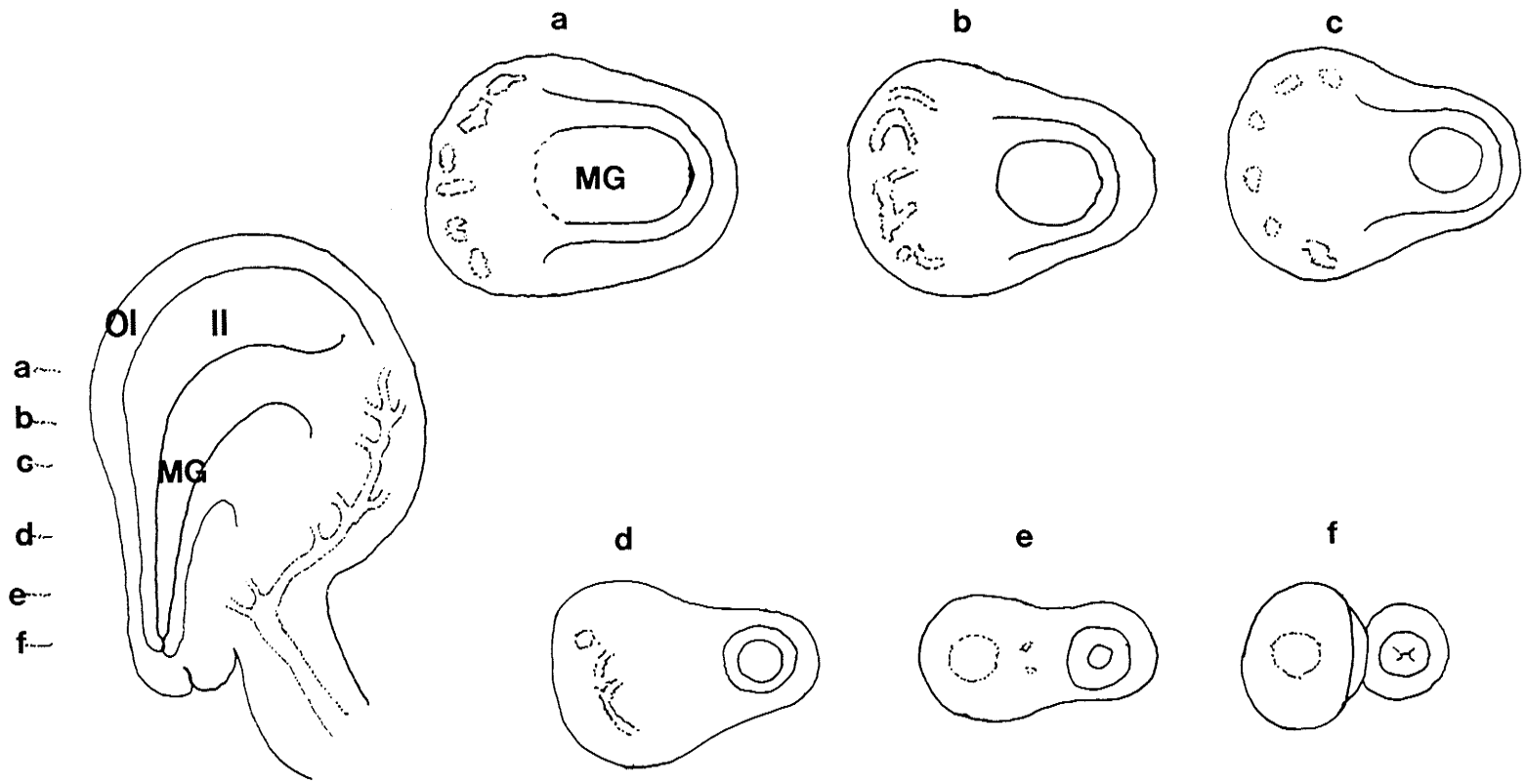

Figure 15-20 Two closely adjacent sections of the same unfertilized megagametophyte 10.5 hours post-anthesis. Figure 15 and 18 were prepared for brightfield microscopy. Figure 16 and 19 were prepared for fluorescence microscopy. Figure 17 and 20 are diagrammatic representations of figure 15 and 18.

Figure 15 Light micrograph of the micropyle region of a megagametophyte. The megagametophyte consists of two connected polar nuclei (pN) in a semi-vacuolated central cell (cc) cytoplasm, a vacuolated (v) egg cell (E), and two intact synergid cells (S) each with a filiform appararatus (Fa). One synergid cell is more densely stained than the other. Other megagametophyte walls are very thin (large arrows) but the longitudinal central cell wall projections have a hazy appearance at the micropyle pole adjacent to the synergid cells (arrow head). The egg and central cell show plastids and starch grains which stain PAS positive (arrows). The inner integument cells (II) adjacent the megagametophyte show increased starch grains (St). Crystal violet /PAS. Scale bar = 23.23 µm.

Figure 16 Epifluorescence light micrograph of figure 15 stained with calcofluor and viewed under UV light. The micropyle lateral wall (arrows) of the egg cell (E), the filiform apparatus (Fa) and inner integument (II) cell show bright fluorescence. Between the first and second inner integument layers adjacent to the megagametophyte, plasmadesmata (Pd) are present; however, plasmodesmata are not visible between the inner integument and central cell (cc). Calcofluor. Scale bar = 23.23 µm.

Figure 17 Diagrammatic representation of figure 15. The megagametophyte consists of two connected polar nuclei (pN) in a semi-vacuolated central cell (cc) cytoplasm, a vacuolated egg cell (E), and two intact synergid cells (S) each with a filiform appararatus (Fa). Scale bar = 23.23 µm.

Figure 18 Light micrograph showing the micropyle region of a developing megagametophyte. The longitudinal section reveals the partially fused polar nuclei (pN) in the semi-vacuolated central cell (cc) cytoplasm. The egg cell (E) has a nucleus and a thin PAS positive apical cell wall. The egg extends from the central cell polar nuclei and is tapered towards the synergid (S) filiform apparatus (Fa). Note the abundance of PAS positive starch grains (St) in the integument cells at the micropyle. Crystal violet/PAS. Scale bar = 23.23 μm.

Figure 19 Epifluorescence micrograph of figure 18 stained with calcofluor and viewed under UV light. The common lateral wall (large arrows) of the synergid (S) cell and the egg cell (E) is shown. The chalazally located egg cell wall shows no fluorescence. The lateral central cell (cc) wall projections (arrow heads) extending from the megagametophyte wall are shown near the egg and synergid cell. Calcofluor. Scale bar = 23.23 μm.

Figure 20 Diagrammatic representation of figure 18. The longitudinal section reveals the partially fused polar nuclei (pN) in the semi-vacuolated central cell (cc) cytoplasm. The egg cell (E) extends from the central cell polar nuclei and is tapered towards the synergid (S) filiform apparatus (Fa). Scale bar = 23.23μm.

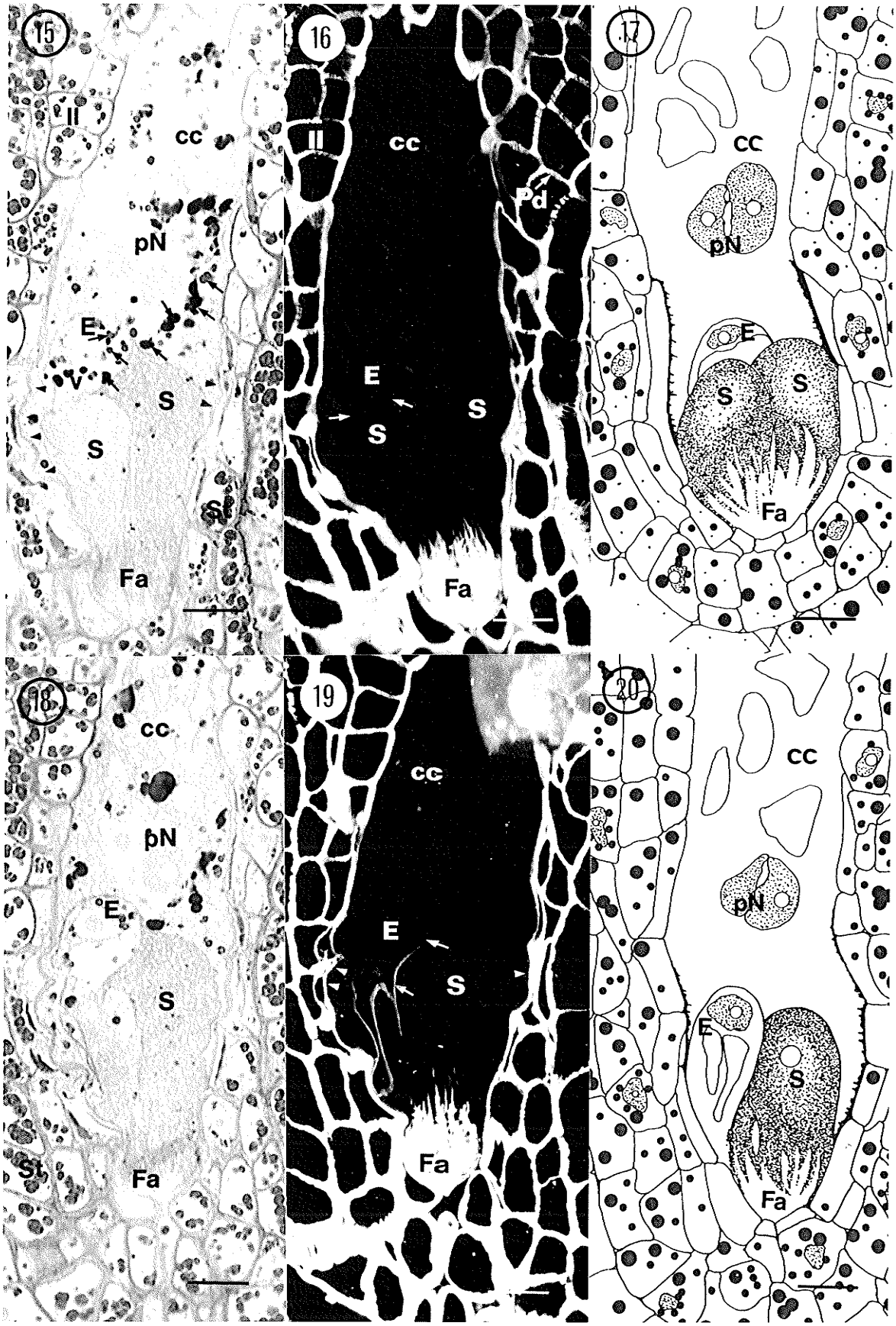
15
II
cc
pN
E
V
S
S
St
Fa
16
II
cc
Pd
E
S
S
Fa
17
cc
pN
E
S
S
Fa
18
cc
pN
E
S
St
Fa
19
cc
E
S
Fa
20
cc
pN
E
S
Fa

Figure 21 Electron micrograph of a region of the central cell in the micropyle adjacent the mature egg apparatus. The central cell (cc) cytoplasm is maintained by a plasma membrane (arrows) which contacts the convoluted central cell wall projections (Wp). The central cell wall is located next to a thick electron-transparent layer of crushed inner integument cells (cII). Note the mitochondria (m) with tubular cristae (arrow heads) located near the wall projections. UA/Pb. Scale bar = 0.39 μm.

Figure 22 Electron micrograph showing a cross-section through the mid-region of a mature egg apparatus at anthesis. The electron transparent-central cell (cc) wall projections (Wp) occur at the micropyle and extend deep into the central cell cytoplasm. The central cell shows small vacuoles (v) and numerous mitochondria (m) and has dilated endoplasmic reticulum (DER) next to the wall projections. The egg cell shows a few mitochondria and endoplasmic reticulum (ER). The synergid (S) cell has numerous small sized mitochondria (m) and several active dictyosomes (D) producing vesicles (Vs). The synergid also shows endoplasmic reticulum throughout the cell. The common cell walls between the central cell, egg and synergid are similar in appearance. The thin cell walls (large arrows, show dilated regions which are electron-transparent with the exception of the egg cell whereby the dilated region contain electron opaque deposits (arrow heads). UA/Pb. Scale bar = 0.63 μm.

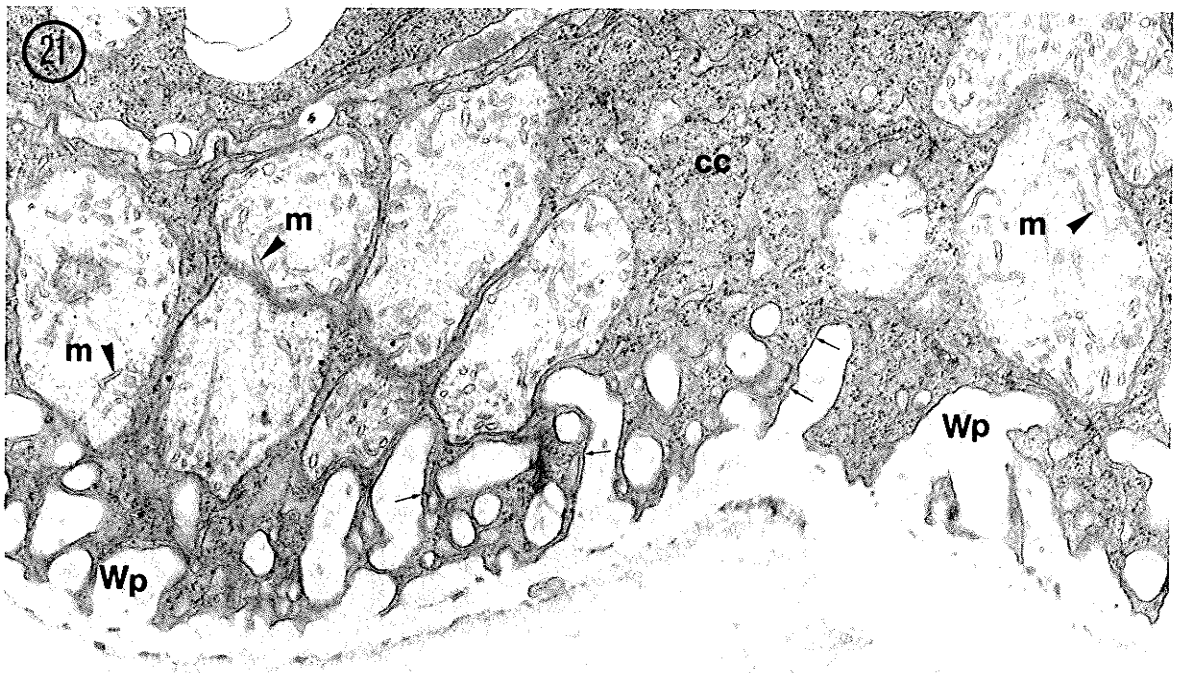
21
cc
m
m
m
Wp
Wp

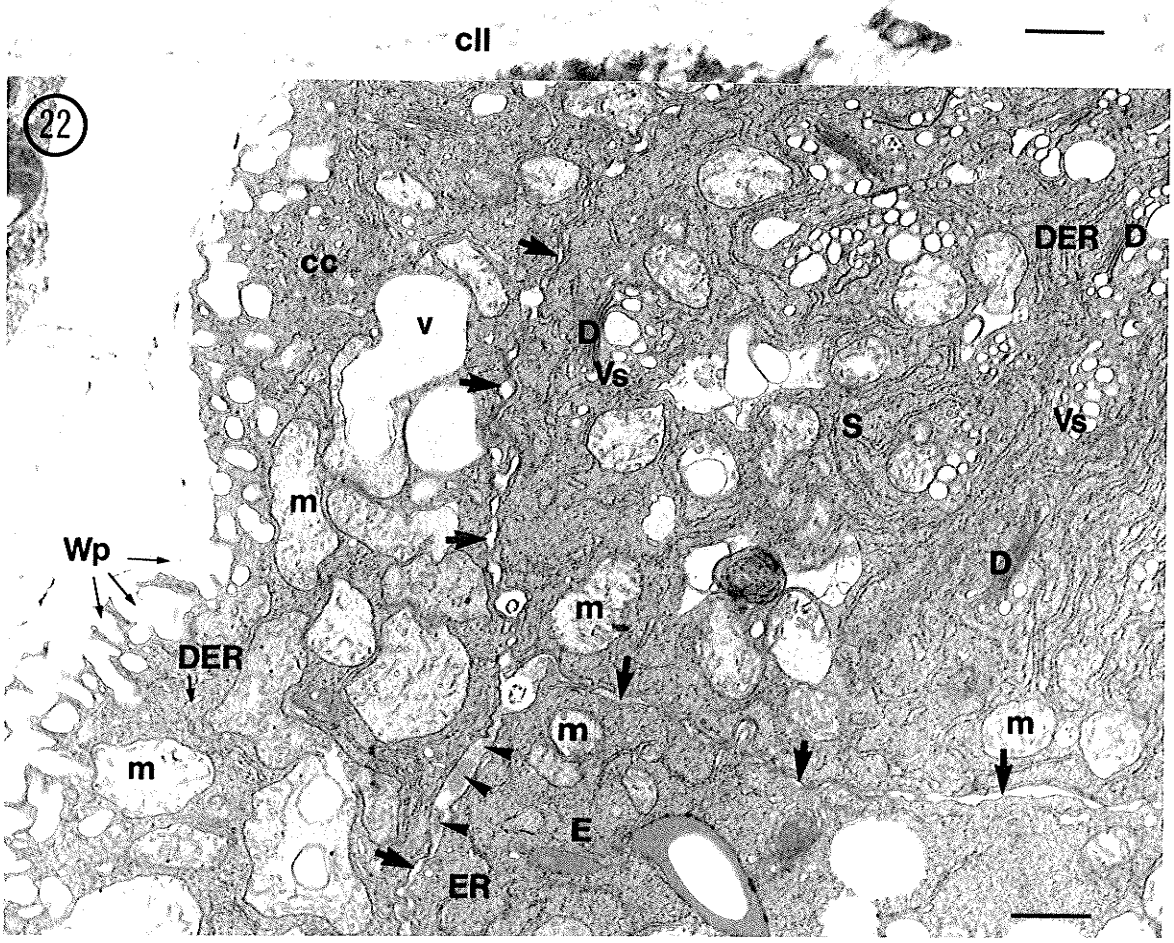
cII
22
cc
v
D
Vs
DER
D
S
Vs
m
Wp
D
m
DER
m
m
m
E
ER

Figure 23 Electron micrograph showing the mid-region of the developing synergid (S) cell at anthesis. The synergid shows mitochondria (m), transition vesicles (Tv) and dictyosome (D) producing vesicles (Vs) of various sizes at the maturing face of the cisternae. The synergid contains dialated endoplasmic reticulum (DER) with some strands (arrow heads) pressed along the thin electron-transparent synergid central cell (cc) common cell wall (large arrows). The thin central cell cytoplasm is invaginated by central cell wall projections (Wp). UA/Pb. Scale bar = 0.63 μm.

Figure 24 Electron micrograph showing the mid-region of the developing synergid cell at anthesis. The centrally located nucleus (N) is surrounded by a nuclear membrane (arrows) which has several nuclear pores (arrow heads). The synergid cell cytoplasm contains cisternae of rough endoplasmic reticulum which periodically becomes dilated (DER) and shown adjacent a nuclear pore (open arrow). Mitochondria (m) with tubular cristae and dictyosomes (D) are also located near the synergid nucleus. UA/Pb. Scale bar = 0.40 μm.

Figure 25 Electron micrograph showing the micropylar region of the synergid (S) and egg (E) cells at anthesis. The electron-transparent common cell wall (cw) between the synergid and egg cell shows electron dense plasmodesmata (Pd). The egg cell contains mitochondria (m) with tubular cristae, rough endoplasmic reticulum (RER) and inactive dictyosomes (D) with few vesicles (arrow heads). The synergid shows mitochondria with tubular cristae and a similar amount of granular free ribosomes to the egg; however, the synergid contains more rough endoplasmic reticulum and dictyosomes with vesicles (Vs). Plastid (Pl). UA/Pb. Scale bar = 0.40 μm.

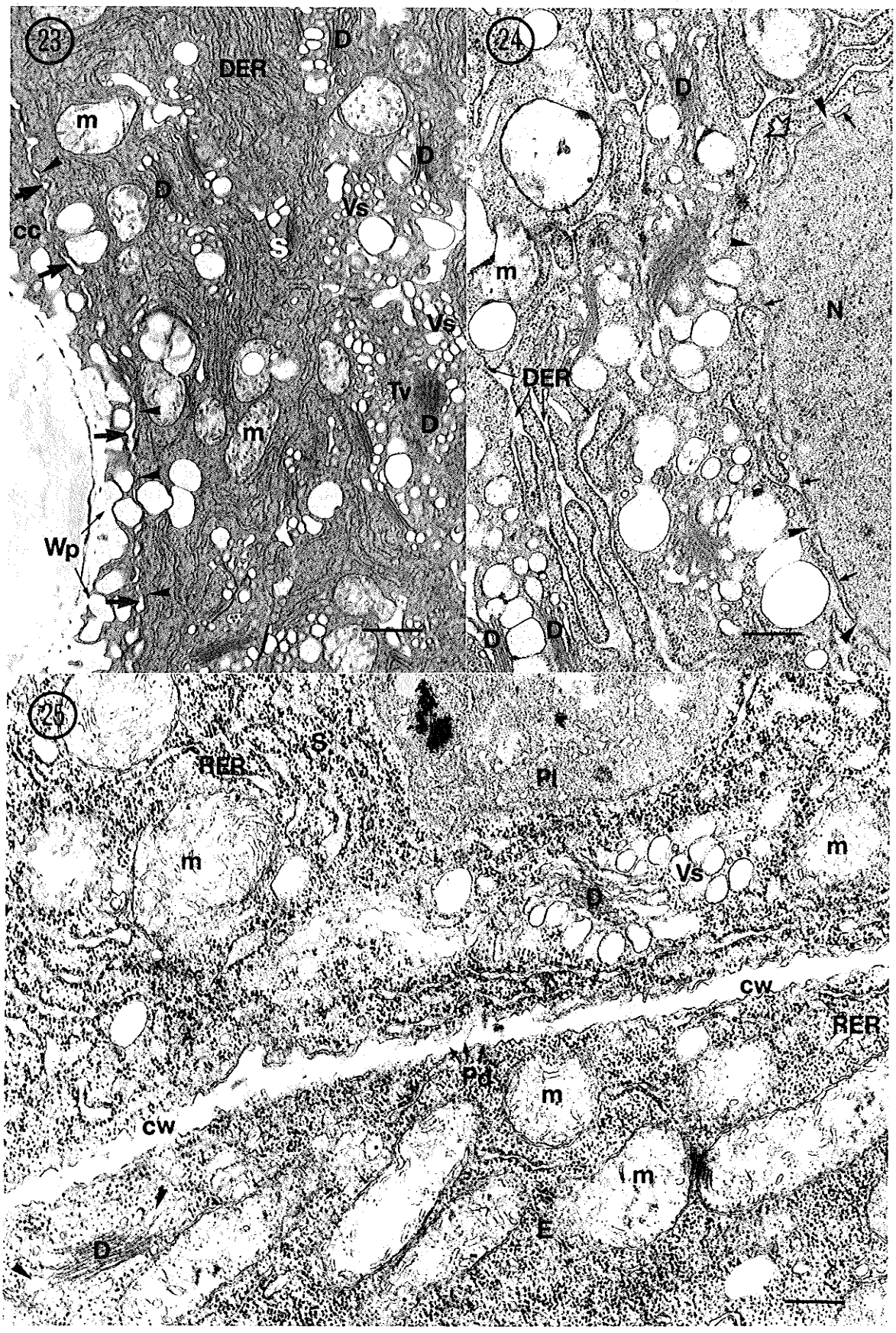
23
DER
D
m
D
D
cc
Vs
S
Vs
Tv
D
m
Wp
24
D
m
N
DER
D
D
25
RER
S
m
Pl
m
Vs
D
cw
RER
Pd
m
cw
m
E
D

Figure 26 Electron micrograph showing a cross section through the mid-region of the mature egg cell after anthesis. The common wall between the egg (E) and the central cell (cc),has intermittent inclusions of electron opaque material (open arrows). Wall projections (Wp) are present on the outside central cell wall. Note starch (St) containing plastid (Pl), mitochondria (m), endoplasmic reticulum (arrow heads) and a central vacuole (v) in the egg cell. UA/Pb. Scale bar = 0.63 μm.

Figure 27 Electron micrograph of a longitudinal section through a mature egg cell. The cell wall (cw) consists of an electron-transparent layer "sandwiched" between the central cell (cc) and egg cell (E) plasma membranes (arrows). Expanded areas of the egg cell wall shows intermittent electron-opaque inclusions (open arrows). The nuclear membrane (arrow heads) circumscribes the chalazally located nucleus (N) which shows a prominent nucleolus (Nu). The egg central cell (cc) cytoplasm consists of perinuclear mitochondria (m), dictyosomes (D) and plastids (Pl) with electron-transparent starch (St). UA/Pb. Scale bar = 0.63 μm.

Figure 28-29 Light micrographs of the developing zygote 22 hours after pollination . Figures 28 and 29 are adjacent sections prepared to view using bright field microscopy.

Figure 28 Light micrograph of a developing zygote (Z) and degenerating synergids (S). The central cell (cc) which surrounds most of the zygote, has a large vacuole (v) near the chalazal tip of the zygote cell. The zygote cell contains a centrally located nucleus (N). Initiation of an ampuliform chalazal tip has begun. The lightly stained filiform apparatus (Fa) extends deep inside the synergid cytoplasm. A portion of the pollen tube (Pt) near the base is visible. Crystal violet. Scale bar = 11.61 μm.

Figure 29 Light micrograph of a developing zygote , and central cell (cc) vacuole (v) at the micropyle. A prominent vacuole (v), adjacent to the zygote, is apparent in the micropylar region of the central cell (cc). A thick walled portion of the pollen tube (Pt) is seen at the base of the synergid filiform apparatus (Fa). The portion of the pollen tube in the degenerate synergid (S) is thin-walled (white arrow). Crystal violet. Scale bar = 11.61 µm.

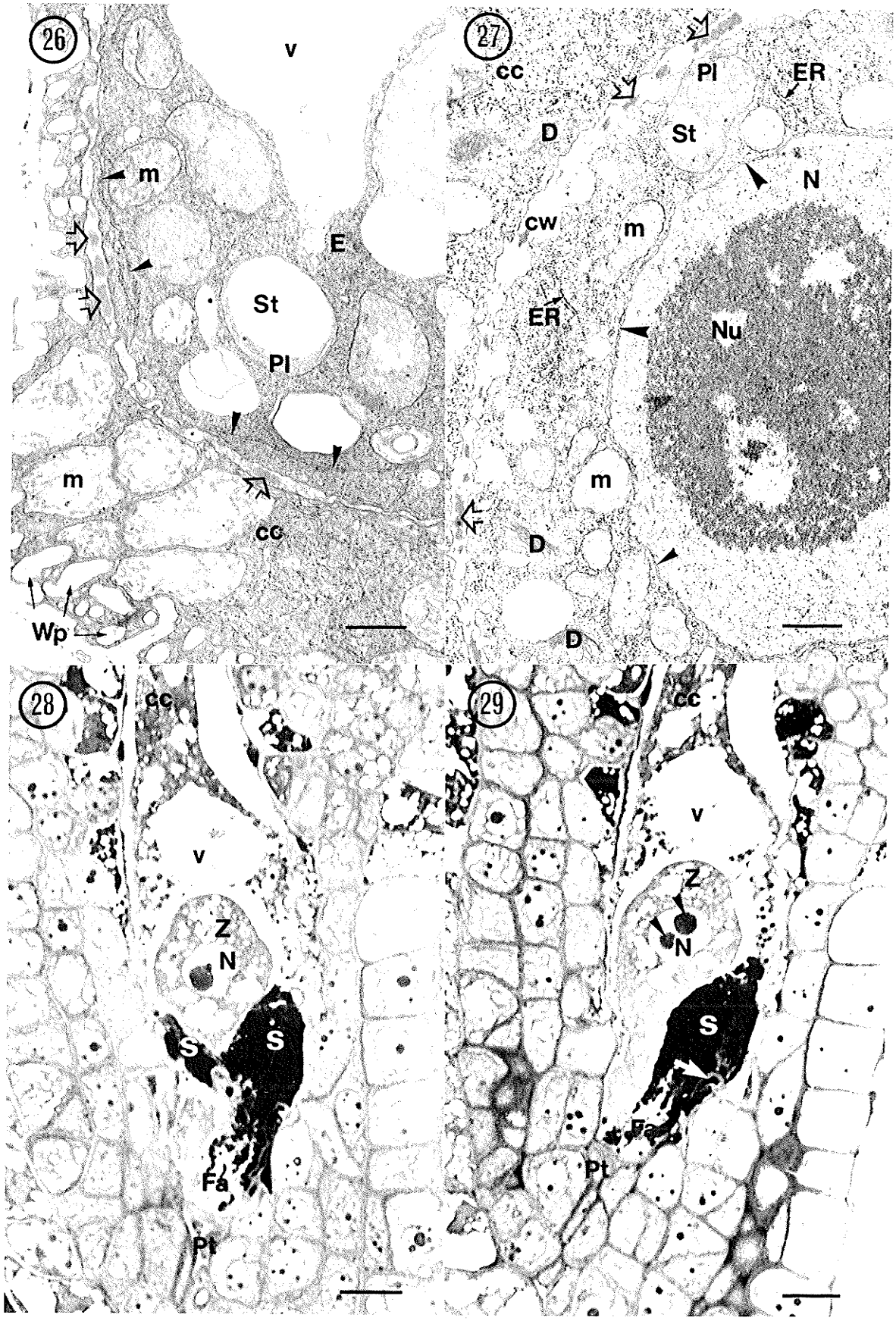
26
v
m
E
St
Pl
m
cc
Wp
27
cc
Pl
ER
D
St
N
cw
m
ER
Nu
m
D
D
28
cc
v
Z
N
S
S
Fa
Pt
29
cc
v
Z
N
S
Fa
Pt

Figure 30-31 Light micrographs of a developing zygote 22 hours after pollination. Figure 30 was prepared to view using brightfield microscopy. Figure 31 was prepared for fluorescence microscopy.

Figure 30 Light micrograph of a zygote (Z), degenerate synergid (S), and central cell (cc). The central cell (cc) has an endosperm nucleus (EN) near the zygote, a small amount of PAS-positive starch grains (arrowheads) and several small vacuoles (v) next to the chalazal tip. The enlarged zygote shows a pronounced ampuliform tip (arrows). The centrally located nucleus (N) shows perinuclear PAS-positive starch (arrows heads). The outer boundary of the megagametophyte is surrounded by the integument cell (II) layer which contain PAS-positive starch grains (arrowheads). Crystal violet/PAS. Scale bar = 13.14 μm.

Figure 31 Epifluorescence light micrograph of figure 30 stained with calcofluor and viewed under UV light. The filiform apparatus (Fa) shows finger-like projections extending deep into the degenerate synergid cell (S) cytoplasm. The lateral cell wall (cc) of the degenerate synergid cells (large arrows) fluoresces slightly compared to the lateral wall (open arrows) of the zygote (Z) cell which fluoresces brightly. The ampuliform tip of the zygote shows only a slight fluorescence (small arrows). The wall projections are hazy along the lateral walls of the central cell (arrow heads). Calcofluor. Scale bar = 13.14 μm.

Figure 32 Electron micrograph of part of a filiform apparatus (Fa), pollen tube (Pt) and inner integument cells (II). The electron-opaque pollen tube cell wall (cw) is thick and shows a portion of the cytoplasm containing spherical particles (arrows). The filiform apparatus extends deep inside the cytoplasm of both synergid cells and consists of an electron transparent core (arrow heads) surrounded by an outer electron transparent margin. KFeCN UA/Pb. Scale bar = 0.16 μm.

Figure 33 Electron micrograph of the micropyle region of the megagametohyte showing a degenerate synergid (S), a portion of the filiform apparatus (FA) and the thick walled pollen tube (Pt). The pollen tube has penetrated a region between the filiform apparatus and the megagametophyte wall. Note wall pojections (Wp) of the central cell near the synergid hook region. UA/Pb. Scale bar = 1.60 μm.

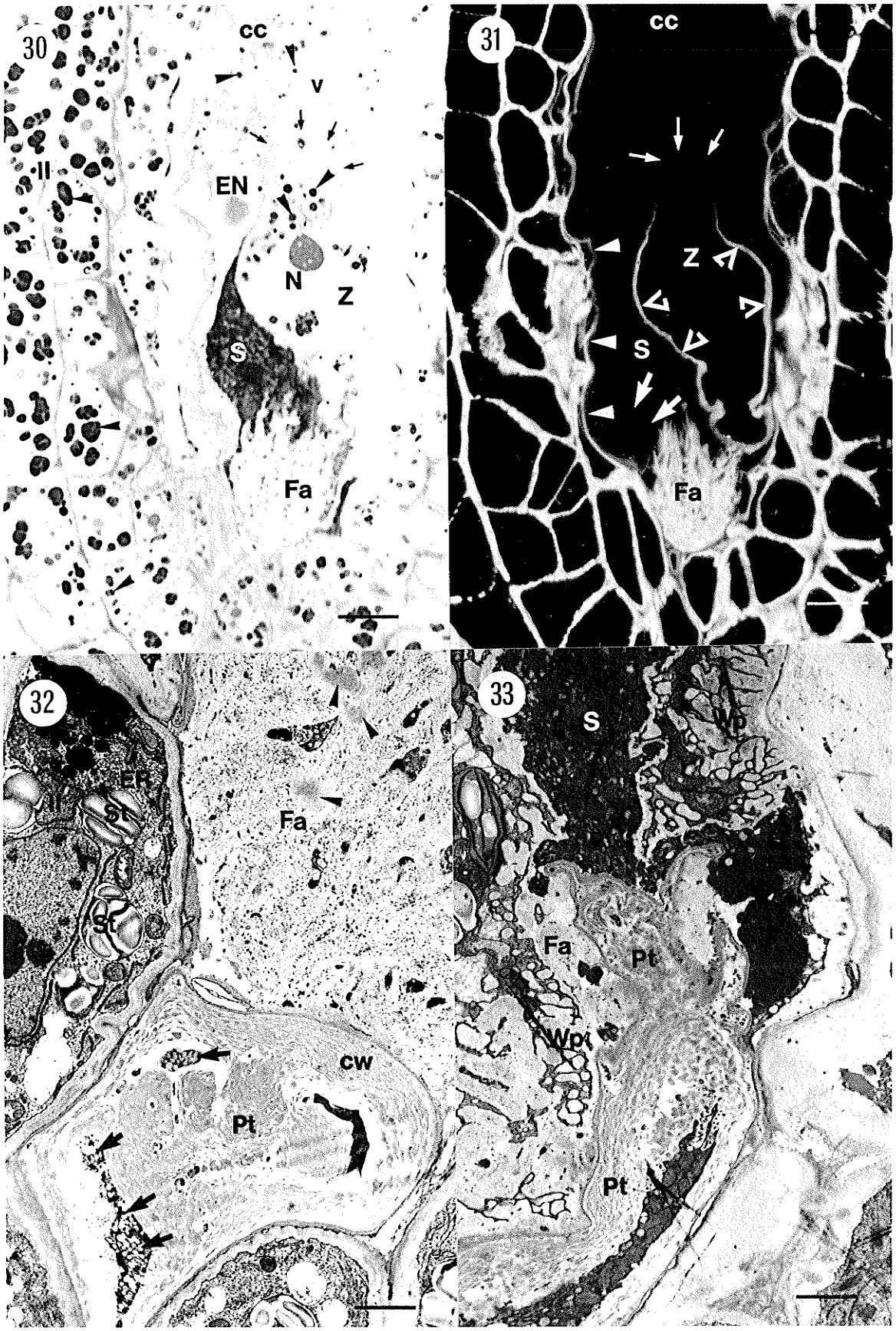
30
cc
v
II
EN
N
Z
S
Fa
31
cc
Z
S
Fa
32
ER
St
St
Fa
cw
Pt
33
S
Wp
Fa
Pt
Wp
Pt

Figure 34 Diagrammatic representation of figure 36 showing a zygote cell (Z), two synergids with filiform apparatus (FA) and the central cell (cc). The megagametophyte is surrounded by a thick layer of inner integument (II) cell wall material. Scale bar = 13.40 μm.

Figure 35 Diagrammatic representation of figure 30 showing the zygote (Z), degenerate synergid (S), and central cell (cc) which has an endosperm nucleus (EN). The megagametophyte is surrounded by a thick layer of inner integument (II) cell wall material. Scale bar = 13.40 μm.

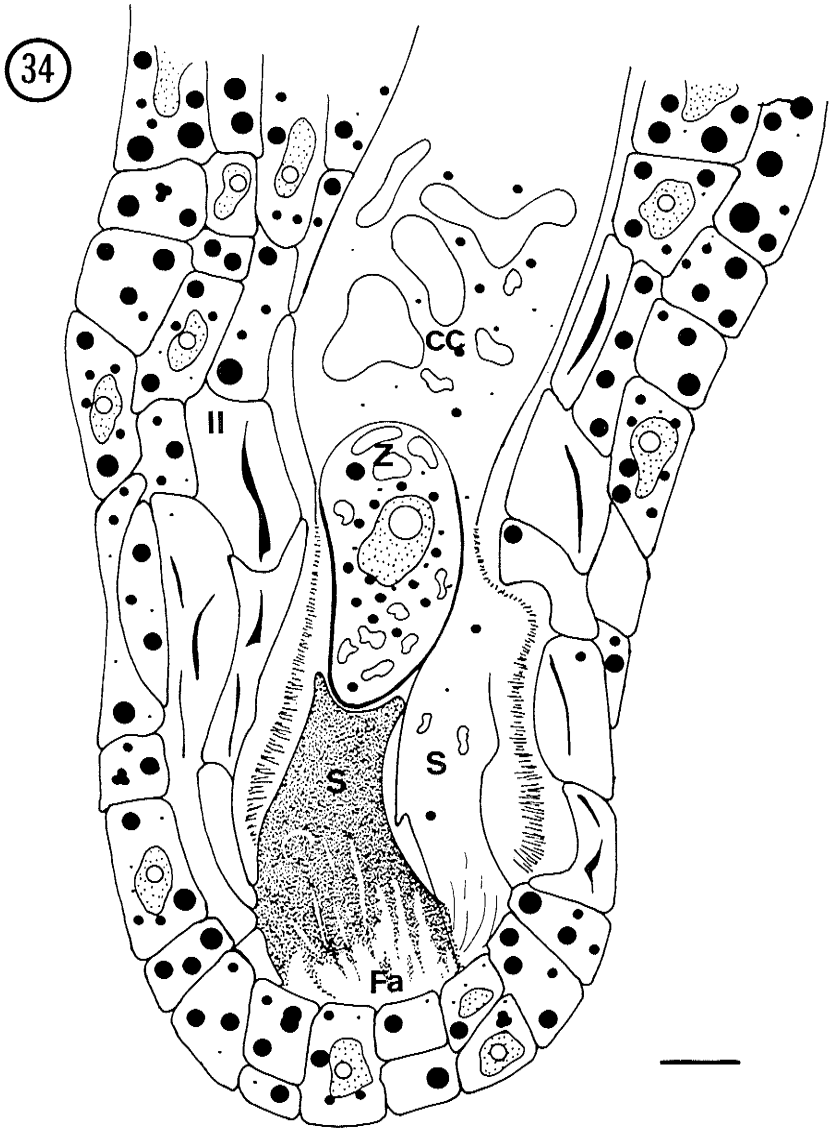
34
CC
II
Z
S
S
Fa

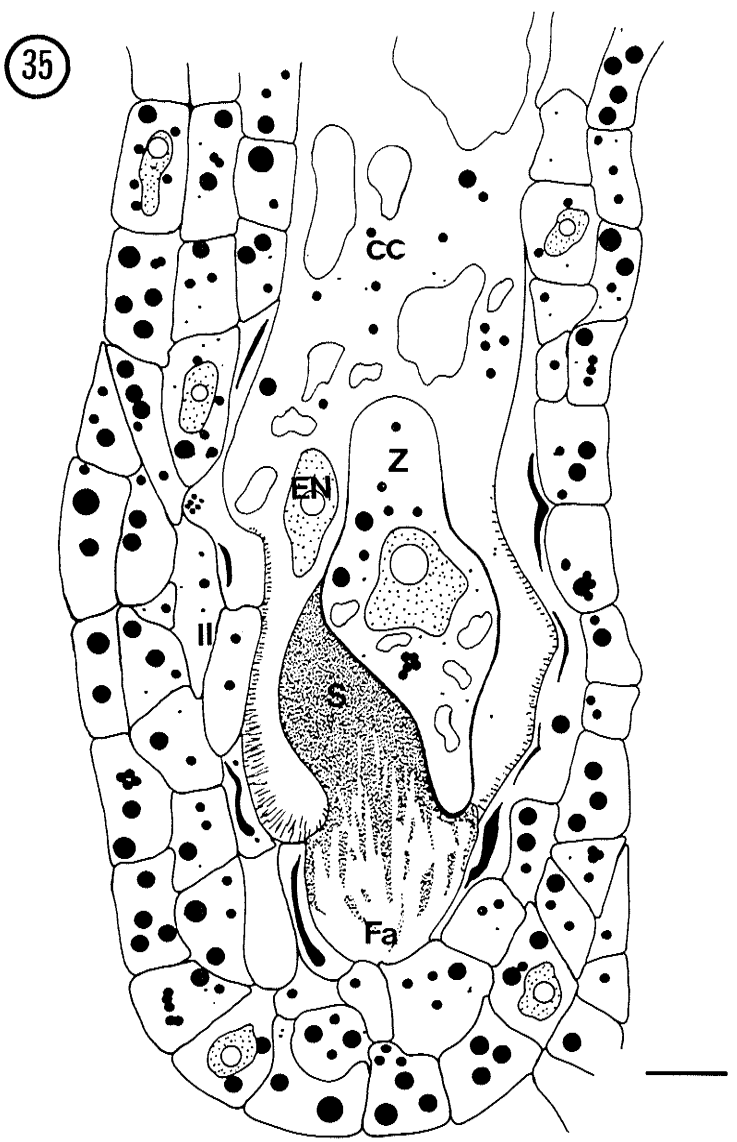
35
CC
EN
Z
II
S
Fa

Figure 36 Electron micrograph of an egg apparatus 22 hours after pollination showing a zygote cell (Z), two synergids and filiform apparatus (FA). The zygote cell is elongated and lacks the large micropyle vacuole seen in the unfertilized egg cell. The zygote cell cytoplasm shows plastids (Pl) containing starch (St), mitochondria (m), lipid bodies (L) and small vacuoles (v). The electron transparent lateral cell walls (cw) of the zygote are thin at the chalazal pole and thick at the micropyle. The zygote is flanked laterally by central cell (cc) which contains mitochondria near the wall projection (Wp). Wall projections cut obliquely adjacent the persistent synergid cell (pS) shows a web-like appearance as the synergid cytoplasm is invaginated by the central cell wall. The persisitent synergid contains few vacuoles, mitochondria, lipids and is separated from the degenerate synergid (dS). The degenerate synergid cell shows a pollen tube (Pt) adjacent the synergid hook (Sh). The pollen tube shows a cone-shaped zone of spherical discharge particles (arrows) extending to the chalazal end of the degenerate synergid cell. The degenerate synergid cell nucleus (N) shows the loss of nuclear membrane integrity. The megagametophyte is surrounded by a thick layer of crushed inner integument (cII) cell wall material. UA/Pb. Scale bar = 2.27 μm.

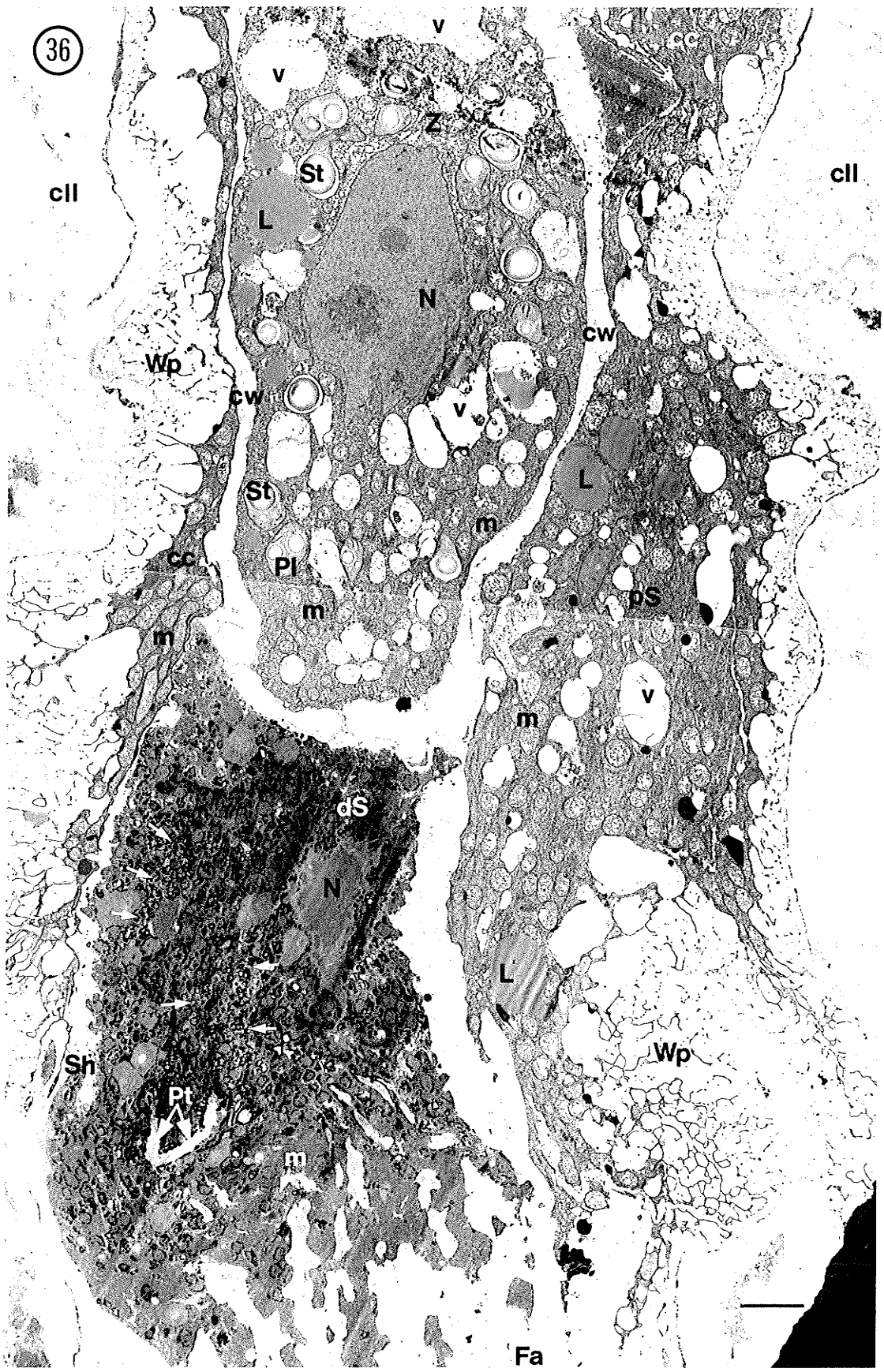
36
v
v
Z
St
cII
L
N
cII
cw
Wp
cw
v
St
L
m
cc
Pl
pS
m
m
v
m
dS
N
L
Wp
Sh
Pt
m
Fa

Figure 37 Electron micrograph showing a portion of the pollen tube wall within the degenerate synergid cytoplasm. The cytosol of the degenerate synergid cytoplasm is very electron opaque and the integrity of many of the organelles has been lost. The starch (St) containing plastid (Pl) shows a non-continuous membrane (arrows) with electron opaque deposits. There are numerous spherical particles (white arrows) near the discharge pore and electron transparent cell wall (cw) of the pollen tube. The spherical particles exhibit an electron-transparent border that circumscribes a granular electron-opaque core. KFeCN UA/Pb. Scale bar = 0.31 μm.

Figure 38 Electron micrograph showing the degenerate synergid (S), central cell (cc) and zygote cell (Z). The micropyle end of the zygote is separated from the central cell (cc) and synergid by a cell wall (cw). The central cell contains numerous mitochondria and is separated from the degenerate synergid cell by a plasma membrane (Pm). The degenerate synergid is necrotic and shows the absence of a plasma membrane. KFeCN UA/Pb. Scale bar = 0.40 μm.

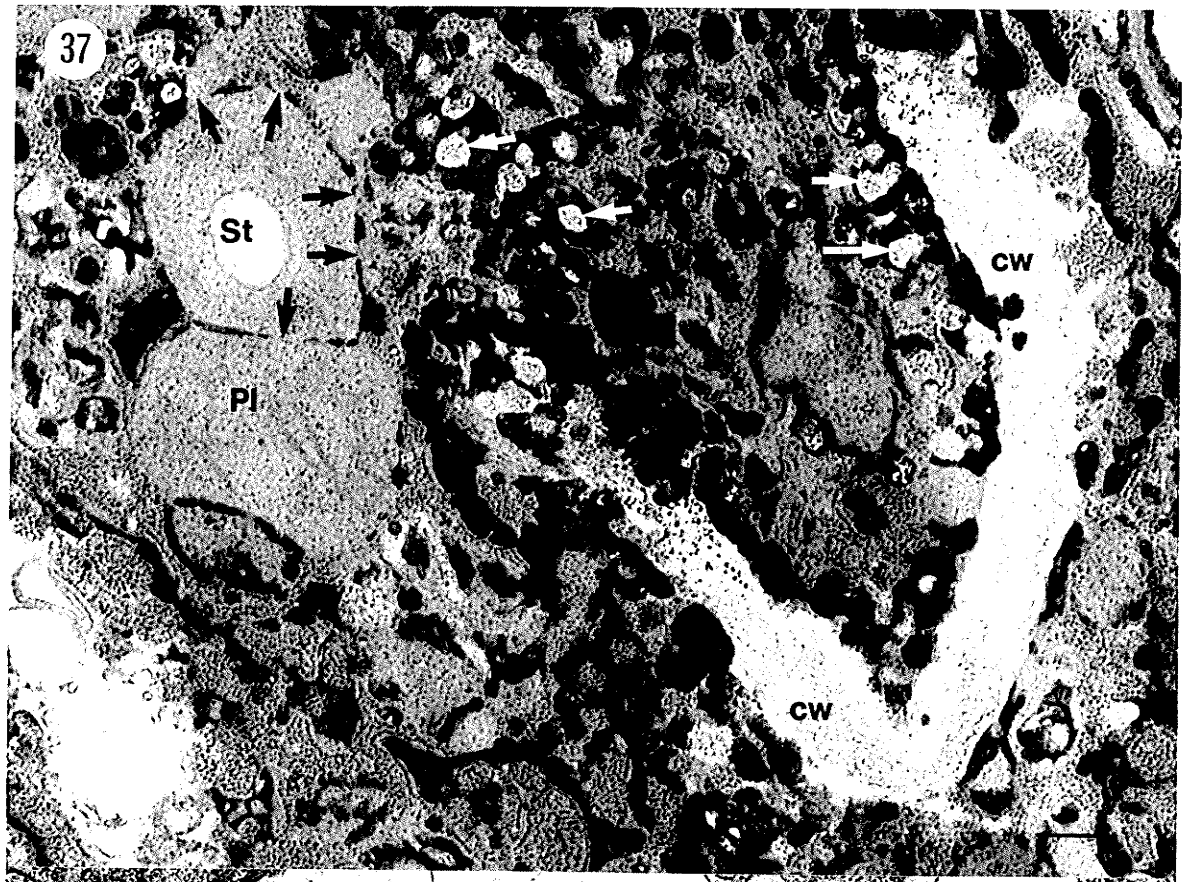
37
St
Pl
CW
CW

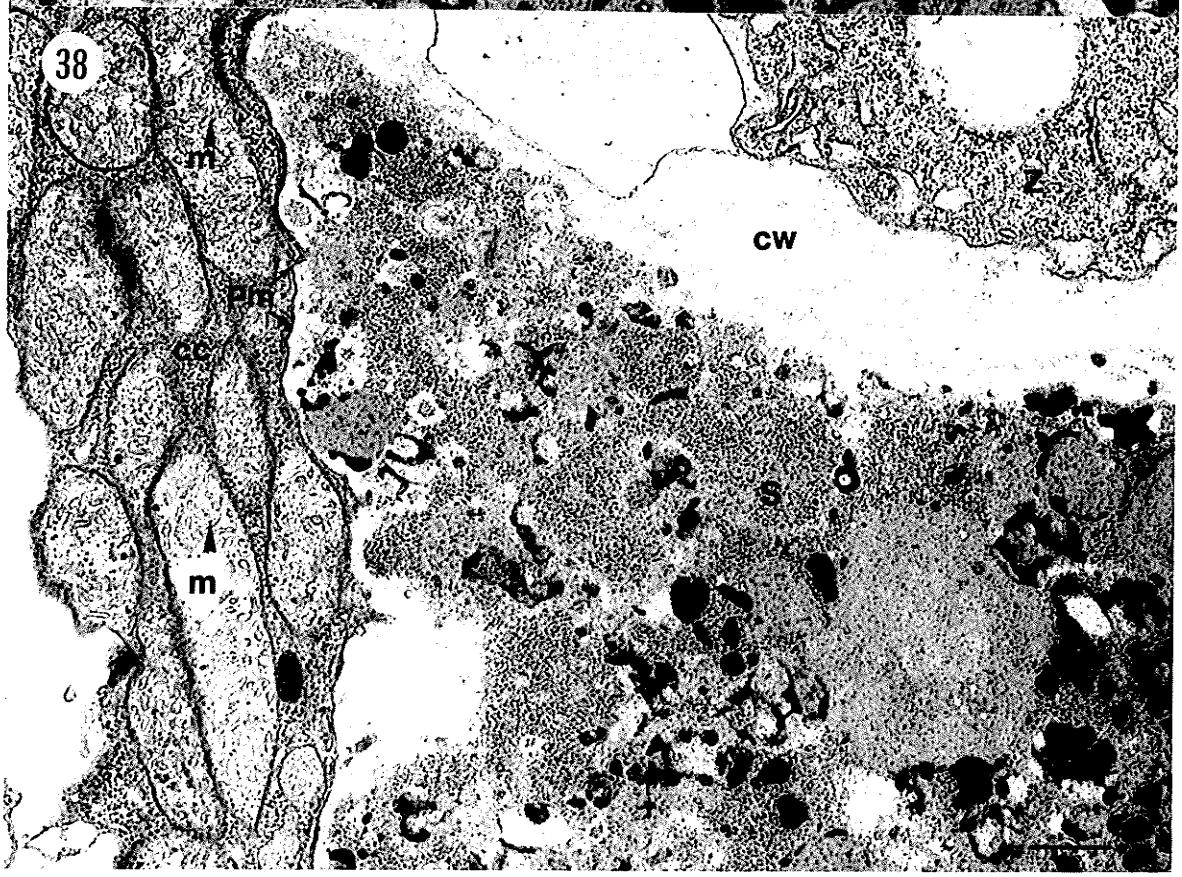
38
m
Pm
cc
m
CW
Z
S

Figure 39 Electron micrograph showing the persistent synergid (S) and central cell (cc). The persistent synergid cytoplasm contains mitochondria (m) and endoplasmic reticulum (ER). The synergid cell is separated from the central cell by a thin cell wall (arrow heads). At the terminal end of the synergid cell, the cytoplasmic composition of the central and synergid cell appears similar. The megagametophyte is surrounded by the central cell lateral walls with electron-transparent wall projections (Wp) and crushed integument cells (cII). KFeCN UA/Pb. Scale bar = 0.79 μm.

Figure 40 Electron micrograph showing the persistent synergid 22 hours after pollination. The synergid contains mitochondria (m), with tubular cristea, plastids (Pl) containing no starch, dilated endoplasmic reticulum (DER), and transition vesicles (Tv). KFeCN UA/Pb. Scale bar = 0.28 μm.

Figure 41 Electron micrograph showing the micropyle portion of the zygote cell. The zygote cytoplasm beneath the nucleus shows several vacuoles (v), mitochondria (m), vesicle producing dictyosomes (D) and endoplasmic reticulum (ER); however, starch (St) containing plasids (Pl) are shown. KFeCN UA/Pb. Scale bar = 0.46 μm.

Figure 42 Electron micrograph showing the mid-region of the developing zygote. The nucleus (N) is centrally located and surrounded by the nuclear membrane (arrow heads). The zygote cell shows vacuoles (v) and several perinuclear starch (St) containing plasids (Pl). Dictyosomes (D), mitochondria (m), and lipids (L) are shown. KFeCN UA/Pb. Scale bar = 1.10 μm.

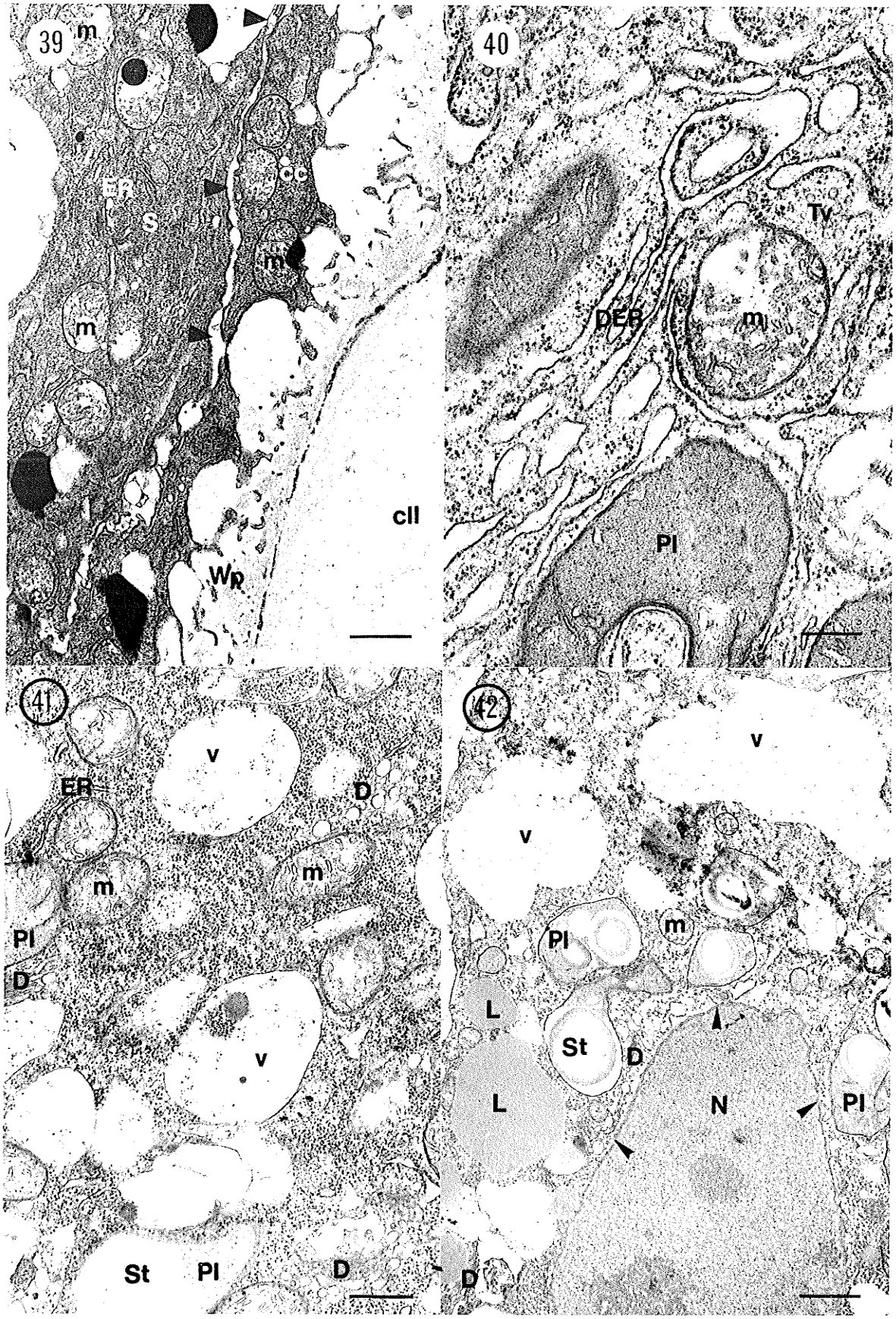
39
m
ER
S
m
m
cc
cII
WR
40
Tv
DEB
m
PI
41
v
ER
D
m
m
PI
D
v
St
PI
D
42
v
v
PI
m
L
St
D
L
N
PI
D

Figure 43 Electron micrograph of the central cell 22 hours after pollination. A plasma membrane (arrows) follows the contours of the central cell wall projections. Active dictyosomes (D), with distinct forming (FF) and maturing (MF) faces, and several dictyosome vesicles (Vs) are located adjacent to the wall projections (wp). UA/Pb. Scale bar = 0.12 μm.

Figure 44 Electron micrograph of the central cell 22 hours after pollination. The dictyosome is composed of five electron opaque cisternae (arrows). Small transition vesicles (Tv) are located at the forming face (arrowheads) while larger electron transparent vesicles (open arrow) are located near the maturing face of the dictyosome. The central cell also contains mitochondria (m), endoplasmic reticulum (ER) and starch (St) containing plastids (Pl). UA/Pb. Scale bar = 0.21 μm.

Figure 45-46 Light micrographs of two adjacent sections showing a well developed ampuliform zygote.

Figure 45 Light micrograph showing a developing zygote (Z) cell and degenerate synergid (S) cell 48 hours after pollination. The central cell (cc) contains heterogeneous vacuoles (v), crystal-violet positive stained bodies (arrows) and free nuclear endosperm (EN). The ampuliform zygote cytoplasm has a peppered appearance, few vacuoles, and a thin cell wall (arrow heads). The degenerate synergid cell has a necrotic appearance with the loss of cell wall integrity. Crystal violet . Scale bar = 11.61 μm.

Figure 46 Light micrograph showing a developing zygote (Z) cell and a degenerating synergid (S) cell 48 hours after pollination. The central cell (cc) cytoplasm contains large PAS positive spheres (large arrow) and endosperm nuclei (EN). The zygote cytoplasm contains PAS positive starch grains at the chalazal end, (arrows) and vacuoles (v) at the micropyle end. The zygote which contains a centrally located nucleus (N) is surrounded a PAS-positive cell wall (open arrows). The degenerate synergid cytoplasm shows a weak PAS-positive reaction and a negative reaction for the cell wall. The inner integument (II) cells, which surround the megagametophyte, contains PAS-positive starch grains (arrows). PAS. Scale bar = 11.61 μm.

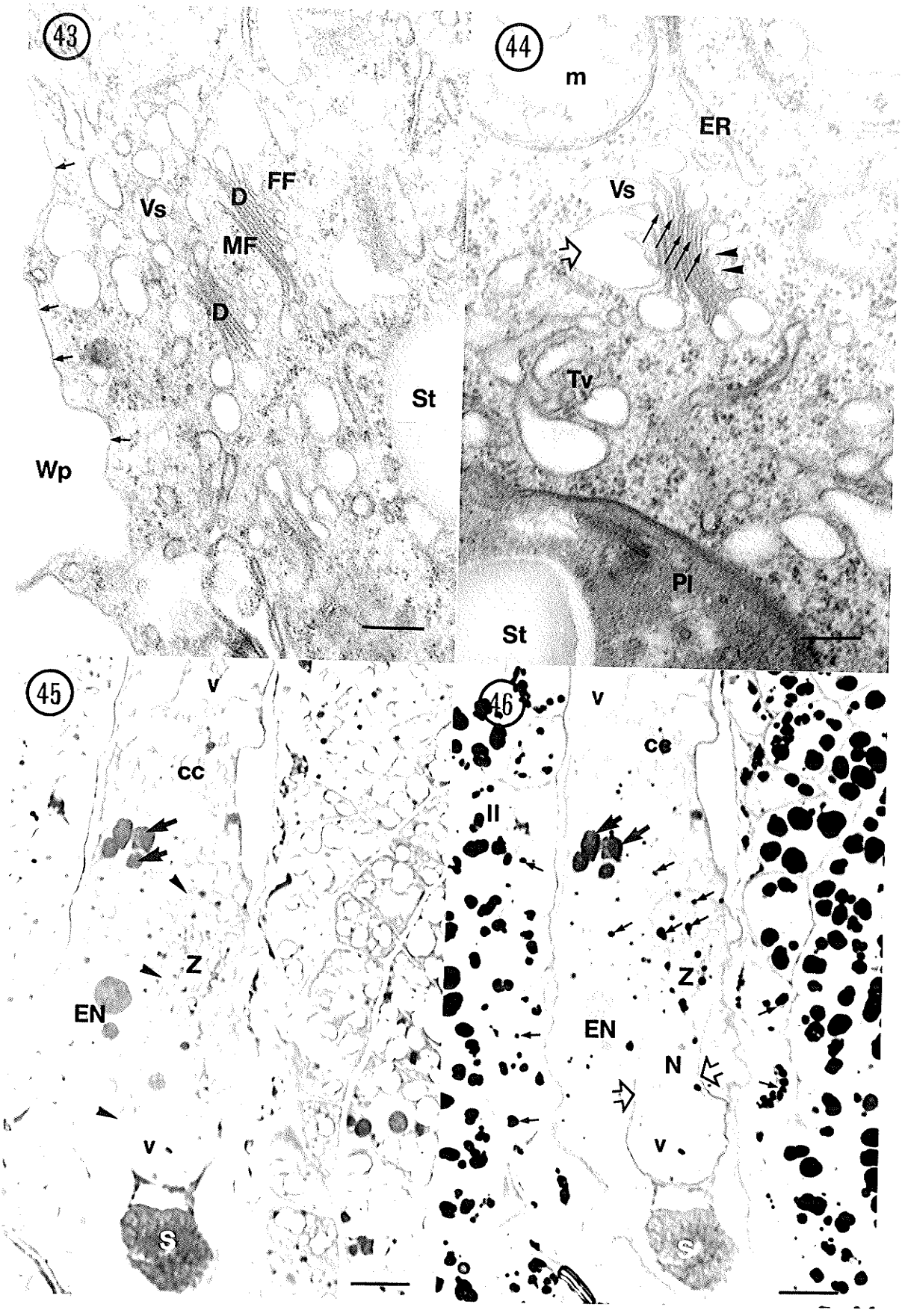
43
Vs
D
FF
MF
D
St
Wp
44
m
ER
Vs
Tv
Pl
St
45
v
cc
Z
EN
v
S
46
v
cc
II
Z
EN
N
v
S

Figure 47 Light micrograph of a zygote (Z), degenerate synergids (S) and the filiform apparatus (Fa) 72 hours after pollination. The micropyle inner integument (II) cells show reduced PAS-positive starch grains (St) relative to the outer integument (OI). The synergid filiform apparatus with its finger-like projections is slightly PAS-positive. Note a thin cell wall (white arrows) is shown between both dark staining synergid cells from the filiform apparatus to the base of the zygote. The elongated zygote extends deep into the central cell (cc). Cytoplasmic strands (arrows) are seen extending across the large zygote cell vacuole (v). From the micropyle, a thin layer of cytoplasm extends along the lateral wall of the zygote to the chalazal apex of the cell (black arrows). ABB/PAS. Scale bar = 14.40 μm.

Figure 48 Epifluorescence light micrograph of figure 47 stained with calcofluor and viewed under UV light. The calcofluor stained filiform apparatus (Fa) shows finger-like projections extending deep into the synergid cells (S). At the base of the filiform apparatus, a portion of the thick walled pollen tube is shown. The zygote cell wall is not fluoresce as intensely as the inner integument (II) cell walls and varies in intensity. The basal cell of the zygote at the micropyle shows more intense fluorescence than the apical wall (arrows). Wall projections of the central cell near the base of the elongate zygote show pale fluorescence which becomes wider in the region of central cell next to the synergids (arrow heads). Calcofluor Scale bar = 14.40 μm.


47
St
Ol
Z
St
II
v
S
S
Fa
48
II
Z
S
S
Fa

Figure 49 Diagrammatic interpretation of figure 47 showing the inner (II) and outer (OI) integuments, the synergid cells (S) with the filiform apparatus (Fa), the zygote (Z) and the central cell (cc). Scale bar = 14.40 µm.

Figure 50-51 Closely adjacent sections through a two-celled proembryo 96 hours after pollination.

Figure 50 Light micrograph of a two-celled proembryo showing the apical cell (*ca*) and the basal cell (*cb*). The apical cell has a dark staining nucleolus (Nu) and the nucleus (N) with dark staining perinuclear spheres (arrow heads). The basal cell has small vacuoles (v) at the chalazal end. The central cell is semi-vacuolated near the proembryo and contains endosperm nuclei (EN). Crystal violet. Scale bar =11.61 µm.

Figure 51 Light micrograph of a two-celled proembryo showing the apical (*ca*) and basal (*cb*) cells. The nucleus (N) of the basal cell is not as intensely stained as the apical cell in figure 50, nor does it contain the dark staining perinuclear spheres in the cytoplasm. The basal cell shows small vacuoles (v) above the nucleus and large vacuoles below the nucleus towards the micropyle. Crystal violet. Scale bar = 11.61 µm.

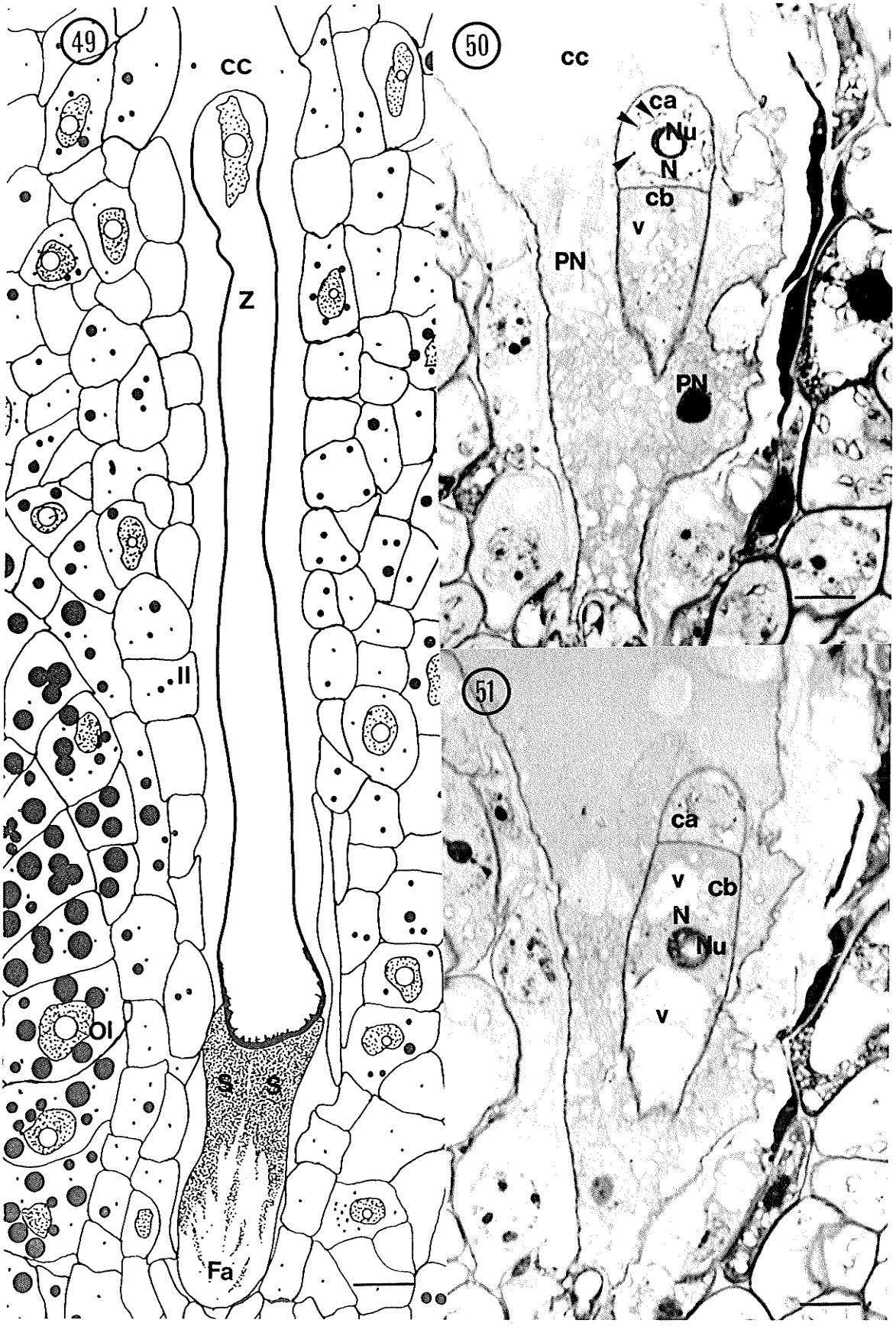
49
cc
Z
Il
Ol
S
S
Fa
50
cc
ca
Nu
N
cb
v
PN
PN
51
ca
v
Cb
N
Nu
v

Figure 52 Light micrograph showing the micropyle end of the basal cell (*cb*) from a two-celled proembryo. The basal cell shows a lightly stained cytoplasm and is vacuolated. The micropyle portion of the basal cell shows projections extending into the cytoplasm (arrow heads), and the basal cell is surrounded by the central cell (cc) cytoplasm. The inner integument (II) cells surrounding the megagametophyte contain few starch grains (St). Crystal violet. Scale bar = 11.61 μm.

Figure 53 Epifluorescence light micrograph of figure 52 stained with calcofluor and viewed under UV light. The central cell wall shows an abundance of projections (arrow heads) along the lateral walls and extending to the base of the basal cell (*cb*). The basal cell wall is intensely stained and evidence of cell wall projections are shown at the micropyle of the basal cell (arrows). Calcofluor. Scale bar = 11.61 μm.

Figure 54-56 Serial sections showing a three-celled proembryo 96 hours after pollination prepared for bright field microscopy.

Figure 54 Light micrograph of a three-celled proembryo showing the apical (ca) cell with a dark staining nucleolus (Nu) within the nucleus (N). The cytoplasm contains few vacuoles and shows dark staining perinucleur spheres (arrow heads). The middle cell (mC) contains a visible nucleus (N) and the presence of dark staining perinucleur spheres. The middle cell is slightly vacuolated. Crystal violet. Scale bar = 11.61 μm.

Figure 55 Light micrograph of a longitudinal section showing the apical (ca), middle (mC), and basal cells (ci). The apical cell shows the same distribution of dark staining perinucleur spheres (arrow heads) and vacuolation (v) as figure 54 except the nucleolus is no longer visible. The middle cell cytoplasm is similar to that of figure 54 and has a dark staining nucleolus (Nu) in a centrally located nucleus (N). The basal cell shows more vacuoles than the apical or middle cells. Crystal violet. Scale bar = 11.61 μm.

Figure 56 Light micrograph of the basal cell (ci) of a three-celled proembryo. The basal cell is elongated and contains large vacuoles divided by a band of cytoplasm containing the nucleus (N) located in the chalazal portion of the cell. Most of the basal cell cytoplasm is located on the lateral walls (arrows). The thickness of the basal cell walls is uniform and no wall projection are shown. Crystal violet. Scale bar = 11.61 μm.

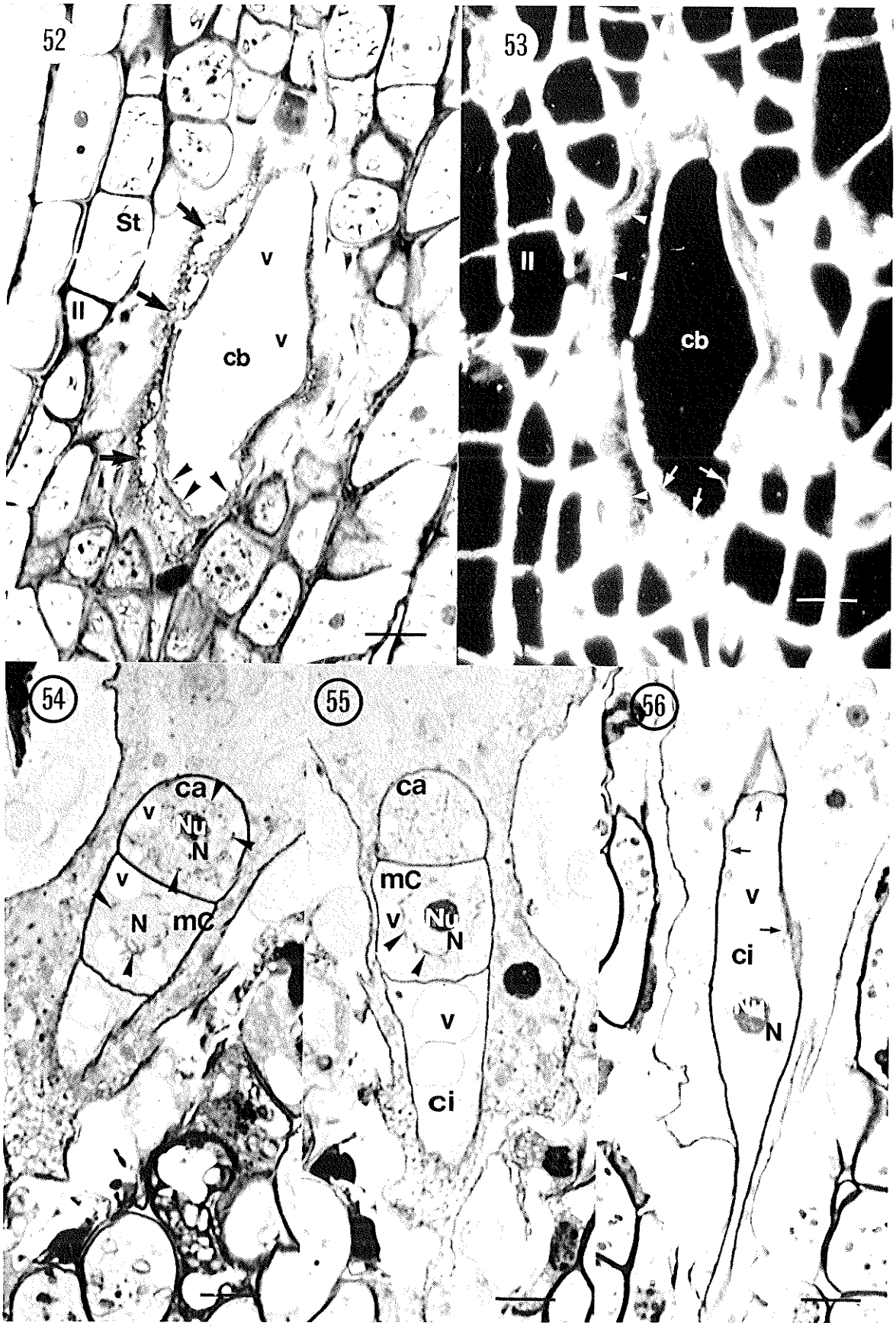
52
St
v
II
v
cb
53
II
cb
54
ca
v
N
v
N
mC
55
ca
mC
v
N
v
ci
56
v
ci
N

Figure 57 Diagrammatic interpretation of the two-celled proembryo from figures 50 and 51 showing the apical cell (ca), the basal cell (cb) and the semi-vacuolated central cell (cc) containing endosperm nuclei (EN). Scale bar = 11.61 μm.

Figure 58 Diagrammatic interpretation of the three-celled proembryo from figures 54 to 56 showing the apical cell (ca), the middle cell (mC), the basal cell (cb) and the central cell (cc) containing endosperm nuclei (EN).. Scale bar = 11.61 μm.

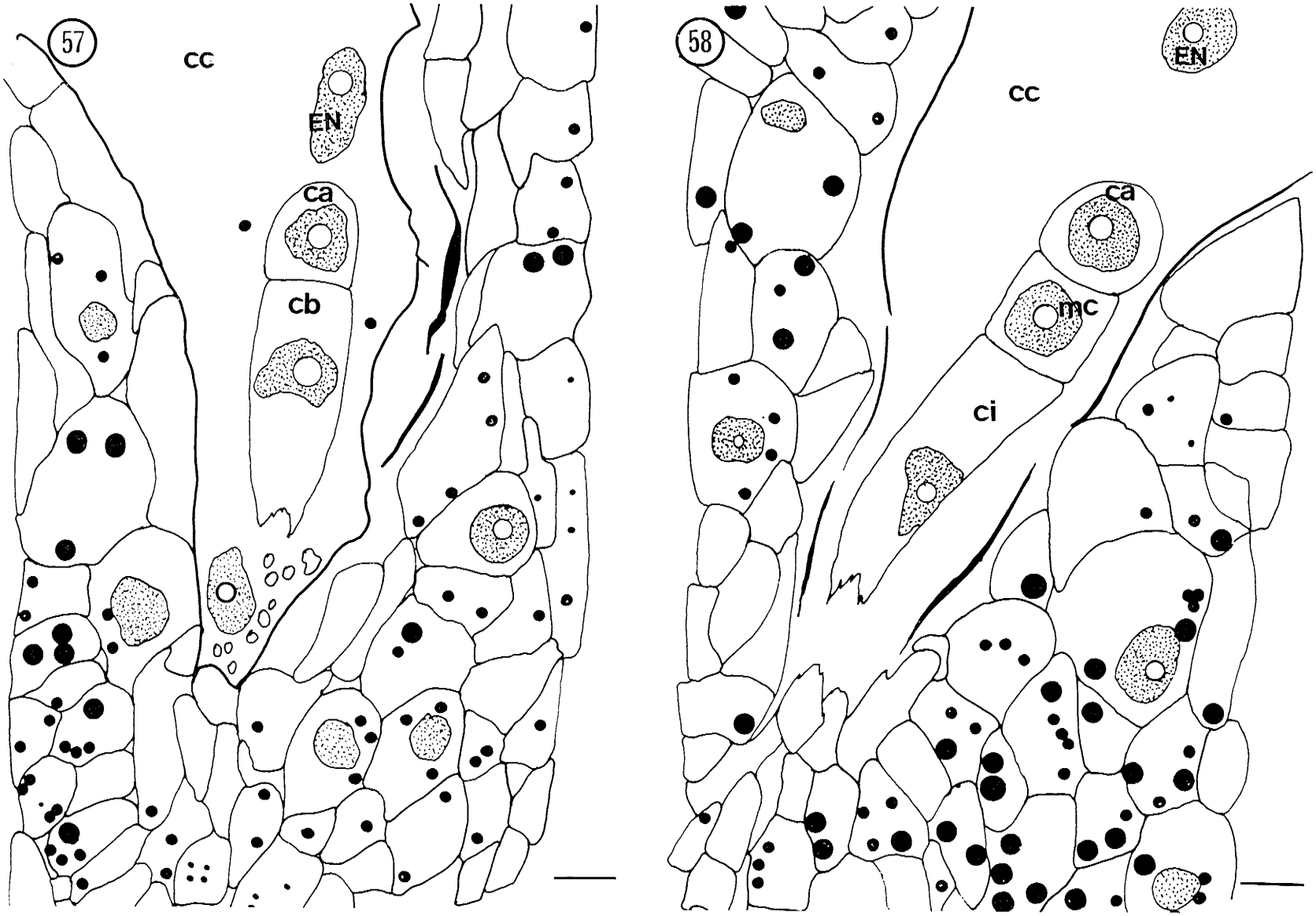
57
cc
EN
ca
cb
58
cc
EN
ca
mc
ci

Figure 59 Light micrograph of a seed 96 hours after pollination. The seed shows the apical cell (*ca*),the middle (*mC*) and basal cell (*ci*) of a proembryo. The chalazal portion of the megagametophyte (MG) central cell is highly vacuolated with a thin parietal cytoplasm lined with endosperm nuclei (arrows). PAS-positive starch accumulations are shown in the inner integument basal body (Bb), the outer integument (OI) of the micropyle and the chalazal inner integument of the seed (large arrows). Some starch is shown in the raphe (Ra) and nucellar proliferation tissue (nP). Vascular tissue (circles) entering the seed through the funiculus (Fu) is seen in the raphe region opposite to the chalazal proliferation tissue adjacent the inner integument at the micropyle. PAS. Scale bar = 45.57 µm.

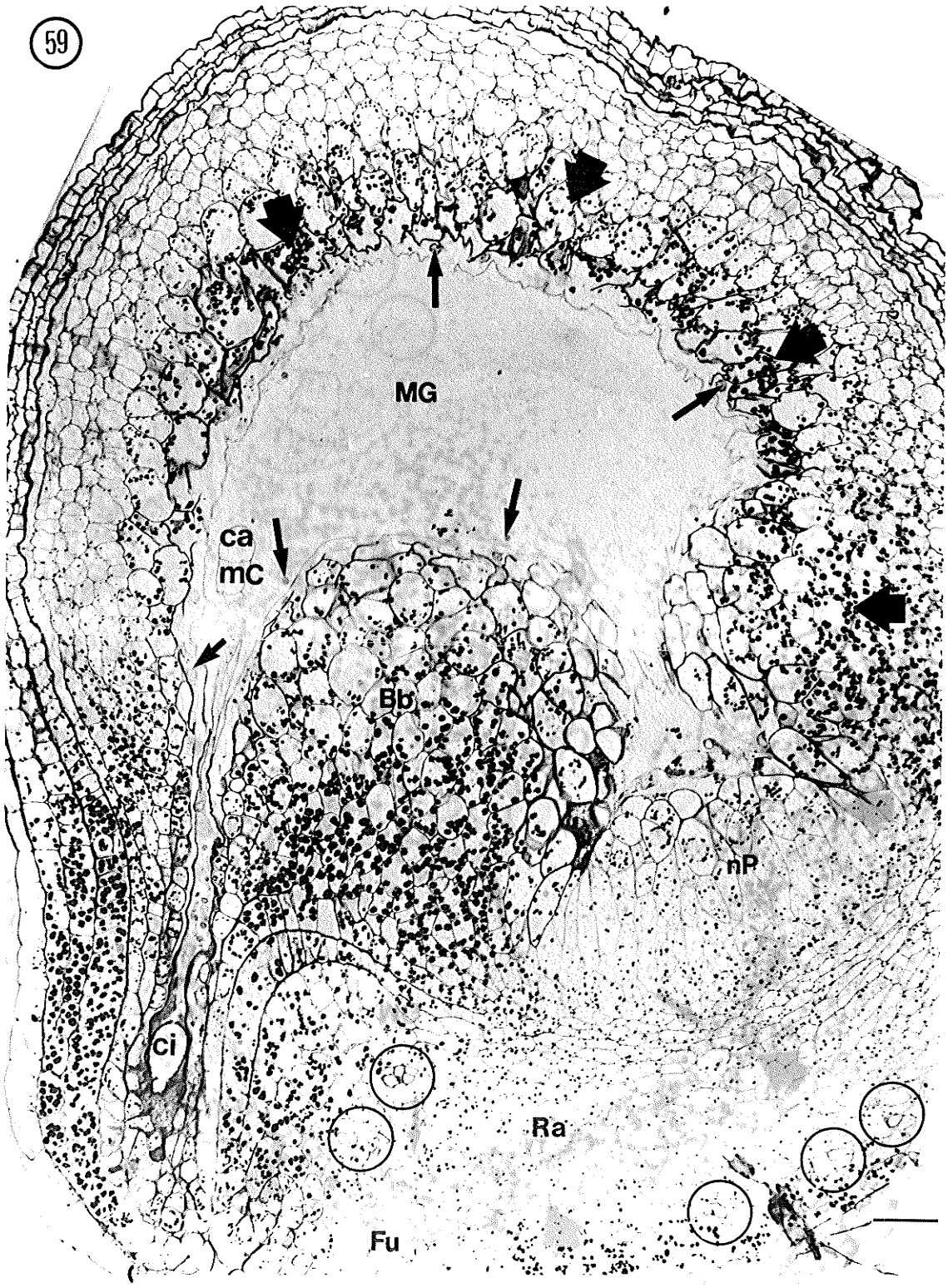
59
MG
ca
mC
Bb
nP
Ci
Ra
Fu

Figure 60 Light micrograph of a 3-celled proembryo and megagametophyte (MG). The lower portion of the basal cell (*ci*) shows cell wall projections (arrows). The cytoplasm of the basal cell is thin and vacuolate (v). The middle cell (*mC*) shows a dark staining centrally located nucleus (N) and nucleolus (Nu). The cell cytoplasm is slightly vacuolated and contains few dark staining perinucleur spheres (arrow heads). The apical and middle cell are similar in size, vacuolation and cytoplasmic distribution. Crystal violet. Scale bar = 18.46 μm.

Figure 61 Diagrammatic representation of the developing proembryo of figure 60 showing the apical cell (ca), the middle cell (mC). and the basal cell (ci). The diagram also shows the position of a synergid cell (S) and central cell (cc) in the megagametophyte which is surrounded by inner integument (II) cell layers. Scale bar = 18.46 μm.

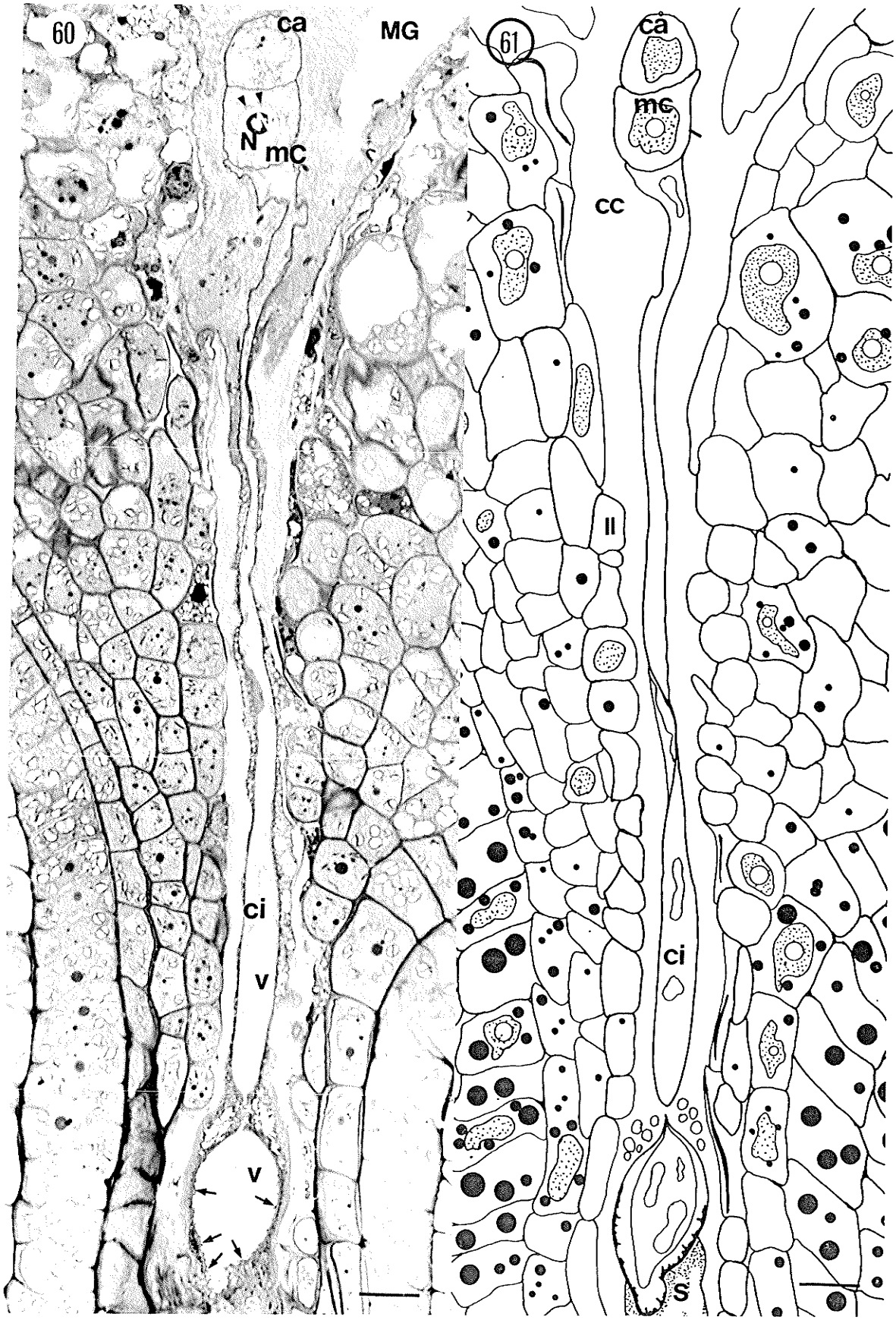
60
ca
MG
N
mc
ci
v
v
61
ca
mc
cc
ll
ci
S

Figure 62 Light micrograph of a 4-celled proembryo and megagametophyte (MG) using differential interface contrast microsopy. The micropyle portion of the basal cell (*ci*) is highly vacuolated and shows cytoplasm extending from the cell walls (arrow). A band of cytoplasm (open arrow) is shown across the chalazal end of the basal cell. The apical cell initial (*ca*) has divided longitudinally producing two sister cells of equal size. The middle cell (*m*C) is larger than the apical cells (*ca*) and is vacuolated (v). The cytoplasm in the middle cell shows a centrally located band of cytoplasm with a nucleus (N) and nucleolus (Nu). The two-celled apex has a bulging appearance and shows no vacuolation. The cell wall between the apical cells is not visible and one apical sister cell shows a centrally located nucleolus (Nu). Endosperm nuclei (EN) are shown in the megagametophyte central cell. Crystal violet. Scale bar = 20 µm.

Figure 63 Diagrammatic representation of the four-celled proembryo as shown in figure 62 showing two apical cell (ca), the middle cell (mC). and the basal cell (ci). The diagram also shows the central cell (cc) which contains several endosperm nuclei (EN). The megagametophyte itself is surrounded by inner integument (II) cell layers.. Scale bar = 20 µm.

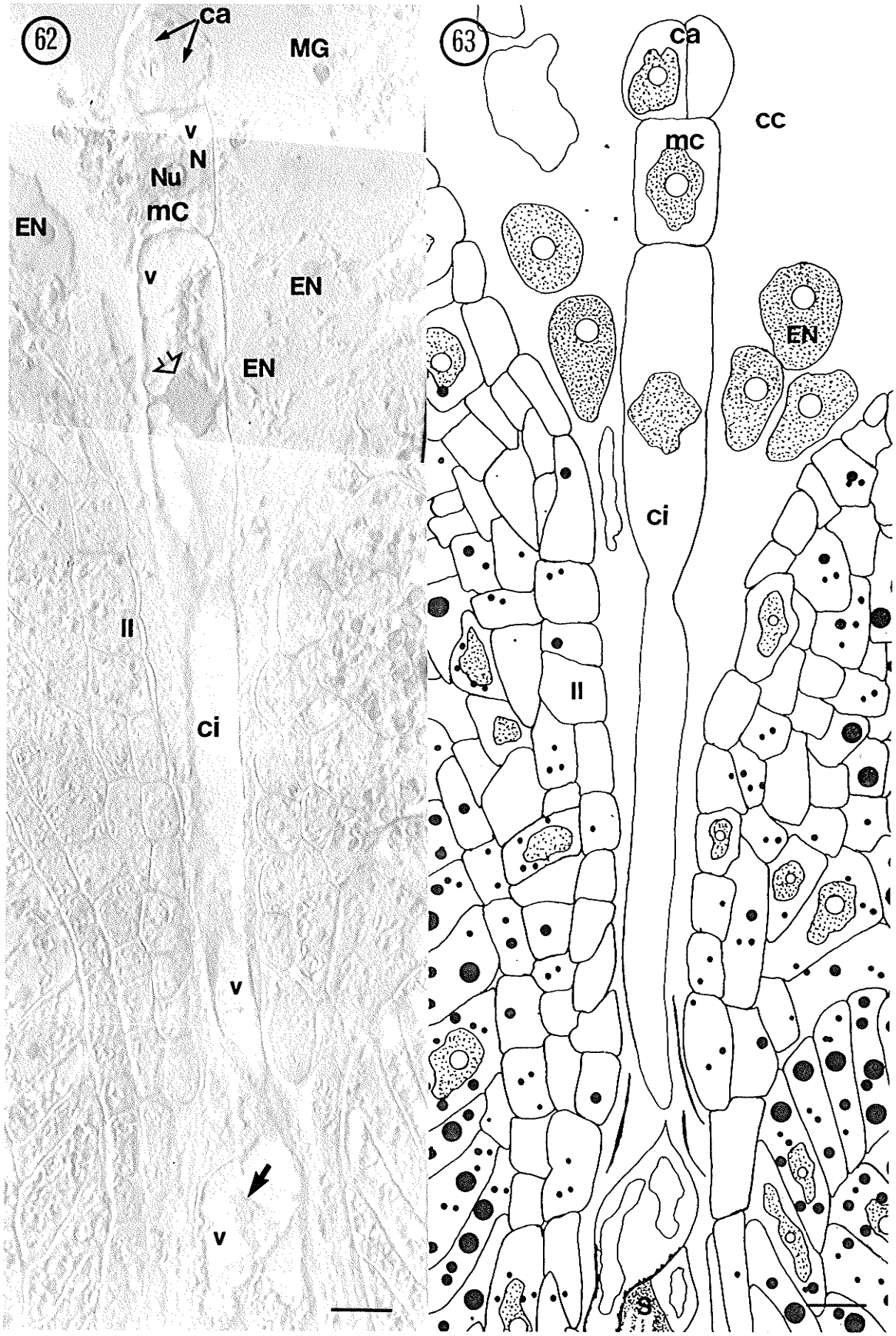
62
ca
MG
v
N
Nu
mC
EN
v
EN
EN
II
ci
v
v
63
ca
cc
mc
EN
ci
II
S

Figure 67 Light micrograph showing the chalazal poles of a seed containing an eight-celled proembryo. On the left of the megagametophyte (MG), the proembryo (PE) is shown and on the right at the chalaza, the central cell contains endosperm nuclei (EN) and lens shaped plastids are shown (arrow heads). Starch grains are shown as small transluscent spheres, which occupies much of the inner integument basal body (Bb). The chalazal nucellar proliferation tissue (nP) shows reduced starch. Crystal violet. Scale bar = 41.14 μm.

Figure 64 Epifluorescence light micrograph of figure 60 stained with calcofluor and viewed under UV light. The cell walls of the inner integument (II) tissues are shown. The proembryo cell walls also show a calcofluor-positive fluorescence; however, the degree of intensity varies. The micropylar portion of the basal cell (*ci*) and filiform apparatus (FA) show brighter fluorescence than the middle (mC) and apical (ca) cells. Calcofluor. Scale bar = 46.45 μm.

Figure 65 Light micrograph of a 4-celled proembryo and megagametophyte (MG) showing an aniline blue-black (ABB) positive staining cytoplasm lining the walls of the basal cell (*ci*). The chalazal end of the cell shows a dark staining cytoplasmic band (Cb). Above the cytoplasmic band is a vacuole (v). The middle (*mC*) and apical sister cells (*ca*) cytoplasmic distribution is clearly shown. The megagametophyte central cell contains free nuclear endosperm nuclei (EN), PAS-positive spheres (arrows) and lens shaped chloroplasts (arrow heads). The inner integument (II) cells at the micropyle (mi) adjacent the megagametophyte show reduced PAS-positive starch (St). Starch is shown in the outer integument (OI) of the micropyle and the inner integument basal body (Bb) region of the seed. ABB/PAS. Scale bar = 46.45 μm.

Figure 66 Epifluorescence light micrograph of figure 62 showing the four-celled proembryo stained with calcofluor and viewed under ultraviolet light. The most intense staining occurs in the integument cell layers. In the proembryo, the most intense fluorescence is shown at the micropyle of the basal cell (*ci*) and filiform apparatus (Fa). The intensity of fluoresence in the outer longitudinal walls of the basal, middle (*m*C) and apical (*ca*) cells is similar; however, the cross wall between the basal, middle and apical cells including the longitudinal wall between the apical sister cells shows a less fluorescence (arrow heads). Calcofluor. Scale bar= 46.45 μm.

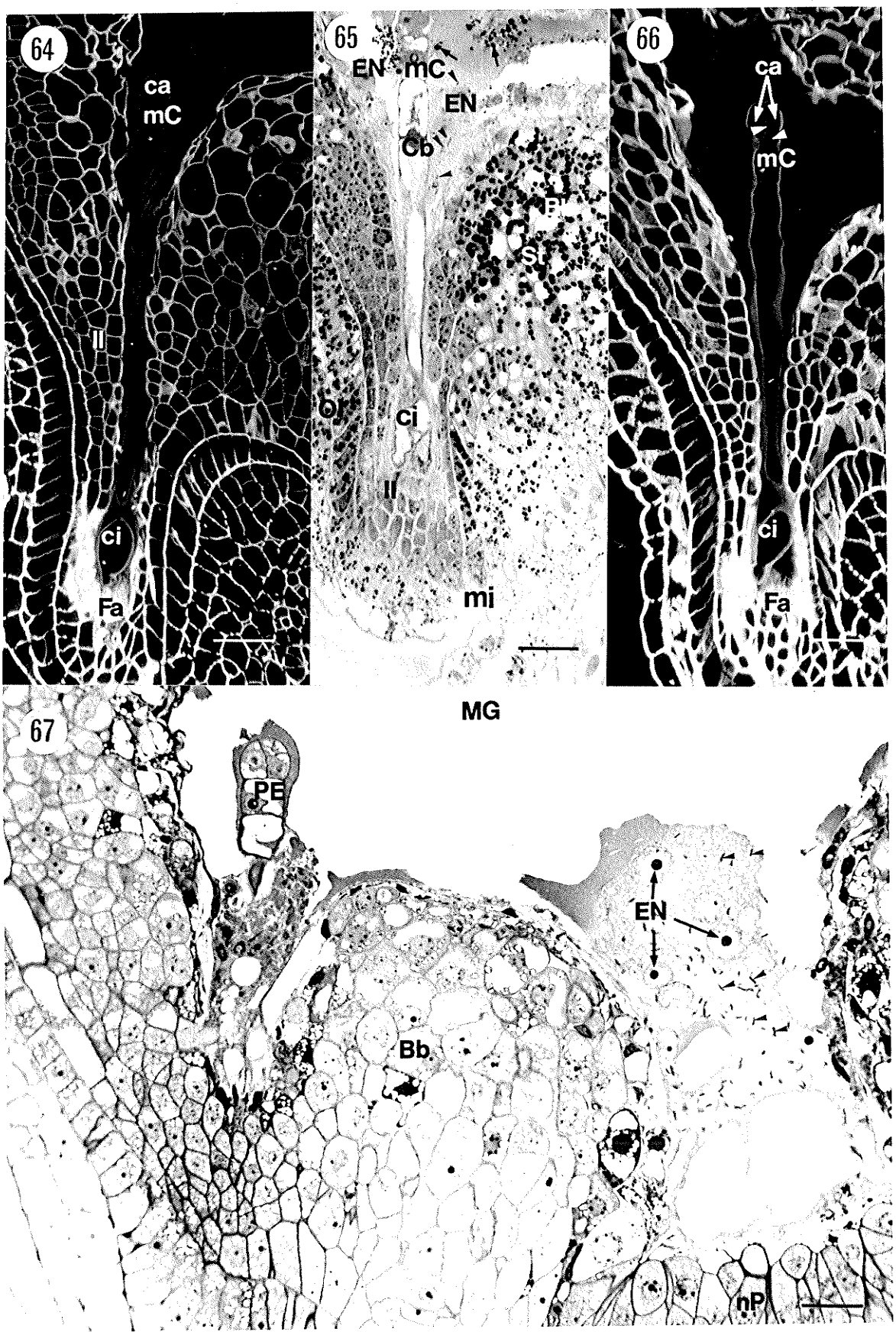
64
ca
mC
ll
ci
Fa
65
EN
mC
EN
Cb
P
S
Or
ci
ll
mi
MG
66
ca
mC
ci
Fa
67
PE
EN
Bb
nP

Figure 68 Light micrograph showing the products of an unsynchronized division of the apical sister cells forming a three-celled proembryo 120 hours after pollination. The apical cells show little vacuolation and the suspensor cell below the apex (*h*) is slightly vacuolated (v) and shows a nucleus surrounded by dark staining perinuclear bodies (arrow heads). The globular proembryo has not changed size at the base next to the suspensor cell; however, the upper third has an enlarged appearance. The central cell (cc) contains endosperm nuclei (EN) and lens shaped plastids (arrowheads). Crystal violet. Scale bar = 11.61 μm.

Figure 69 Light micrograph showing the quandrant embryo stage of an 8-celled proembryo 120 hours after pollination. The globular apex (*ca*) has little vacuolation and one sister cell shows a nucleus (N). The central cell (cc) shows lens-shaped plastids (arrow heads) and endosperm nuclei (EN) near the proembryo. Crystal violet. Scale bar = 11.61 μm.

Figure 70 Information gathered from serial sectioning shows diagrammaticly an eight-celled proembryo. The quandrant apical sister cells (*ca*) of the proembryo are symmetrical and slightly vacuolated (v). The suspensor unit includes the *h, k, f* and *ci* cells which are larger than the apical cells and exhibit a higher degree of vacuolation. The central cell (cc) also shows a certain degree of vacuolation and contains some edosperm nuclei (EN). Scale bar = 14.70 μm.

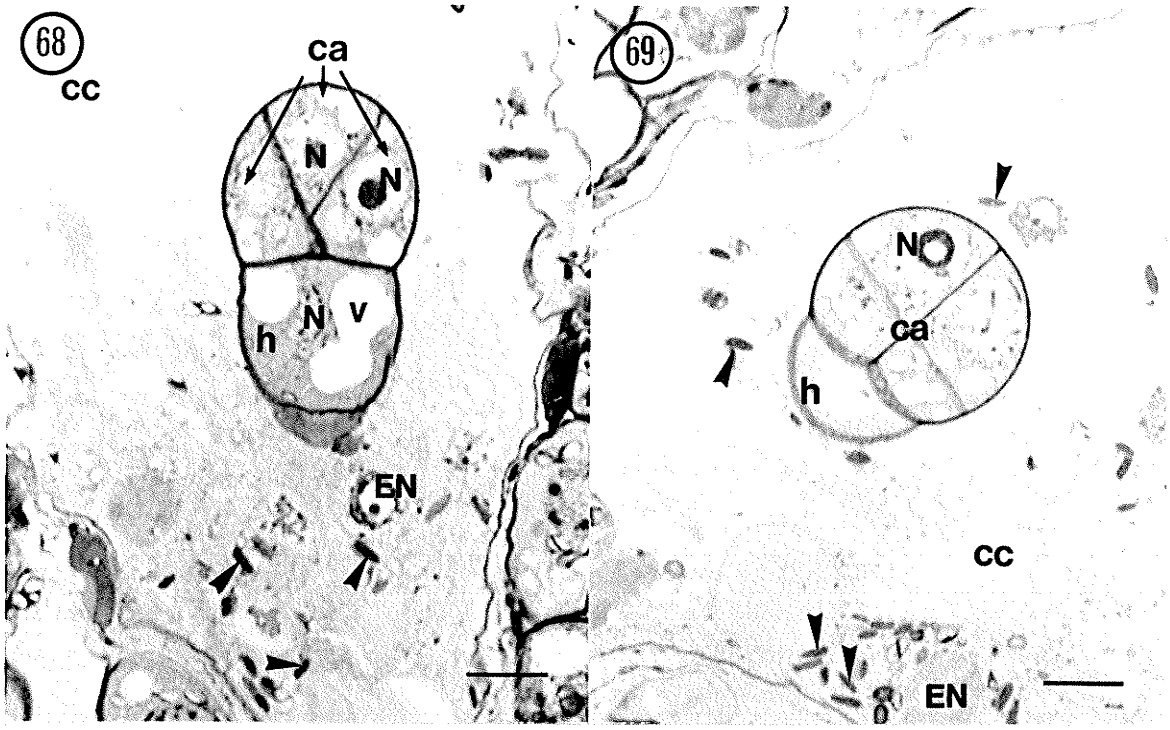
68
cc
ca
N
N
h
N
v
EN
69
N
ca
h
cc
EN

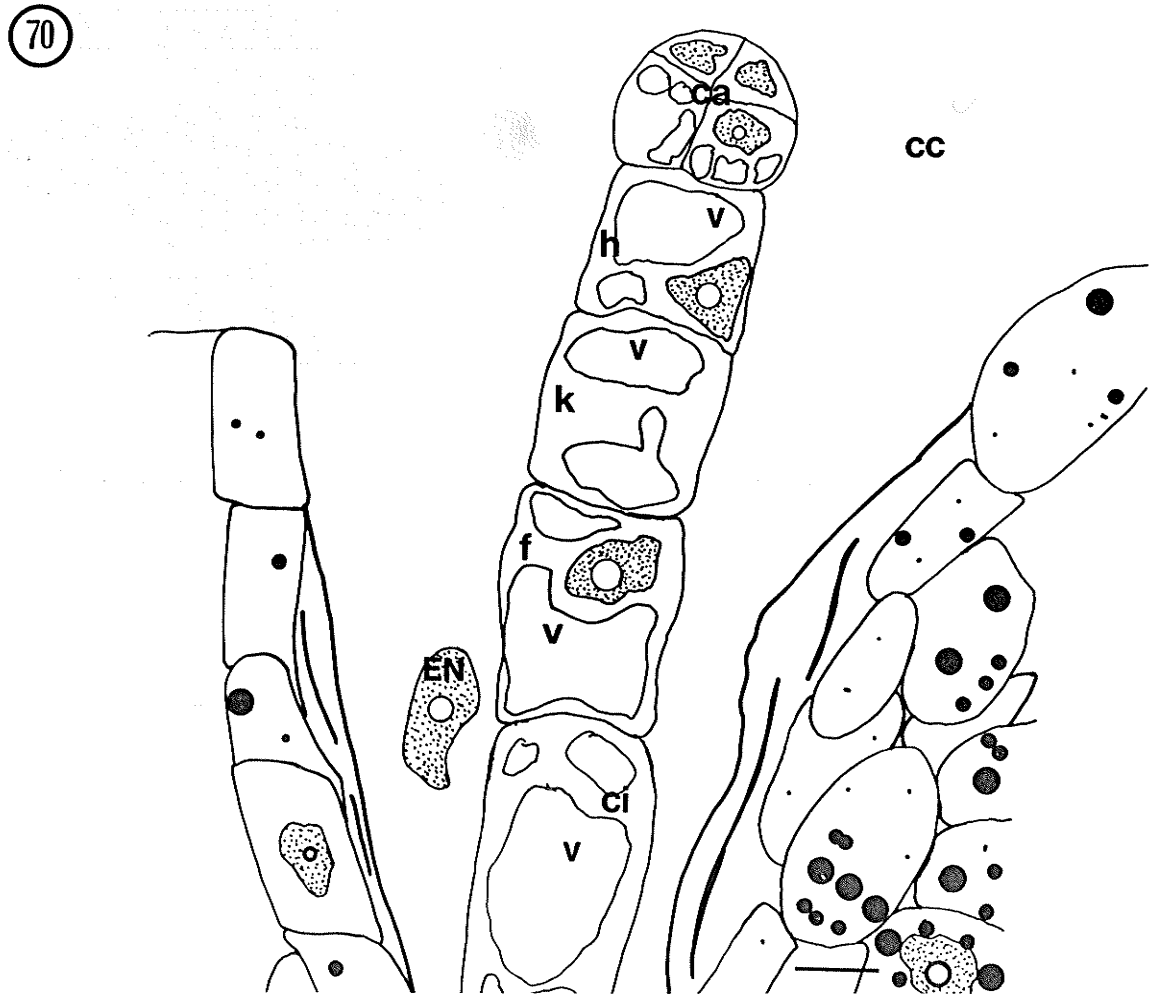
70
ca
cc
v
h
v
k
f
v
EN
ci
v

Figure 71 Electron micrograph showing the apical sister cells (*ca*) and the first suspensor cell (*m*C) of a seed 72 hours after pollination. Both apical cells show similar organelle composition and frequency. The apical cells show mitochondria (m), endopasmic reticulum (ER) and are highly vacuolated (v). The proembryo has the characteristic globular appearance with the upper 1/3 of the *ca* cells having a larger diameter than the base of the cell. The electron-transparent cell wall (cw) surrounding the apex is even in thickness; however, the common cell wall between sister cells appears thinner (arrows). The first suspensor cell (*m*C) shows a centrally located nucleus (N) between two large vacuoles (v). UA/Pb. Scale bar = 1.62 μm.

Figure 72 Electron micrograph showing the (*m*C) suspensor cell of a seed 72 hours after pollination. The *m*C cell shows two large vacuoles (v) on either side of a cytoplasmic band which contains a centrally located nucleus (N) with a dark staining nucleolus (Nu). Next to the nuclear membrane (arrow heads) are perinuclear mitochondria (m) and plastids (Pl). Other structures include several dictyosomes (D) with maturing vesicles (arrows) distributed throughout the cell; however, many appear near the lateral cell walls (cw) of the embryo. UA/Pb. Scale bar = 0.97 μm.

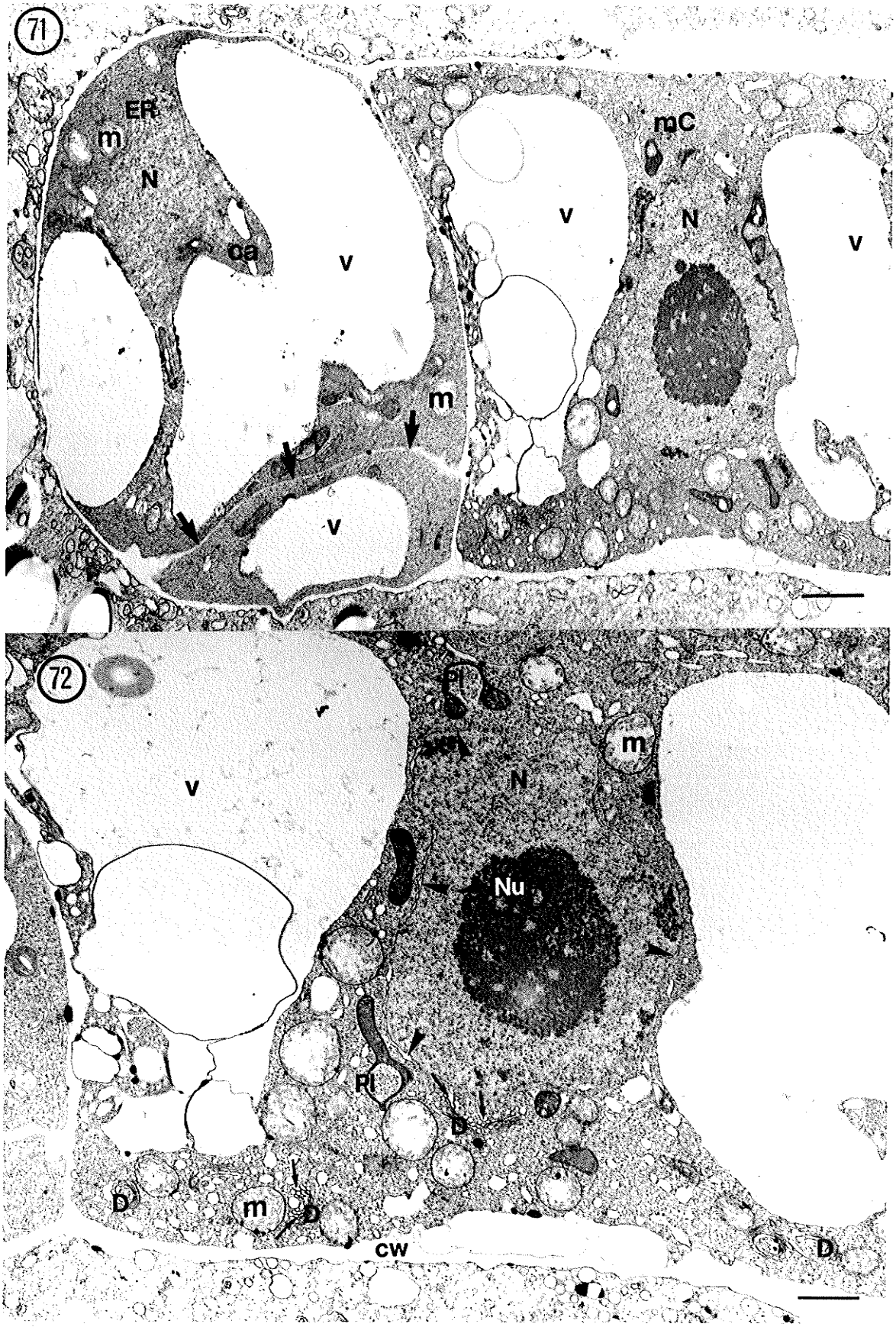
71
ER
m
N
ca
v
v
mC
N
v
m
v
72
v
Pl
m
N
Nu
Pl
D
D
m
D
cw
D

Figure 73 Electron micrograph showing the *m C* suspensor cell cytoplasm. Cytoplasmic composition includes the peppered appearance from the ribosomes, active dictyosomes (D) producing vesicles (Vs), and mitochondria (m) adjacent the proembryo cell wall (cw). The common electron transparent cell wall of the proembryo and central cell (cc) shows a dark staining middle lamella (arrow heads). The central cell contains few ribosomes with some bound to expanded vesicles near the cell wall (arrows). UA/Pb. Scale bar = 0.38 μm.

Figure 74 Electron micrograph showing the *mC* and *ci* suspensor cells of a seed 72 hours after pollination. The cross-section shows plasmadesmata (Pd) that traverse the common cell wall (cw). UA/Pb. Scale bar = 0.27 μm.

Figure 75 Electron micrograph showing the basal *ci* cell of a proembryo 72 hours after pollination. The centrally located nucleus (N) is surrounded by perinuclear mitochondria (m) and plastids (Pl) devoid of starch. Active dictyosomes (D) producing vesicles (Vs) are present as are periodic dilated strands of endoplasmic reticulum (ER). UA/Pb. Scale bar = 0.91 μm.


73
D
m
Vs
cw
D
Vs
D
m
74
mc
D
cw
Pl
75
m
ER
m
Pl
m
Vs
D
N
D
Pl

Figure 76 Electron micrograph showing the basal cell (*ci*) and central cell (cc) of a seed 72 hours after pollination. The *ci* cell cytoplasm shows more ribosomes and provides a more electron-opaque cytoplasm in comparison to the central cell. The *ci* cell contains mitochondria (m) and dictyosomes (D) near the electron-transparent common cell wall (cw). The central cell cytoplasm shows dark staining perinuclear bodies which appear to be phagocytosed by vesicles (arrows). Mitochondria (m), and transition vesicles (circles) appear throughout. UA/Pb. Scale bar = 0.65 μm.

Figure 77 Electron micrograph showing the basal cell *ci* cytoplasm of a seed 72 hours after pollination. The enlarged view of an active dictyosome (D) shows a forming face (FF) composed of segments of intermittent cisternae (arrows) which appear to coalesce forming larger individual golgi cisternae towards the maturing face (MF). Semi-transparent vesicles (Vs) appear to be released from the maturing face of the active cisternae. UA/Pb. Scale bar = 0.15 μm.

Figure 78 Electron micrograph of the central cell in a seed 68 hours after pollination. The central cell contains free nuclear endosperm (FNE) and shows plastids (Pl) with thylakoid stacks (arrows), mitochondria (m), active dictyosomes (D) producing vesicles (Vs), increased dilated endoplasmic reticulum (DER) and reduced vacuoles (v). UA/Pb. Scale bar = 0.80 μm.

Figure 79 Electron micrograph of the micropyle region of the central cell with free nuclear endosperm (FNE) cut in cross section. Starch (St) containing plastids (Pl) show thylakoid stacks (arrows). The FNE shows the well developed wall projections (Wp). UA/Pb. Scale bar = 1.08 μm.

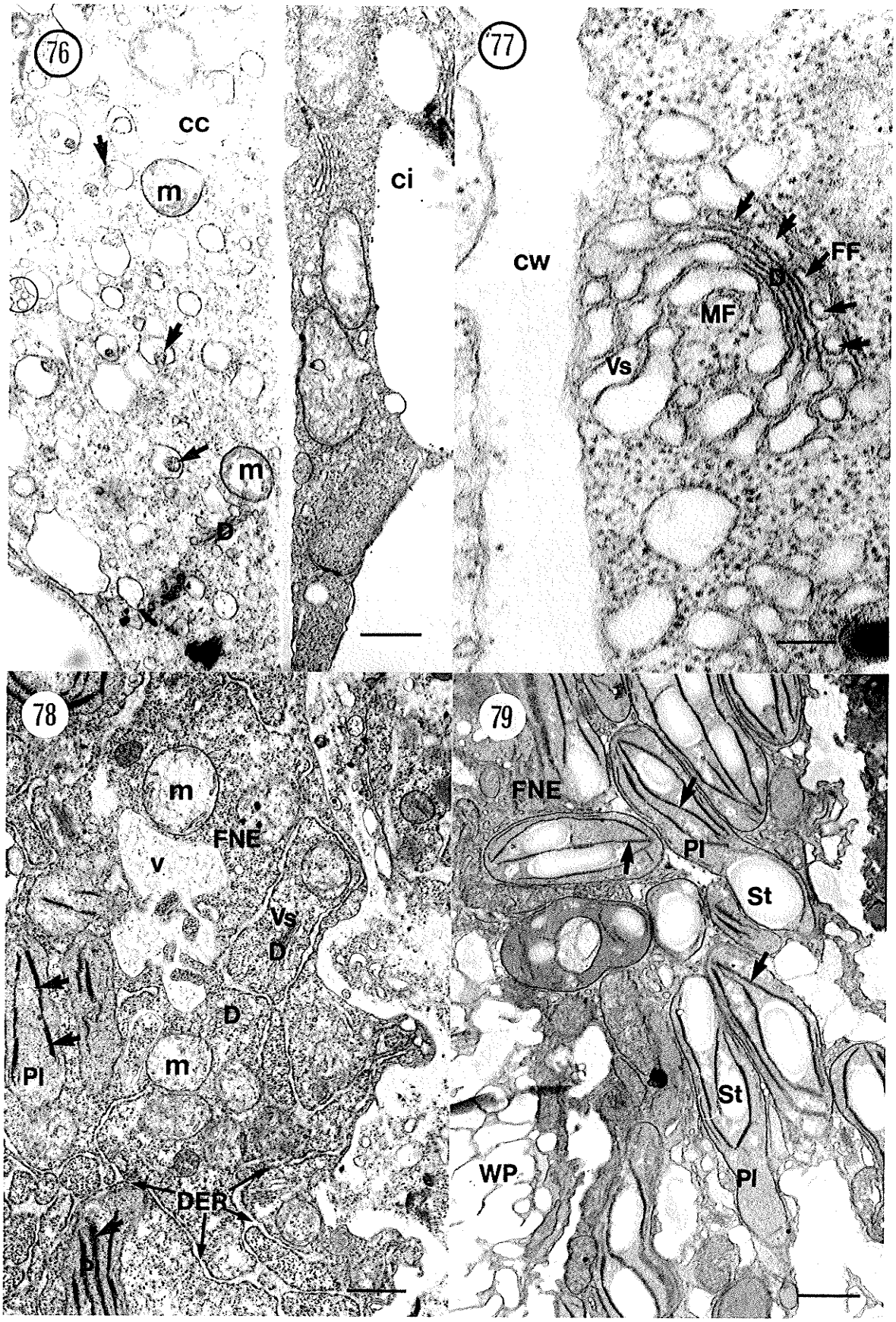
76
cc
m
m
D
ci
77
cw
FF
MF
Vs
78
m
FNE
v
Vs
D
D
m
Pl
DER
Pl
79
FNE
Pl
St
St
WP
Pl

Figure 80 Electron micrograph showing a longitudinal section through the centre of the basal suspensor cell (*ci*) 68 hours after pollination. The *ci* cell has a large central vacuole (v) and thin cytoplasm lining the inner surface of the cell wall (cw). The *ci* cytoplasm in this section contains mitochondria (m) along the length of the cell. The central cell containig free nuclear endosperm (FNE) shows dilated endoplasmic reticulum (DER), and plastids (Pl). The central cell is surrounded by a thick megagametophyte cell wall (open arrows). The megagametophyte wall is electron-transparent; however, dark staining bodies (arrows) in the cell wall and the cuticular (Cu) layer appears electron-opaque. UA/Pb. Scale bar = 1.31 μm.

Figure 81 Electron micrograph showing the micropyle portion of a basal cell (*ci*) 68 hours after pollination. The basal cell shows a high frequency of mitochondria (m) evenly distributed throughout the cytoplasm. The basal cell wall (cw) shows uniform thickness along its length; however, irregularities occur near the hook region (Zh). The basal cell wall projections invaginate the surrounding cytoplasm and increase cell wall surface area. The central cell nuclear endosperm (FNE) is electron-dense and shows a complex maze of convoluted electron-transparent central cell wall projections (Wp). UA/Pb. Scale bar = 0.52 μm.

Figure 82 Electron micrograph showing a higher magnification of the basal cell (*ci*) wall projections from figure 81. The micrograph shows the convoluted configuration of the *ci* wall projections (Wp). The finger-like projections have an electron-dense matrix (arrows) with electron-transparent margins (arrow heads). Small vesicles are seen in or near some of the wall projections of the suspensor cell (circles). UA/Pb. Scale bar = 0.46 μm.


80
Pl
ci
FNE
v
cw
m
Cu
m
DER
81
cv
ci
DER
Wp
FNE
Zh
m
ll
m
Wp
82
m
m
ci
Wp

Figure 83 Electron micrograph showing the micropyle portion of the *ca* and *d* cells. Plasmadesmata (Pd) appears between the elecron-transparent common cell walls of the *ca* sister cells and *d* suspensor cell. Both sister cells show mitochondria (m) and prominent dictyosomes (D) producing vesicles (Vs). UA/Pb. Scale bar = 0.46 μm.

Figure 84 Electron micrograph showing the *d* suspensor cell cytoplasm in a seed 84 hours after pollination. The cross-section reveals a centrally located nucleus (N) surrounded by perinuclear plastids (Pl). The cytoplasm is peppered with ribosomes and shows mitochondria (m), active dictyosomes (D) with vesicles (arrows), endoplasmic reticulum (ER) and the electron-transparent cell wall (cw). UA/Pb. Scale bar = 1.14 μm.

Figure 85 Electron micrograph showing a magnified view of the *d* suspensor cell cytoplasm. Mitochondria (m), plastids (Pl) and some micro-bodies (Mb) appear near the nuclear envelope (arrow heads). Also shown is endoplasmic reticulum (ER) and many ribosomes. UA/Pb. Scale bar = 0.38 μm.

Figure 86 Electron micrograph showing a portion of the *d* suspensor cell (d) cut in cross section and the central cell free nuclear endosperm (FNE). The central cell has an endosperm nuclei (EN), mitochondria (m), long strands of rough endoplasmic reticulum (RER) and three configurations of plastids. Plastids (Pl) containing starch (St), plastids with prominent thylakoids (arrow heads) and plastids containing only starch (arrows). UA/Pb. Scale bar = 1.14 μm.

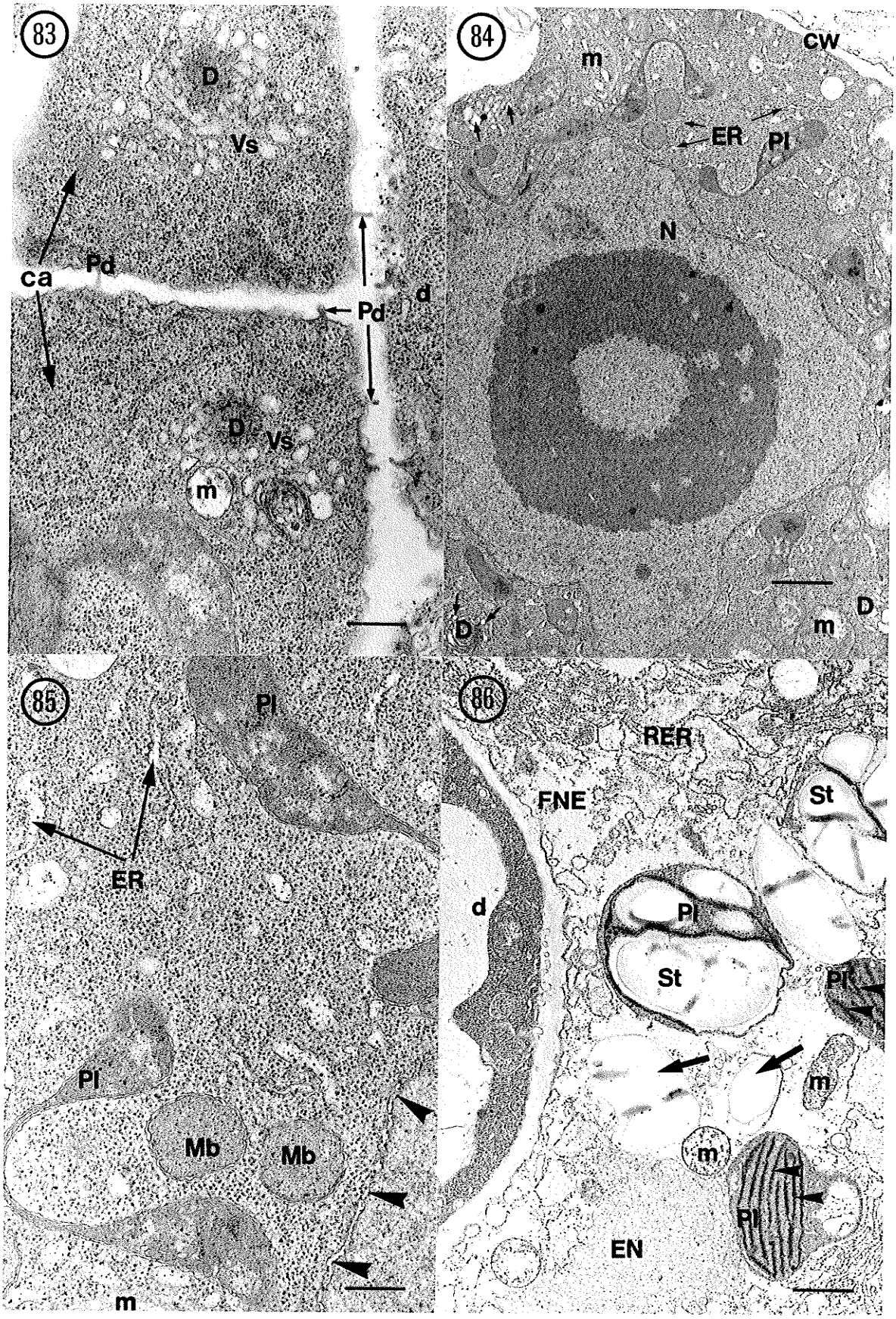
83
D
Vs
ca
Pd
Pd
d
D
Vs
m
84
m
CW
ER
Pl
N
D
D
m
85
Pl
ER
Pl
Mb
Mb
m
86
RER
FNE
St
d
Pl
St
Pl
m
m
Pl
EN

Figure 87 Electron micrograph showing the cell wall interface between the central cell (cc) and the *d* and *f* cells of a proembryo 84 hours after pollination. The cell wall (cw) shows some density at the middle lamella (mL), but the margins are electron-transparent and plasmadesmata (Pd) are shown between the cells of the suspensor; however, they are non-existent between the proembryo and the central cell. UA/Pb. Scale bar = 0.30 μm.

Figure 88 Electron micrograph showing the darkly stained f cell cytoplasm 84 hours after pollination. The portion of cytoplasmic strand shows a duck-shaped tonoplast (arrow heads) which extends into the vacuole and reveals a dense community of organelles such as mitochondria (m), active dictyosomes (D) producing vesicles (arrows), plastids (Pl) with no starch and ribosomes. UA/Pb. Scale bar = 0.91 μm.

Figure 89 Electron micrograph showing an expanded view of the chalazal end of the *d* cell in figure 86. The central cell free nuclear endosperm (FNE) shows isolated starch grains and starch (St) containing plastids (Pl) which also show reduced thylakoid stacks (arrows). Within the central cell and *d* cell is a common cell wall (cw) with electron-transparent margins (arrow heads) and an increasingly dense matrix at the middle lamella (mL). Convoluted cell wall projections (open arrows) appear radiating into the common cell wall from the *d* cell plasma membrane. UA/Pb. Scale bar = 0.23 μm.

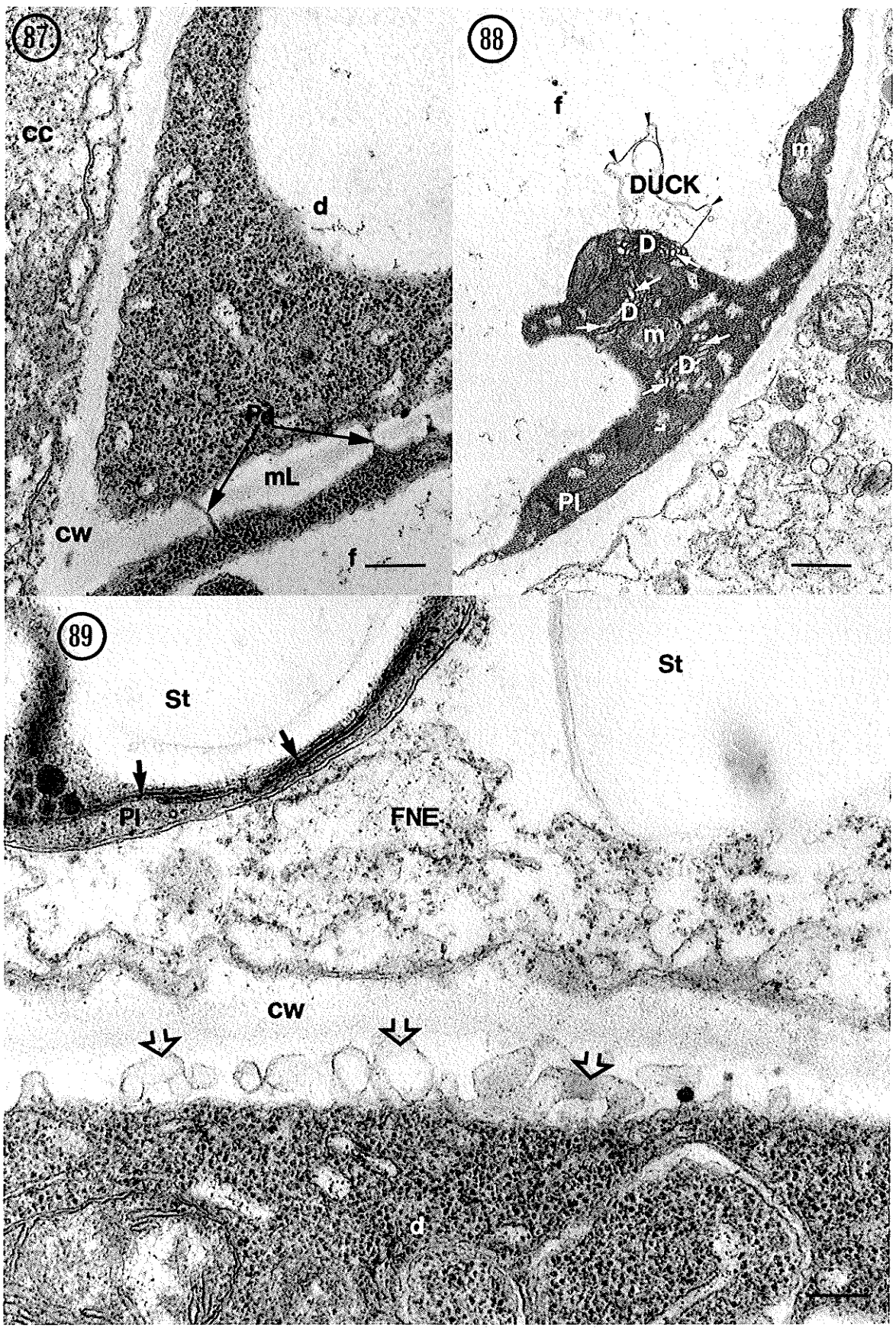
87
cc
d
Pl
mL
CW
f
88
f
DUCK
D
D
m
D
Pl
89
St
St
Pl
FNE
CW
d

Figure 90 Electron micrograph showing the f suspensor of a seed 84 hours after pollination. The dictyosomes (D) are located in the thin cytoplasm with the forming face (FF) next to the vacuole (v) and the maturing face towards the common cell wall (cw). The maturing vesicles (Vs) pinching off the ends of the cisternae are near the plasma membrane (arrows). Two large paramural bodies (PM) are shown adjacent the *f* cell plasmadesmata. UA/Pb. Scale bar = 0.11 μm.

Figure 91 Electron micrograph showing the central cell free nuclear endosperm (FNE) near the *f* suspensor cell of a seed 84 hours after pollination. Rough endoplasmic reticulum (RER) in the central cell is surrounded by few ribosomes in comparison with the *f* cell. The *f* cell shows a paramural body (PM) which appears to be a component of the common cell wall (cw). UA/Pb. Scale bar = 0.15 μm.

Figure 92 Electron micrograph showing dictyosomes in the developing *f* suspensor cell of a proembryo 84 hours after pollination. Each dictyosome (D) cut in cross-section shows the forming face (FF) and a maturing face (MF). Vesicles (Vs) appear to be pinching off the ends of the individual cisternae. The vesicles appear to be directed towards the plasma membrane (Pm) or the tonoplast (T). UA/Pb. Scale bar = 0.11 μm.

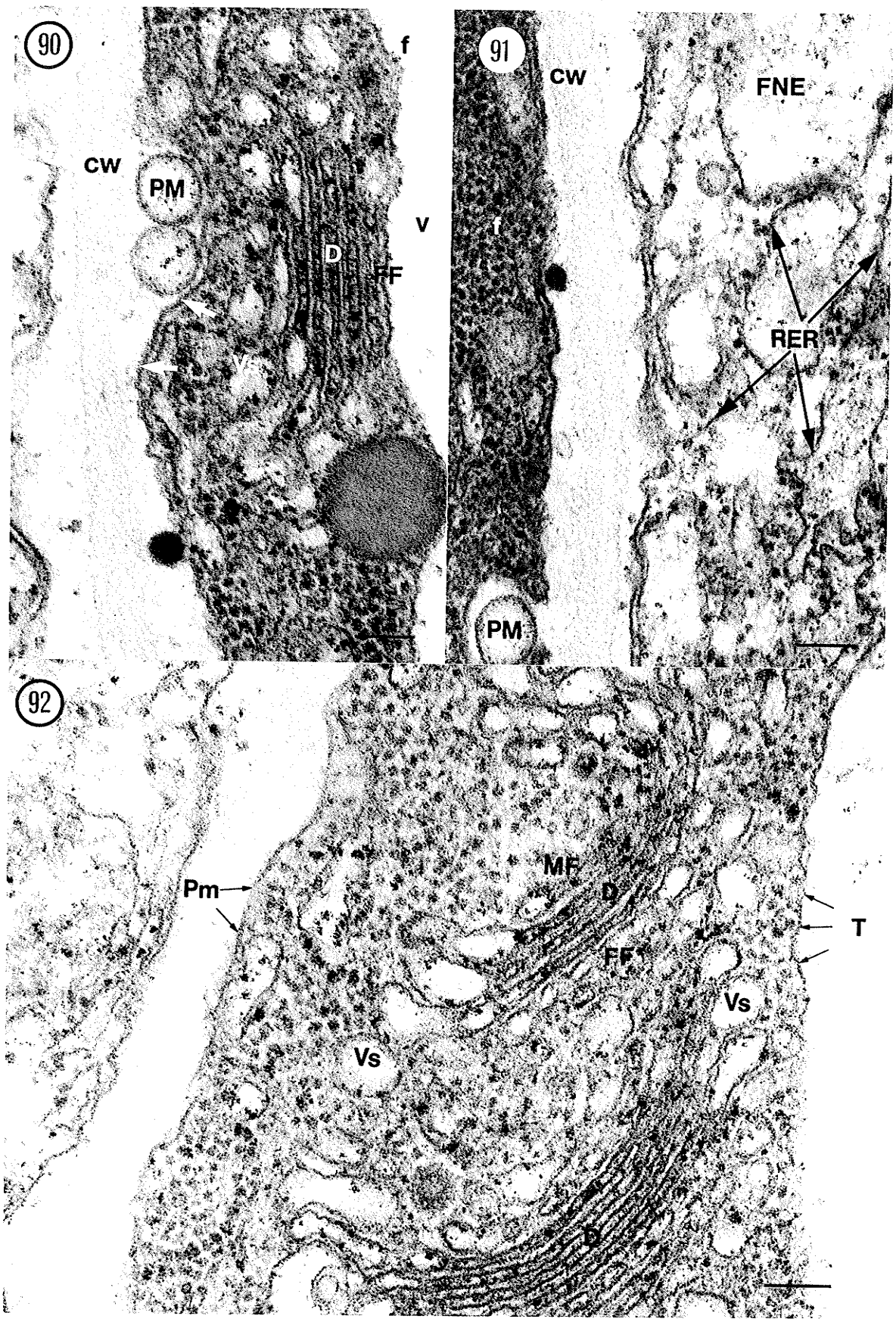
90
f
CW
PM
V
D
FF
91
CW
FNE
f
RER
PM
92
Pm
MF
D
T
FF
Vs
Vs

Figure 93 Electron micrograph showing the *f* suspensor cell cytoplasm in a seed 84 hours after pollination. The *f* suspensor cell of the proembryo cut in cross section has cytoplasmic strands (arrows) extending through a large central vacuole (v). The electron-transparent cell wall (cw) around the circumfernce of the *f* cell is even in thickness. The cytoplasm contains mitochondria (m) and dictyosomes (D) and vesicles (arrow heads). Scale bar = 0.65 μm.

Figure 94 Electron micrograph showing the *f* suspensor cell of the proembryo and the central cell free nuclear endosperm (FNE) in a seed 84 hours after pollination. The cross-section reveals a centrally located nuclues (N) in a cytoplasmic band bordering the cell wall (cw). Next to the developing embryo in the central cell are starch (St) grains, mitochondria (m) and large strands of rough endoplasmic reticulum (RER). Scale bar = 1.83 μm.

Figure 95 Electron micrograph showing the endosperm nuclei (EN) from figure 94. The nuclues (N) has a distinct nuclear membrane (arrows) and shows numerous perinuclear mitochondria (m). The central cell free nuclear endosperm (FNE) also contains ribosomes and rough endoplasmic reticulum (RER). The *f* suspensor cell shows a more electron-opaque cytoplasm in relation to the free nuclear endosperm and also contains several mitochondria and ribosomes. UA/Pb. Scale bar = 0.91 μm.

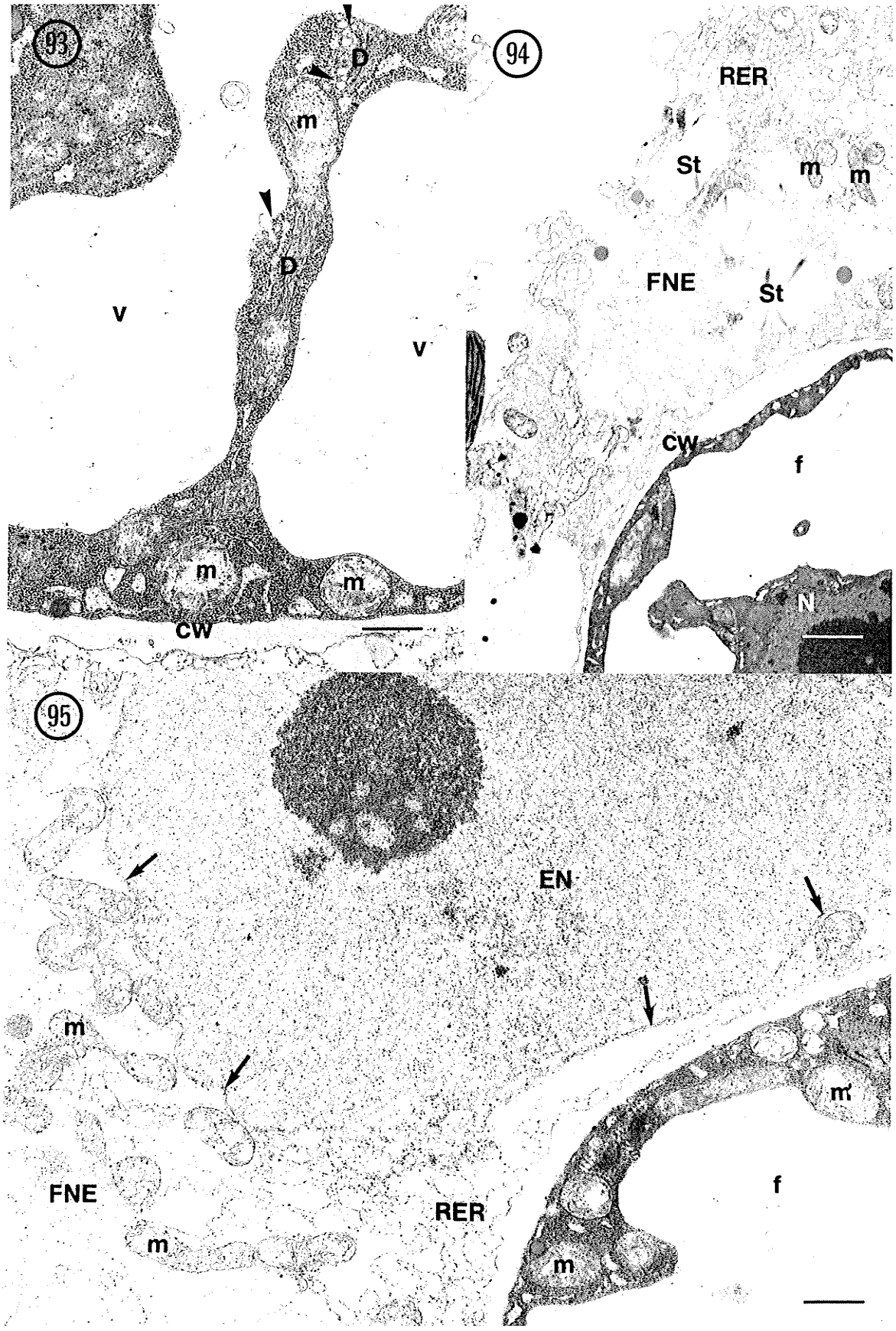
93
D
m
D
v
m
m
CW
94
RER
St
m
m
FNE
St
v
CW
f
N
95
EN
m
FNE
m
RER
m
f
m

Figure 96 Electron micrograph showing the *f* and *ci* suspensor cells in a seed 84 hours after pollination. The *f* cell has a more electron-opaque cytoplasm than the *ci* cell. The *f* cell has a large central vacuole (v). The *ci* cell shows a large central vacuole as well as many small vacuoles. The walls (cw) surrounding the two cells have similar electron density and there are no plasmodesmata. UA/Pb. Scale bar = 1.27 μm.

Figure 97 Electron micrograph showing the common cell wall (cw) between the *f* and *ci* suspensor cells in a seed 84 hours after pollination. The *f* cell cytoplasm contains mitochondria (m) and long strands of endoplasmic reticulum along the cell wall (arrow heads). Plasmadesmata (Pd) are shown within the common cell wall. UA/Pb. Scale bar = 0.70 μm.

Figure 98 Electron micrograph showing the *f* suspensor cell and the central cell free nuclear endosperm (FNE) of an embryo 84 hours after pollination. The active dictyosomes (D) in the *f* cell cytoplasm appear to release vesicles (Vs) towards the tonoplast (T) of the cell. A vesicle at the top left of the micrograph appears to have fused with the tonoplast (arrows). The central cell shows large expanded rough endoplasmic reticulum (RER). UA/Pb. Scale bar = 0.26 μm.

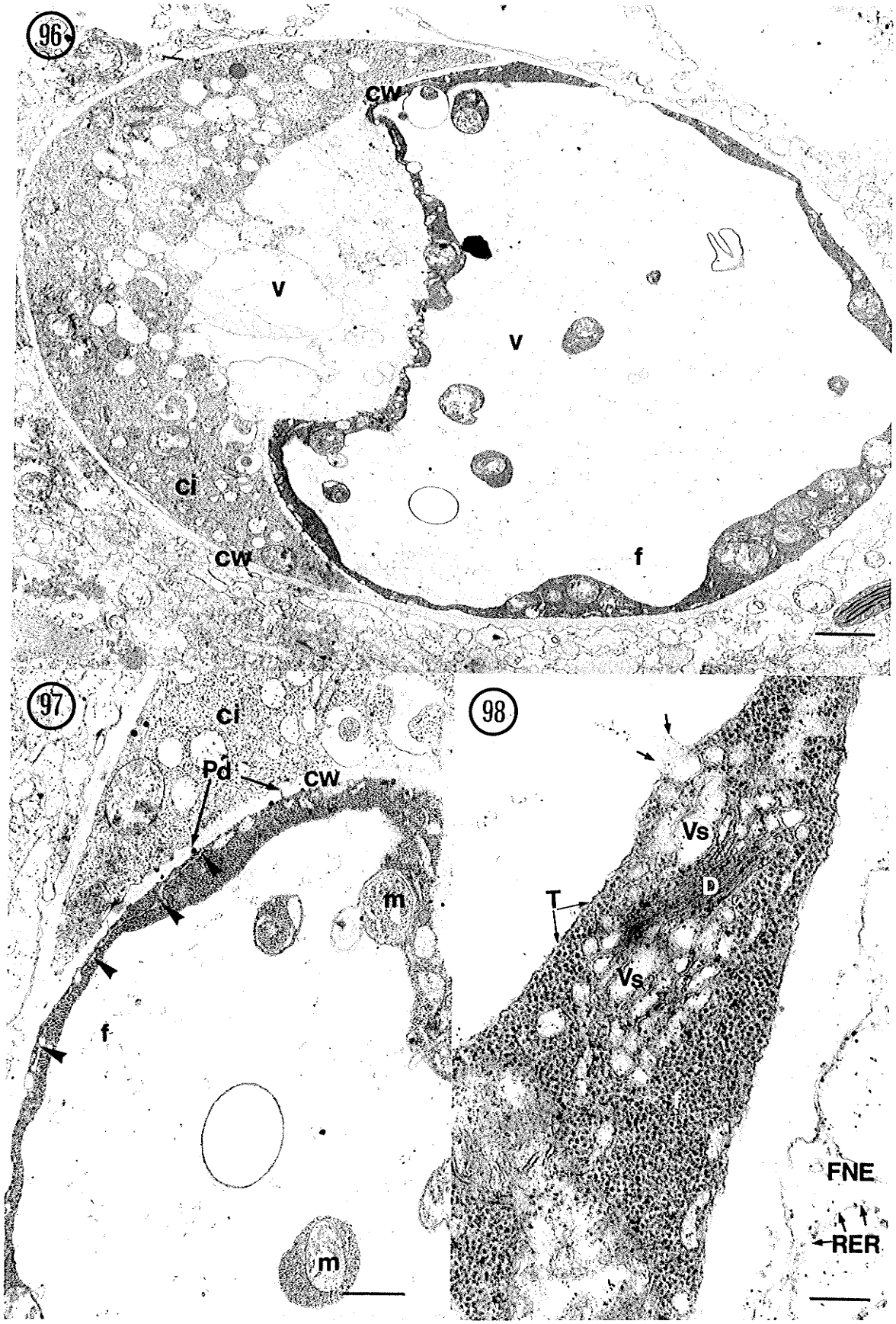
96
cw
v
v
ci
cw
f
97
ci
Pd
cw
m
f
m
98
Vs
D
T
Vs
FNE
RER

Figure 99 Electron micrograph showing the *ci* suspensor cell of an proembryo 84 hours after pollination. The cross-section reveals the proembryo *ci* cell surrounded by a cell wall (cw) of even thickness. The cytoplasm is shown near the cell wall and contains many vacuoles (v) of various sizes occupying a large portion of the cell volume. The cell has a centrally located nucleus (N) which is surrounded with perinuclear plastids (Pl) containing no starch. Mitochondria (m), dictyosomes (D), endoplasmic reticulum (arrows) are located near the cell wall and are less frequent than the plastids. UA/Pb. Scale bar = 0.96 μm.

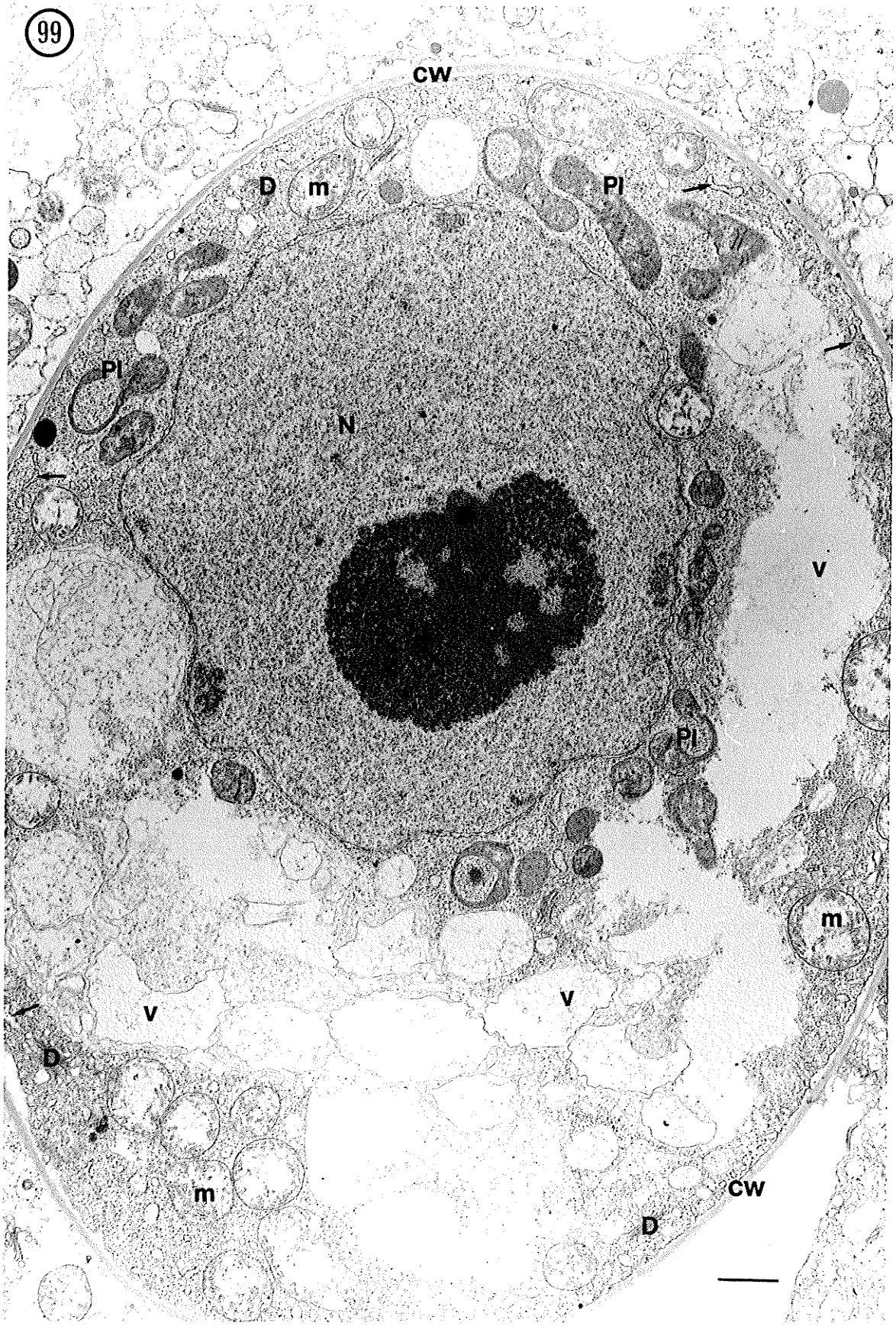
99
CW
D
m
Pl
Pl
N
V
Pl
m
V
V
D
m
CW
D

Figure 100 Electron micrograph showing the central portion of the *ci* suspensor cell of an proembryo 84 hours after pollination. The cross-section reveals that the cell diameter is reduced when approaching the micropyle. The large central vacuole (v) is ringed by cytoplasm which shows mictochondria (m), endoplasmic reticulum (arrows), active dictyosomes (D) microbodies (Mb) and vesicles (circles) bordering the cell wall (cw). Other small paramural bodies (open arrows) are shown beyond the plasma membrane (arrow head) next to the cell wall. The central cell free nuclear endosperm (FNE) has a heterogeneous appearance surrounded by a thick inner integument (II) cell wall which reveals an electron-dense cuticle (Cu). UA/Pb. Scale bar = 0.97 μm.


100
m
CW
m
Mb
m
v
D
Mb
CW
D
Cu
II

Figure 101 Electron micrograph showing the micropylar portion of the *ci* suspensor cell of an proembryo 84 hours after pollination. The circular *ci* suspensor cell is located in the centre surrounded by the central cell free nuclear endosperm (FNE) which is contained by a ring of crushed inner integument (cII) cell wall material and an electron-dense cuticle (arrows). The layer of crushed integument cells are adjacent three cell layers of inner integument (II) followed by several more outer integument (OI) cell layers. UA/Pb. Scale bar = 3.86 μm.

Figure 102 Electron micrograph showing inner integument of the seed. The cell cytoplasm shows starch (St) containing plastids (Pl), circular mitochondria (m) and a dark staining stack of endoplasmic reticulum (ER) adjacent the nucleus (N). KFeCN. Scale bar = 0.77 μm.

Figure 103 Electron micrograph showing inner integument of the seed. The cytoplasm shows starch (St) containing plastids (Pl), long strands of endoplasmic reticulum (arrows) and elongated mitochondria (m) located along the cell wall. KFeCN. Scale bar = 0.77 μm.

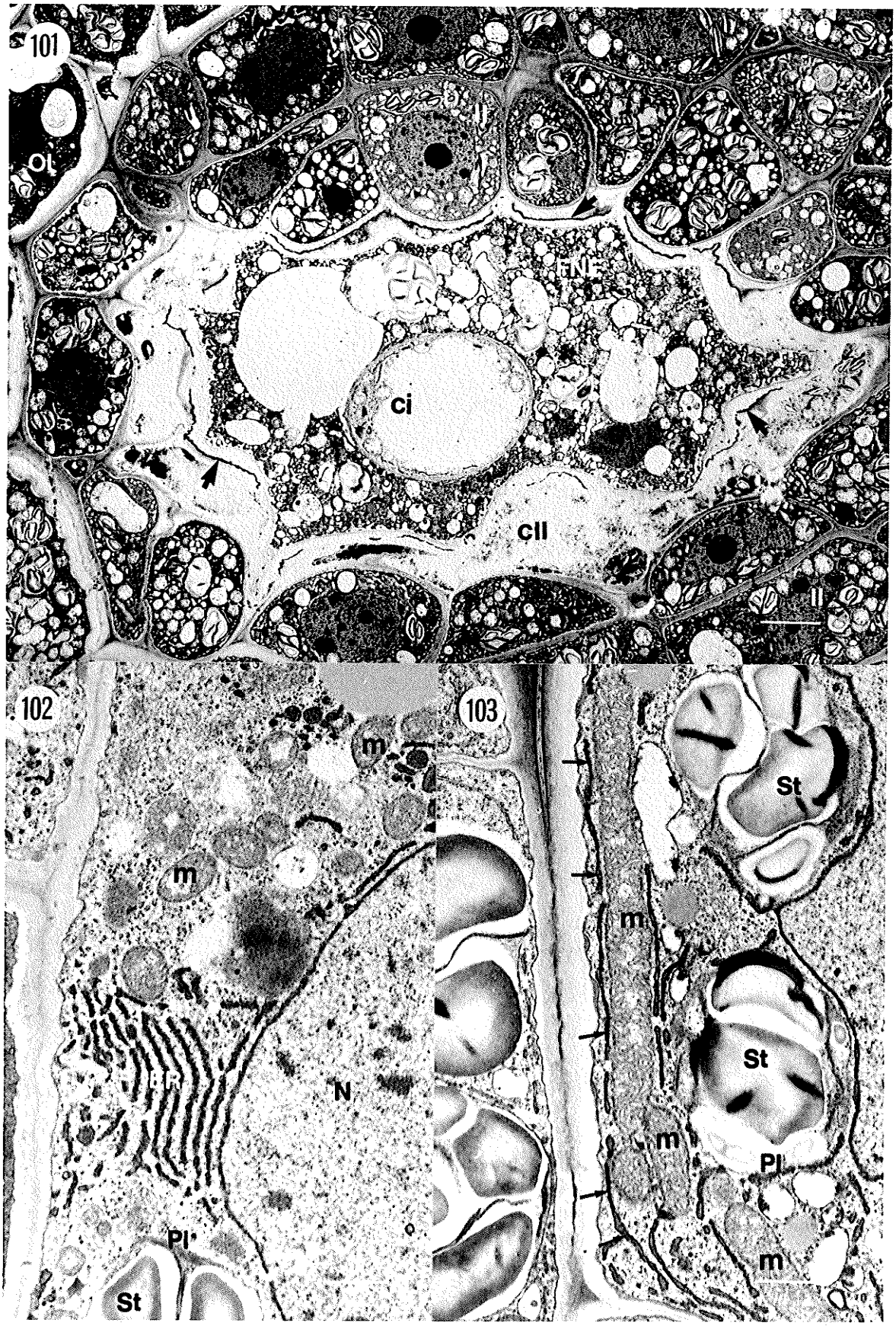
101
Ot
II
FNE
Ci
CII
II
102
m
m
N
Pl
St
103
St
m
St
m
Pl
m

Figure 104 Electron micrograph of microtubules (arrows) adjacent to the lateral wall of inner integument cells. The microtubules are near the cell wall (cw), adjacent the plasmadesmata (Pd). UA/Pb. Scale bar = 0.19 μm.

Figure 105 Electron micrograph showing the inner integument (II) cells, and the central cell free nuclear endosperm (FNE) in a developing seed 84 hours after pollination. The central cell is bordered by a layer of crushed inner integument (cII) which forms a barrier around the megagametophyte. Beyond the cII is the inner integument cells. The inner integument cells appear typical; however, they show the presence of extremely dilated endoplasmic reticulum which contains striated inclusions cut in cross and longitudinal sections (arrows). KFeCN. Scale bar = 2.05 μm.

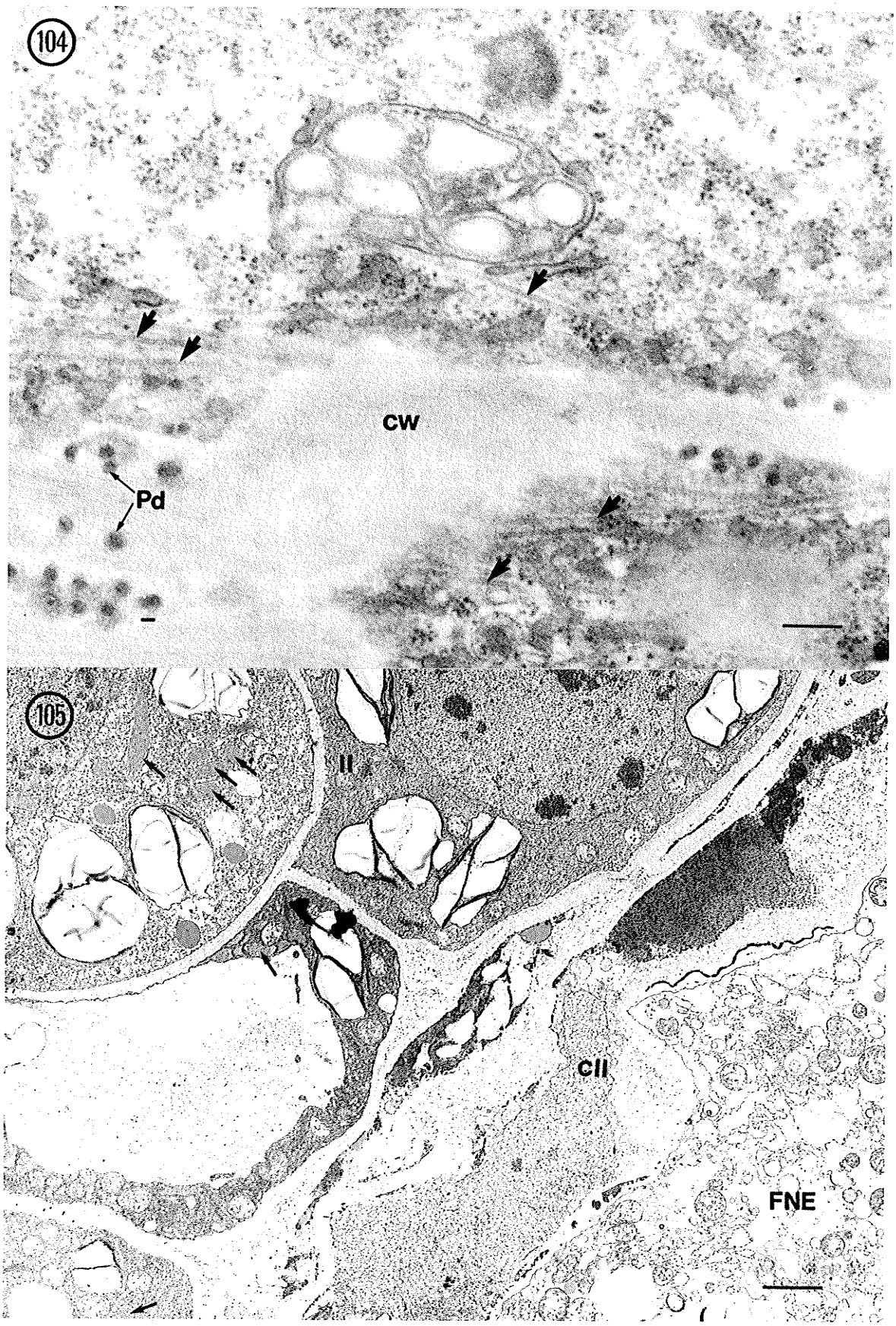
104
CW
Pd
105
II
CII
FNE

Figure 106 Electron micrograph showing the striated inclusions cut in cross section of the integument cell in a seed 84 hours after pollination. The outer membrane has ribosomes adjacent to it (arrows). The striated inclusions give the dilated endoplasmic reticulum a "honey comb" appearance. UA/Pb. Scale bar = 0.23 μm.

Figure 107 Electron micrograph showing dilated endoplasmic reticulum with striated inclusions sectioned longitudinally (arrows). UA/Pb. Scale bar = 0.14 μm.

Figure 108 Electron micrograph representing the control for the PATCH-SP staining technique in the integument cells. Note the lipids (L) and endoplasmic reticulum (arrows) reacted positively; however, the large starch grains did not react with the stain. Scale bar =0.69 μm.

Figure 109 Electron micrograph of the inner integument cells stained using PA-TCH-SP. The large starch grains and the cell wall of the integument cell reacted positively and exhibited a granular electron opaque appearance. Scale bar = 0.24 μm.

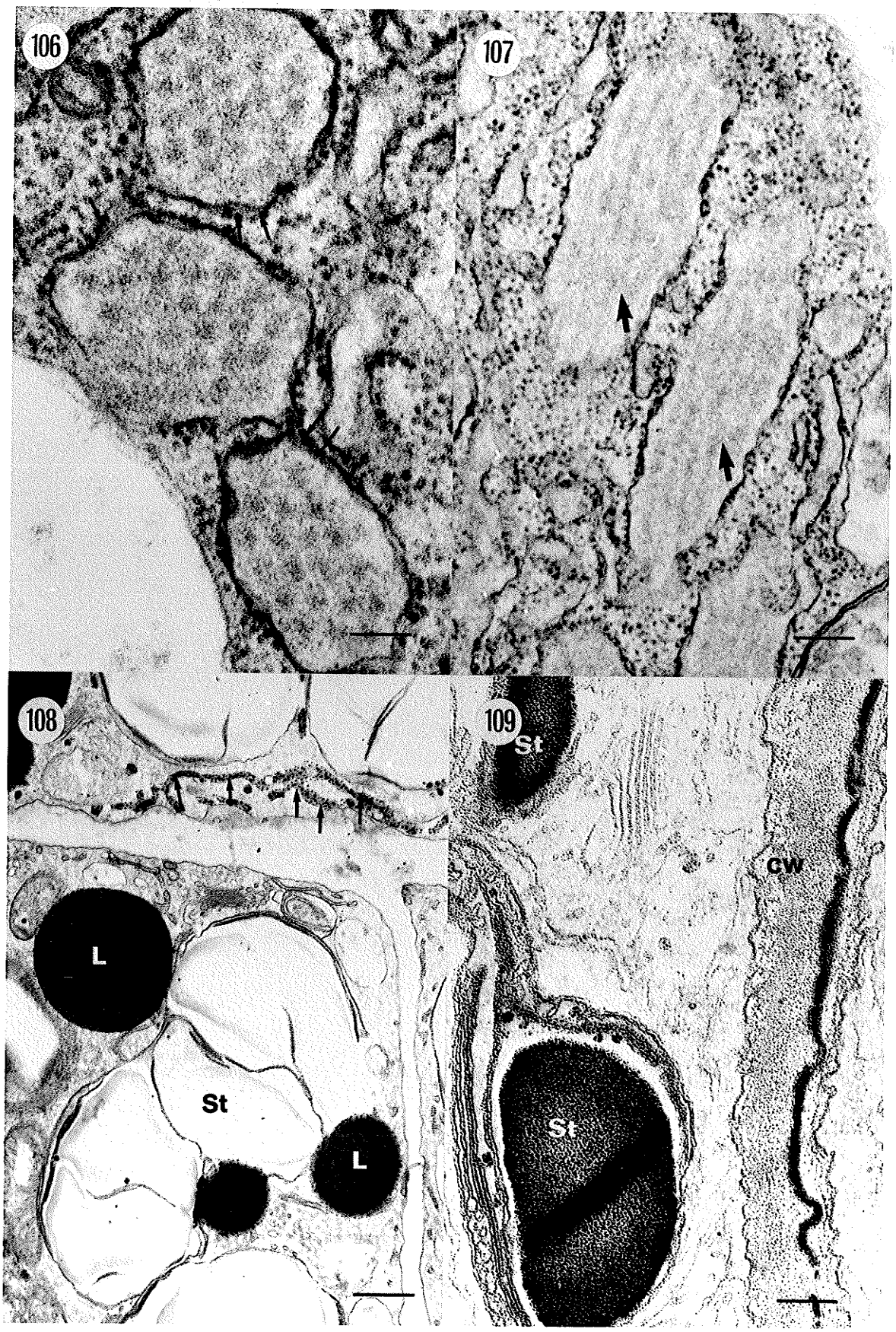
106
107
108
L
St
L
109
St
St
CW

Figure 110-112 Light micrograph of a aberrant ovule 22 hours after pollination. Figure 110 and 111 were prepared for bright field microscopy and figure 112 is the same section prepared for epifluorescence microscopy.

Figure 110 Light micrograph showing the polar nuclei (pN) and synergid (S) cells of an normal appearing megagametophyte. The filiform apparatus end of the synergids protrudes out of the micropyle normally enclosed by the inner (II) and outer (OI) integument cell layers. The chalazal portion of the megagametophyte shows the presence of nucellar tissue (NU). Crystal violet. Scale bar = 14.75 μm.

Figure 111 Light micrograph showing the starch (St) distribution in the aberrant ovule in figure 110. The longitudinal section shows a large number of PAS-positive starch (St) grains in the micropyle (mi) inner integument (II) layers surrounding the megagametophyte. PAS. Scale bar = 11.61 μm.

Figure 112 Epifluorescence micrograph of figure 111 stained with calcofluor and viewed under UV light The calcofluor-positive filiform apparatus (Fa) is shown protruding out of the micropyle (mi). A slightly calcofluor-positive synergid (S) cell wall (arrow heads) is shown in the megagametophyte. Calcofluor. Scale bar = 11.61 μm.

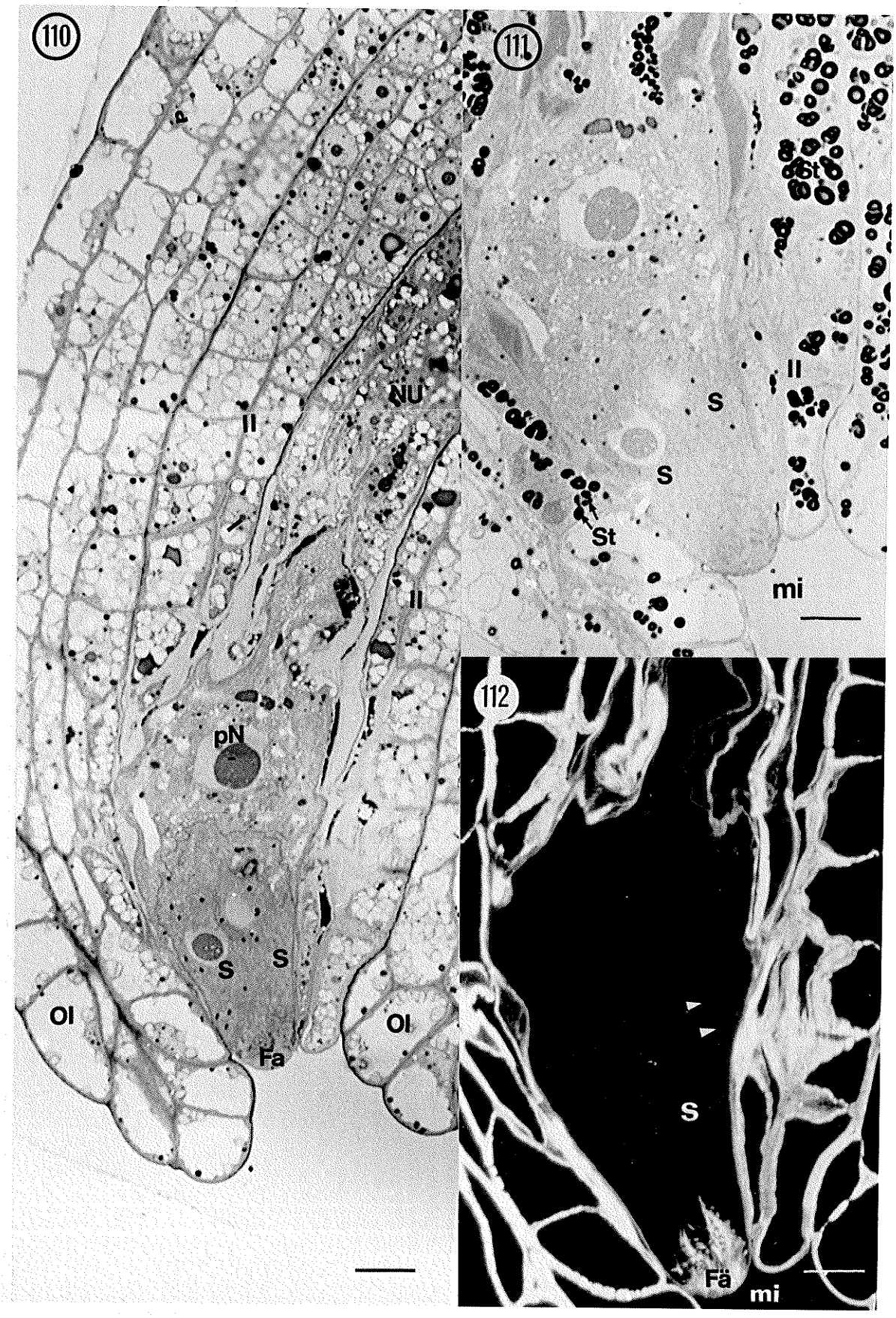
110
a
NU
Il
Il
pN
S
S
Ol
Ol
Fa
111
St
St
S
S
Il
mi
112
S
Fä
mi

Figure 113 Light micrograph of aberrant ovule 10.5 hours after pollination. The nucellar epidermis (arrow heads) surrounds nucellar tissue (Nu) in the area of normal megagametophyte development; however, there is no evidence of megagametophyte development. The largest PAS- positive starch accumulations are in the inner (II) and outer (OI) integuments at the micropyle (mi). Reduced starch is shown in the chalazal nucellus and raphe region of the ovule (Ra). This ovule is similar in size to a fertile seed 10.5 hours after pollination. PAS/ABB. Scale bar = 11.61 μm.

Figure 114 Light micrograph of a aberrant 96 hours after pollination. The nucellar epidermis (arrowheads) surrounds nucellar tissue (Nu) in the area of normal megagametophyte development; however, there is no evidence of megagametophyte development. The inner integument (II) basal body does not contain starch. A large open space (open arrow), adjacent the nucellus, appears to be a preparation artifact. Fertile seeds 96 hours after pollination show a morphology similar to the 96 hour aberrant ovule. PAS/ABB. Scale bar = 46.45 μm.

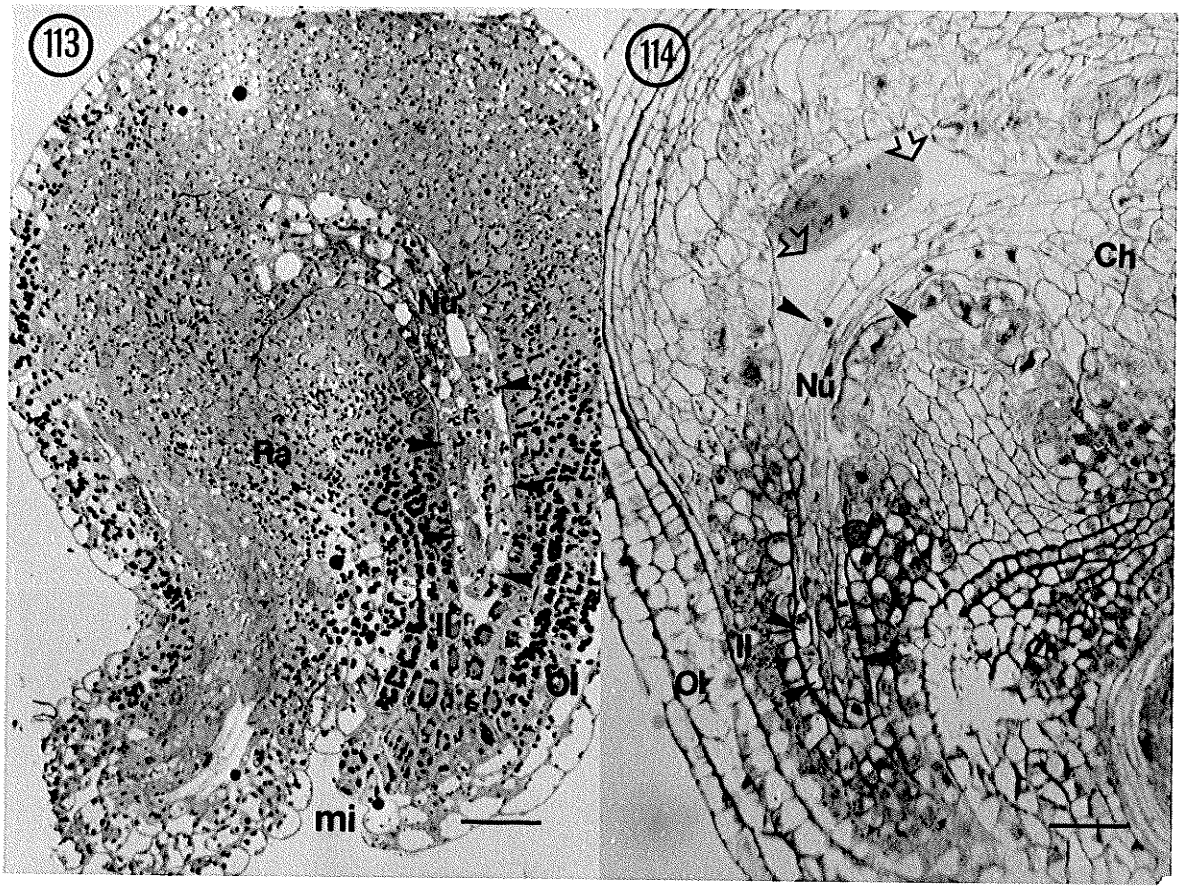
113
Ra
Nu
Il
Ol
mi
114
Ch
Nu
Il
Ol

5.0 Discussion

5.1 Pre-Fertilization Development of the Egg

Prior to fertilization, the egg cell of *Brassica napus* L. cv. Regent (Canola-Rapeseed) is cone-shaped and shows definite polarization. The chalazal 1/3 of the egg cell is occupied by the nucleus and contains much of the cytoplasm (Figs 4, 15, 18). The remaining 2/3 of the egg cell is occupied by a large vacuole. Egg cell polarity has been demonstrated in many species such as *Arabidopsis* (Mansfield *et al.* 1991a) and *Brassica campestris* (Sumner and VanCaeseele 1989); however, in *Stipa*, vacuole size and distribution differ from the above mentioned (Maze and Lin 1975).

Although the egg cell polarity is similar in many species, cytoplasmic ultrastructure may vary greatly. The egg cell cytoplasm of *Brassica napus* is similar in composition to *Zea mays, Spinacia, Brassica campestris* and *Helianthus* (Diboll and Larson 1966, Wilms 1981a, Sumner and VanCaeseele 1989, Yan *et al.* 1991). The chalazal cytoplasm of *Brassica napus* shows perinuclear plastids containing some starch, numerous mitochondria and a few lipid droplets. The presence of starch and lipid deposits in the cytoplasm suggests the accessibility of energy reserves to the egg upon fertilization. Dictyosomes present throughout the cytoplasm and near the cell walls appear quiescent, producing few vesicles. Cytoplasmic ultrastructure of *Brassica napus* varies greatly with *Petunia*, which show few mitochondria, plastids and dictyosomes (Went 1970b).

In many species including *Capsella, Epidendrum,* and *Arabidopsis* (Schulz and Jensen 1968b, Cocucci and Jensen 1969, Mansfield *et al.* 1991b) polarization has been shown to occur prior to fertilization; however, in

Gossypium polarization occurs after fertilization (Jensen 1968a). Little is known about the purpose or the induction of polarization in the developing egg cell.

It is unknown if polarization is important for fertilization and if polarization is maintained in the unfertilized *Brassica napus* egg after anthesis because most of the material observed in this study was fertilized.

5.1.1 Synergids

The development of the synergid cell prior to fertilization in *Brassica napus* is similar to that described in *Brassica campestris* and *Capsella* (Sumner and VanCaeseele 1989, Schulz and Jensen 1968a). After fertilization, the persistent synergid appears metabolically active prior to the extensive zygote elongation phase where it shows similar staining characteristics as the degenerate synergid (Fig 47). In seeds older than 96 hours after pollination, no evidence of the dark staining synergid cytoplasm remains (Fig 60).

Following fertilization, the cell wall of the persistent synergid appears discontinuous at the chalazal end of the cell (Figs 36, 39). The lack of a synergid cell wall in this region allows the synergid and central cell cytoplasm to mix. Similar observations by Sumner (1986) and Schulz and Jensen (1968a) report cytoplasmic mixing in *Brassica campestris* and *Capsella* respectively. These observations suggest the persistent synergid cell is a preferential route of metabolite translocation directly into the central cell early in the embryogenesis. The synergid cell translocation is suspected to continue provided the cell remains viable. For example, in *Helianthus* the persistent synergid is observed up to the heart-stage of embryogenesis (Newcomb 1973b).

In the *Plumbago* egg cell, Russell (1989) describes a filiform-like structure which simulates the synergid filiform apparatus complex of most species. In *Brassica napus,* only the calcofluor-positive synergid filiform apparatus remains present in the megagametophyte after the synergid cells degenerate (Fig 60). This suggests that the synergid filiform apparatus has an important role during embryogenesis other than possible nutrient translocation and is suspected to have a role in synergid viability. Russell and Mao (1990) also speculate the filiform apparatus is linked to the synergid degeneration; however, conclusive evidence is lacking. Although the role of the degenerate synergid could not be linked directly to the pollen tube, the constant success of the pollen tube in identifying the micropyle and eventually the megagametophyte synergid cell remains a mystery (Fig 6). Russell *et al.* (1990) speculate the degenerate synergid participates in pollen tube guidance through a chemical manifestation; however, conclusive evidence identifying the chemotropic chemical is lacking.

5.2 Post-Fertilization, Pre-Division Development of the Zygote

In *Brassica napus,* a loss of polarity occurs soon after fertilization. Consequently, there is a reorganization of the cytoplasm and the migration of the irregular shaped nucleus to a central position (Fig 36). Reorganized cytoplasmic polarity has also been shown in *Zea mays* (Lammeren 1981) and *Papaver nadicaule* (Olson and Cass 1981); however, in these species the nucleus is situated at the micropyle end of the egg prior to fertilization and migrates to the chalazal end following fertilization. In post-pollinated *Brassica campestris* , Sumner (1992) mentions the pre-fertilization movement of the egg nucleus to a central position. Zaki and Dickinson (1990) observed a similar nuclear migration

from a peripheral location to a central position in *Brassica napus* microspore cultures. This evidence suggests the pre-fertilized nuclear migration is a normal developmental sequence not influenced by external factors.

Several small vacuoles, distributed throughout the *Brassica napus* zygote, replaces the single pre-fertilized egg vacuole. Although fragmentation of the large pre-fertilized egg vacuole probably reduces the cell size, the cytoplasmic volume appears to remain constant. A few larger vacuoles are shown clustered at the chalazal end of the cell. In the young non-polarized *Brassica napus* zygote, vacuoles forming at the chalazal end suggest the initiation of ampuliform elongation. Vacuolar distribution in the young *Brassica napus* zygote appears to be similar to the post-fertilized *Arabidopsis* zygote recently described by Mansfield *et al.* (1991b).

Upon fertilization, the *Brassica napus* zygote exhibits a slight reduction in size. Similar observations were made in *Capsella* (Schulz and Jensen 1968b) and *Brassica campestris* (Sumner 1992); however, Schulz and Jensen (1968b,c) show that the zygote increases in size for a short period of time after the initial reduction in size. The loss of vacuolation probably causes a sudden reduction in turgor resulting in a reduction of cell size. When a decrease of cell turgor pressure occurs, signs of plasmolysis are shown in the *Brassica napus* zygote; however, the zygote cell is not destroyed. Plasmolysis in figure 36 suggests fixation artifact; however, a portion of the plasmolysis is probably caused by a normal development reduction in cell turgor. Little is known what causes the reduction in turgor or subsequent plasmolysis; although in a review, Schnepf (1986) indicates the disturbance in cell polarity is probably caused by plasmolysis. Sumner (1986) also reports a change in polarity in *Brassica*

campestris and suggests the immature zygote will sustain less injury resulting from plasmolysis because the zygote cell walls contain little cellulose. In *Brassica napus,* a reduced calcofluor-positive reaction of the young zygote cell walls indicates a similar lack of cellulose (Fig 31).

Ultrastructural observations of the chalazal 1/3 of the young *Brassica napus* zygote showed regions of electron-opaque material in the common zygote central cell wall. Similar electron-opaque deposits have been shown in *Capsella* (Schulz and Jensen 1968b), *Plumbago* (Russell 1983) and *Brassica campestris* (Sumner and VanCaeseele 1989). Russell speculates the purpose of electron-opaque deposits are to stabilize the egg cell during fertilization; however, Sumner and VanCaeseele (1989) suggest the electron-opaque deposits in the central cell zygote common wall helps prevent zygote plasmolysis during zygote shrinkage by stabilizing the plasma membranes of both the central and zygote cells. The absence of the electron-opaque deposits at the chalazal pole of the mature *Brassica napus* zygote suggests the deposits have an important developmental role prior to the extensive elongation phase. Observations of the young *Brassica napus* zygote support the adhesion theory proposed by Sumner and VanCaeseele (1989).

Ultrastructural investigations of *Gossypium* (Jensen 1968a,b), *Capsella* (Schulz and Jensen 1968b,c) and *Epidendrum* (Cocucci and Jensen 1969) show an increase in organelles such as endoplasmic reticulum, ribosomes and clusters of plastids and mitochondria near the nucleus of the zygote cell. Similar observations were made in *Brassica napus.* Additional observations in *Brassica napus* reveal the reduction and relocation towards the ampuliform chalazal tip of the PAS-positive perinuclear starch grains present earlier in the egg cell (Fig 30), and the

increase of lipid droplets throughout the zygote. The increase in energy producing organelles such as mitochondria and plastids suggests the zygote is preparing for an energy requiring process. A review by Natesh and Rau (1984) supports this observation and suggests that high metabolic activity is achieved in the enlarging zygote by an increase in the numbers of mitochondria and plastids. As the zygote matures, the insoluble starch and lipid bodies disappear. A similar reduction of starch in *Arabidopsis* (Mansfield *et al.* 1991b) and oil droplets in *Jasione Montana* (Erdelská and Klasovà 1978) during the early zygote elongation has also been reported and suggests starch and lipids provide a readily available energy source in the initial stages of zygote elongation.

In *Brassica napus,* dictyosomes with little active vesicle production and short strands of rough endoplasmic reticulum are shown throughout the zygote with some strands lining the plasma membrane. Although it was not possible to show wall synthesis, the presence of these organelles suggests a possible involvement with cell wall synthesis. In *Epidendrum, Nicotiana,* and *Helianthus* an increased number of active dictyosomes, and endoplasmic reticulum adjacent the cell wall after fertilization implies dictyosomes may be involved in cell wall formation (Cocucci and Jensen 1969, Mogensen and Suthor 1979, Yan *et al.* 1991). Salisbury and Ross (1991) indicate golgi vesicles released from dictyosomes probably fuse with the plasma membrane of a plant cell increasing membrane surface area. The vesicles incorporated into the plasma membrane contain wall material synthesized in the dictyosomes including the cellulose synthase complex described by Herth (1985). Mizuta and Brown (1992) confirm cellulose is synthesized in the plasma membrane; however, they propose a

more elaborate cellulose synthase model than the "rosette" type described by Herth (1985).

In species such as *Capsella* (Schulz and Jensen 1968b), *Epidendrum* (Cocucci and Jensen 1969), *Papaver* (Olson and Cass 1981) and *Brassica campestris* (Sumner and VanCaeseele 1989) a partial cell wall exists prior to fertilization. Sumner (1992) has shown cytological changes within the cell wall of the developing zygote using calcofluor, which will stain β 1-4 glucans such as cellulose, in combination with enzymatic extraction. Cellulosic material visualized in the egg and immature zygote cell walls of *Brassica campestris* are similar to those observed in *Brassica napus*.

Soon after fertilization, a complete PAS-positive cell wall surrounded the *Brassica napus* zygote; however, a calcofluor-positive reaction in the cell walls of this immature zygote at the micropyle suggested the presence of cellulose. At the initiation of the ampuliform elongation, the entire zygote shows a PAS-positive reaction for non-cellulosic cell wall (Fig 30). When stained with calcofluor, a positive reaction for cellulose deposition occurs in the cell walls at the micropyle and the lateral cell walls; however, a reduced or no reaction for cellulose is shown at the chalazal tip of the zygote 22 hours after pollination. The *Brassica napus* zygote undergoes an extensive elongation phase (Fig 47). When stained with calcofluor the zygote shows a poor fluorescence at the chalazal tip suggesting diminished amount of cellulose material in the cell wall (Fig 48). In the cell wall of *Brassica napus*, cellulose appears to provide rigidity and permanence. Verneulenen and Wessels (1984) indicate a complex of β D-glucans and chitin in the hyphal cell walls of *Schizophylum commune* increased stability. Therefore, areas of the zygote lacking cellulose suggests the cell walls have plastic properties.

This permits the zygote cell wall adjustments, resulting from sudden changes in turgor such as the reduction in the recently fertilized egg and rapid zygote cell elongation. Early investigations by Folsom and Peterson (1984) suggest synthesis of cellulosic wall material is related to dictyosomes near the cell wall; however, an investigation by Herth (1985) and Mizuta and Brown (1992) shows convincing evidence that cellulose synthesis occurs at the plasma membrane.

Twenty two hours after pollination, the zygote cell begins to show initial ampuliform elongation at the chalazal portion of the zygote (Figs 30, 35). The ampuliform development shown in this investigation is not apparent in *Capsella* (Schulz and Jensen 1968a,b) or *Arabidopsis* (Mansfield *et al.* 1991b) and is not mentioned by Tykarska (1976) in *Brassica napus*; however, Sumner (1992) showed the ampuliform development in *Brassica campestris*. Forty eight hours after pollination, the elongated basal cell is 58μm in length. The chalazal and middle regions are narrow (13 μm) in comparison to the proximal end of the cell (Figs 45, 46). Seventy two hours after pollination, the seed shows an extended zygote 235 μm of length (Figs 47, 48) positioned deep into the free nuclear endosperm. Similar zygote and early proembryo developmental patterns were shown in *Arabidopsis* and *Capsella* (Mansfield *et al.* 1991b, Schulz and Jensen 1968a,b) Previous studies by on *Brassica napus* (Tykarska 1976) indicate that the post-cytokinetic proembryo including the apical cell is 45-55 μm in length . From Tykarska's interpretive diagrams, it appears extensive basal cell elongation occurs after apical cell formation; however, photographic evidence gathered during this study indicates much of the *Brassica napus* proembryos length is acquired prior to basal cell division.

5.2.2 Cell Polarity and Elongation.

According to Schnepf (1986), factors including the plasma membrane, cell walls, phytohormones and cell turgor may influence cell polarity and cell elongation. Two types of polarity are shown in the developing *Brassica napus* zygote cell. The most visible change in polarity involves the cytoplasm and the second change in polarity is obscure and involves the zygote cell walls.

Cytoplasmic polarity occurs in a cell when there is an uneven distribution of organelles in different parts of the cell. This is the case with *Brassica napus* zygote prior to the first basal cell division The cytoplasm stains more intensely with aniline blue-black at the chalazal apex. This region was showed to have little vacuolation and contains the nucleus. The cytoplasmic polarization which occurs in the elongated zygote is probably essential for continued embryo development since it positions the nucleus and a large portion of the cytoplasm at the chalazal pole prior to the first cell division. Perinuclear and chalazal PAS-positive starch grains of the pre-ampuliform stage of development are absent in the cytoplasm suggesting nutrition is provided to the developing zygote and future embryo by other means (Figs 47, 49).

In *Brassica napus* the central portion of the zygote is occupied by a large unstained vacuole. The size of the vacuole increases as the zygote enlarges and appears to maintain cytoplasmic cell polarity throughout cell development. When describing the zygote cell development process, the importance of the large central vacuole is often overlooked. Ultrastructural investigations suggest that the vacuoles are formed by vesicles derived from golgi and endoplasmic reticulum (Salisbury and Ross 1991). Vesicles from the transface of *Brassica napus* zygote cell

dictyosomes appear destined for the tonoplast (Figs 92, 98). The large centrally located vacuole shown in the mature zygote was probably formed by the coalescence of smaller pre-existing vacuoles within the immature depolarized zygote and the membrane-forming organelles described above. Boller and Wiemken (1986) indicate that vacuoles have an important role maintaining homeostatic functions in plant cells. This includes regulation of the cytoplasmic proton concentration (pH), osmotic adjustments (K^+ Cl^-), cytoplasmic inorganic ions (Ca^{+2}) and intracellular partitioning of newly assimilated photosynthates. Of all vacuole functions, cell turgor pressure within the zygote cell is the most interesting since it probably affects cell polarity and cell wall elongation.

Cell walls may also be important in maintaining cytoplasmic polarity. Investigations by Burgess and Linsted (1982) show that naked moss protoplasts regained cytoplasmic polarity once a cell wall is formed. This evidence indicates that plant cell walls and plasma membrane are important for cytoplasmic polarity.

Polarity is also expressed as an increasing gradient of cellulose deposition from the proximal to the distal end of the elongating *Brassica napus* zygote cell wall. A similar cellulose gradient has been described in the caulonema tip cells of the *Funaria* moss by Reiss *et al.* (1984) and in *Brassica campestris* zygote by Sumner (1992). The change in cell wall chemistry in *Brassica napus* occurs after the loss of cytoplasmic polarity with cellulose deposition increasing in the proximal end of the zygote cell wall once turgor is restored and elongation begins. Sumner (1986) indicates that reduced cell volume and increased cellulose deposition in the cell wall of the post-anthesis *Brassica campestris* egg cell do not occur unless the egg is fertilized. This implies the loss and subsequent

restoration in cell turgor after fertilization in *Brassica napus* and *Brassica campestris* may trigger cellulose synthesis in the elongating zygote cell walls. Variations in cytoplasmic and cell wall polarity occur throughout zygote development and appear to halt prior to cell division. This suggests polarity in the zygote cell influences cell elongation and its termination.

Cosgrove (1987) proposed that irreversible plant cell elongation results from water absorption and cell wall yielding. He explains the normal plant cell wall is maintained reversibly stretched because of pressure placed on "load-bearing" parts of the cell wall by the protoplast. The first step of the proposed "Yield / Creep" cell elongation theory occurs when the cell wall "yields". This results in an elongation of the plastic element in the cell wall and a contraction of the elastic elements with relatively unchanged cell wall dimensions. Cell wall yielding causes an immediate reduction in cell turgor pressure and water potential. In an effort to maintain a minimum cell turgor, the cell increases its volume by water influx which subsequently elongates the elastic elements of the cell wall. This portion of cell elongation is referred to by Cosgrove (1987) as "Creep".

Although wall yielding is shown experimentally in plants, there is a lack of conclusive evidence to explain the mechanism which triggers this process. Hormones have been speculated to induce cell wall loosening. Ray (1987) reviewed the acid growth theory which proposed auxins caused a reduction in cell wall pH by activating cell wall degrading enzymes that were inactive at higher pH. Kutschera *et al.* (1987) questioned this theory and indicated that other factors were involved, since maize coleoptile experimentation showed treatments where auxins did not cause wall

loosening. The most recent attempts to explain cell wall loosening have been simplified by Salisbury and Ross (1991) who suggested that hormones (auxins) activate enzyme synthesis in the plasma membrane, which probably loosen cell walls. However, this has never been proven.

Few reports in the literature have shown conclusive evidence outlining the mechanisms controlling the direction and termination of cell elongation. In the young *Brassica napus* zygote, the apex has been shown to lack the stabilizing matrix of cellulose. The apex would then be a preferred site for a reduction in cell wall load. The direction of cell growth in the *Brassica napus* zygote could, therefore, be in part directed by the gradient of cellulose deposition within the cell walls. No other investigations to date speculate on the influence of cell wall polarity in directing cell elongation; however, it is interesting to note that a similar cell wall gradient has been reported in the elongating cells of fungal hyphae (Vermeulen and Wessels 1984).

Schnepf (1986) proposes that the termination of cell elongation occurs when a physical barrier is encountered. However, in *Brassica napus*, a more probable barrier terminating zygote elongation may be cell turgor. In the mature elongated zygote, cellulose is shown within the chalazal tip cell wall. Since cellulose provides increased stability to the zygote cell wall, yielding of the cell wall would be reduced. The zygote cell would soon achieve an optimum turgor and elongation would cease. The termination of zygote cell elongation could possibly signal cell division prior to continued cell enlargement.

5.3 Cells of the Embryo Proper

Proembryo differentiation in *Brassica napus* is in accordance with the Onagrad development described by Johansen (1950). The *Brassica*

napus proembryo has a developmental pattern similar to that described in *Capsella* (Schulz and Jensen 1968b), *Diplotaxis* (Simoncioli 1974), *Brassica napus* (Tykarska 1976) and in *Arabidopsis* (Mansfield *et al.* 1991b).

The first cell division is asymmetrical. A transverse cell wall divides the elongated zygote cell into a large basal cell (*cb*), forming the distal portion of the proembryo, and a small semi-circular apical cell (*ca*), located at the proximal end of the proembryo (Figs 50, 51, 57). Although the asymmetrical cell division in *Brassica napus* is under genetic influence, Zaki and Dickinson (1990) show that the first cell division of cultured *Brassica napus* microspores is symmetrical suggesting that other unknown factors influence the site of cytokinesis.

From this point the *ca* cell will give rise to the future embryo proper and the *cb* cell will give rise to the suspensor unit (Johansen 1950). The first vertical *ca* cell division produces two sister cells of approximately the same size. Prior to cell division, the *ca* cell enlarges; however, the cell width never exceeds its height. Once the two apical sister cells have an enlarged bulbous appearance, both cells will subsequently divide in a vertical direction producing the quadrant apex (Figs 69, 70). Cell enlargement in the proembryo is not as extensive as the elongating zygote cell. The large vacuole of the zygote cell is not evident and therefore cytoplasmic cell polarity is not obvious and the cellulosic cell wall gradient shown in the zygote is no longer present. The cellulosic material present in the *cb* cell of the proembryo is now uniformly distributed and according to Vermeulenen and Wessels (1984) the cellulose stabilizes the cell walls. As a result, cell enlargement through the "yielding and creep" mechanism described by Cosgrove (1987) is probably reduced. The mechanism controlling termination of cell enlargement is not completely understood;

however, cytokinesis appears to occur before the apical cell height exceeds the width or when cell enlargement ceases in *Brassica napus*. An extensive review by Baskin and Candle (1991) recently described cytokinesis with special reference to the participation of microtubules in flowering plants. Webb and Gunning (1991) made a similar comment about cytokinesis in the proembryo of *Arabidopsis*. In *Brassica napus*, cytokinesis appears to occur very rapidly since no observations were made of a dividing proembryo cell. In this study, unsynchronized cytokinesis often resulted in the production of a three-celled apex (Fig 68) which eventually becomes four-celled (quadrant). Similar observations have been made in the proembryo of *Arabidopsis* (Mansfield *et al.* 1991b, Webb and Gunning 1991) and *Brassica napus* (Tykarska 1976). It is impossible to detect if the unsynchronized division is caused by the accelerated division of a single apical cell or the retardation of an apical cell; however, the probable influence of one apical cell over another cannot be disregarded.

In species such as *Capsella* (Schulz and Jensen 1968b), *Diplotaxis* (Simoncioli 1974), *Brassica napus* (Tykarska 1976) and *Arabidopsis* (Mansfield *et al.* 1991b) tissue differentiation is more clearly detectable later in the globular stages upon dermatogen formation. In this investigation the *Brassica napus* proembryo was described up to the quadrant stage. Each cell of the quadrant embryo proper showed little notable cytoplasmic differences. A similar observation in *Arabidopsis* led Mansfield *et al.* (1991b) speculate the cytoplasmic uniformity between the apical proembryo cells indicates each individual cell maintains its totipotency and does not yet have a predetermined developmental sequence. This speculation is similar to the "regulative theory of organization" proposed by Wardlaw (1950); however, unsynchronized cell division during the

formation of the quadrant embryo of *Brassica napus* indicates possible cell inheritance and a predetermined sequence of development as proposed by the"theory of mosaic inheritance" (Wardlaw 1950).

Although microtubules were observed in the integument cells surrounding the megagametophyte (Fig 104), they were never observed in the *Brassica napus* proembryo; however, microtubules were shown to exist in the proembryo of *Arabidopsis* (Mansfield *et al.* 1991b , Webb and Gunning 1991). Webb and Gunning (1991) describe the importance of the microtubular cytoskeleton distribution throughout zygote and proembryo stages of embryogenesis. Prior to this report, evidence showing the sequence of cytokinesis and the origin of embryo cells during embryogenesis was done after the fact. Few if any investigations show the occurrence of cytokinesis in an embryo; therefore, the origin and sequence of cells in an embryo over time was typically predicted from morphological investigations. Using antibodies and embryo isolation techniques, Webb and Gunning (1991) were able to show the preprophase bands present during embryogenesis in *Arabidopsis*. As a result, the ability to visualize the preprophase band lengthens the time of observation for cytokinetic events and subsequently allows the prediction of embryo cell origin and sequence. The evidence gathered by Webb and Gunning (1991) confirms the proembryo cells in *Brassica napus* have similar origin to its relative *Arabidopsis* up to the quadrant stage of development. Webb and Gunning's experiment confirms the presence of the pre-prophase band present in the *Arabidopsis* zygote prior to cytokinesis; however, a similar investigation using *Brassica napus* seeds remains to be undertaken.

The cytoplasm of the proembryo apical cells show little vacuolation, dark staining nucleus and orthochromatic perinuclear plastids when stained with crystal violet (Fig 50). Ultrastructurally the apical cells show an increased numbers of ribosomes, perinuclear mitochondria and plastids, and dictyosomes with maturing vesicles which appear adjacent the cell wall (Fig 65). The volume of the apical cells increases and the apex shows a globular appearance. The increased number of mitochondria, dictyosomes and plastids reflects the increased cellular activity (Natesh and Rau 1984) including cell enlargement (Boller and Wiemken 1986). The *cb* cell nucleus located in the chalazal region of the cell does not stain as intensely with crystal violet as the *ca* cell of figure 50, nor does it contain the dark staining perinuclear plastids. Ultrastructurally the density of mitochondria, dictyosomes and plastids in the *cb* cell is similar to the *ca* cell; however after the two-celled stage of embryo development, the *cb* cell appears to increase in endoplasmic reticulum and shows a reduction in the quantity of ribosomes .

During embryogenesis in *Brassica napus*, the suspensor cell elongates and continues cell divisions forming an absorptive organ known as the suspensor unit (Johansen 1950).

5.4 Cells of the Suspensor

In *Brassica napus*, suspensor cell division proceeds at the same time as the embryo proper. After the two-celled proembryo is formed, the suspensor unit continues to divide transversely resulting in an unequal and differential division of the *cb* cell. The chalazal portion of the *cb* cell divides and produces the *mC* cell (Figs 54, 55, 58). The reduced *cb* cell is now termed the *ci* cell. After the *m* cell is produced, any subsequent suspensor divisions do not occur at the expense of the *ci* cell. The

cytoplasm of the middle cell in figure 54 is slightly vacuolated and darkly stained with crystal violet. Ultrastructurally the *mC* cell contains energy producing organelles which suggest a future energy requiring process such as cytokinesis (Figs 71, 72). This appears to be the case since prior to quadrant apex formation, the *mC* cell of the suspensor unit divides producing the *d* and *f* cells. The next division occurs when the *d* cell divides to produce the *f* and *k* cells (Fig 70). The *f, k* and *h* suspensor cells have a similar ultrastructural appearance. The cytoplasm reveals a dense community of organelles such as mitochondria, active dictyosomes, plastids with abscence of starch and dense staining ribosomes which pepper the cytoplasm (Figs 83, 84, 85). In the literature, variations in suspensor cell cytoplasmic makeup is observed. For example, *Capsella* shows dictyosomes dispersed throughout the suspensor cells with the highest concentration located in the basal cell (Schulz and Jensen 1968b). The active dictyosomes distributed throughout the suspensor cells of *Brassica napus* shows maturing vesicles which appear to be migrating towards the tonoplast and the plasma membrane (Fig 90) to possibly participate in membrane formation, important during cell elongation (Boller and Wiemken 1986) (Figs 92, 98). During suspensor unit proliferation the *ci* cell ultrastructure is similar to other actively dividing suspensor cells; however, the *ci* is largely vacuolated.

In *Brassica napus*, once the quadrant embryo proper is formed the suspensor unit is composed of the *h, k f,* and *ci* cells. This confirms earlier findings by Tykarska (1976) who shows that the suspensor unit in other cultivars of *Brassica napus* consisting of three to four cells at the quadrant stage of embryogenesis. A similar number of cells form the suspensor of *Capsella* (Schulz and Jensen 1969), yet Mansfield *et al.* (1991)

only observed a three to four-celled suspensor unit at the mid-globular stage of *Arabidopsis* embryogenesis. At maturity, the suspensor unit increases in size and cell number prior to degeneration. Mansfield *et al.* (1991b) showed 7 to 9 celled *Arabidopsis* suspensors, Thompson (1933) described the suspensor in *Brassica oleraceae* as having 10 to 12 cells and Tykarska (1976, 1979) observed 14 cell suspensor in some cultivars of *Brassica napus*.

Although variations in suspensor morphology exists between species, the literature describing early embryogenesis suggests that the suspensor cells have two important roles. Firstly, the suspensor is a source of nutrients and growth regulators for the developing embryo. Secondly, it acts as an organ which absorbs nutrients from the somatic tissue of the seed and translocates them to the developing embryo proper (Schulz and Jensen 1969, Nagl 1974, Tykarska 1976, Yeung and Clutter 1979, Yeung and Sussex 1979, Yeung 1980, Folsom and Cass 1986, Bohdanowicz 1987, Dute *et al* 1989, Nagl 1990, Mansfield *et al.* 1991b).

5.4.1 Nutrients and Growth Regulators

From the literature it appears the suspensor unit provides nutrients and growth regulators to the embryo proper during early embryogenesis; however, little conclusive evidence has shown the mechanism controlling proembryo development. During early embryogenesis in *Capsella* and some cultivars of *Brassica napus*, the initial nutrient supply are have been thought to have derived from insoluble polysaccharides and lipid bodies within the suspensor cells (Schulz and Jensen 1968c, 1969, Tykarska 1982, 1987a). In later stages, Yeung and Clutter (1979) and Gartner and Nagl (1980) suggest that the plastids are the site of nutrient synthesis or substances which control embryo development in *Phaseolus*. Picciarelli

et al. (1984) and Bohdanowicz (1990) also report that the suspensor has a secretory function and speculate that the suspensors of *Tropaeolumm, Cytisus* and *Alisma* controls the output of certain hormones or are the site of production of these hormones. Investigations using *Phaseolus* by Cionini *et al.* (1976) and Brady and Comb (1988) demonstrated embryo proper survival when the suspensor unit is replaced with the addition of exogenous GA on the suspensorless embryos. This provides strong evidence that the suspensor secretes growth regulators into the embryo proper and possibly has an important role other than that of nutrition during early embryo development. Hormone concentrations, however, do not remain constant in the proembryo suspensor and have been shown to increase in the enlarging embryo proper later in embryogenesis. For example, Lorenzi *et al.* (1978) observed high levels of biologically active cytokinins in the suspensor of *Phaseolus* at the heart-shaped stage of embryo development and the embryo proper showed little; however, when the embryo reaches the mid-cotyledonary stage, the concentration of cytokinins was lower in the suspensor and higher in the embryo proper. Simoncioli (1974) showed that the reduction in the hormone concentration of the suspensor cells resulted in slower *Diplotaxis* suspensor growth. Little is known how embryo growth is regulated, Simoncioli (1974), Lorenzi *et al.* (1978) and Marsden *et al.* (1985) suggested that increased hormone concentrations in one embryonic area has an influence over another area. For example, in *Arabidopsis*, once the embryo proper differentiates into a mature embryo, the suspensor begins to degenerate. Using an embryo-lethal mutant, Marsden and Meinke (1985) showed continued suspensor development upon the degeneration of the embryo proper, suggesting yhat suspensor development is

influenced by the embryo proper late in embryogenesis. Because *Brassica napus* embryogenesis is similar to those of *Diplotaxis* and *Arabidopsis*, hormones may have an important role during embryogenesis as proposed by Simoncioli (1974) and Lorenzi *et al.* (1978).

From the literature it appears hormonal interaction between the embryo proper and the suspensor influence embryogenesis, yet little information exists describing a possible control mechanism. Well documented in animal systems is the regulated development or controlled secretion of material through a "Feedback Inhibition" mechanism. This mechanism of control of embryogenesis has never been shown to exist in plant systems; however, ethylene biosynthesis in plants has been shown to be positively or negatively modulated by itself (ethylene) (Mattoo and Aharoni 1988).

5.4.2 Organ Which Absorbs and Translocates Nutrients.

Some of the early literature suggests that an important function of the suspensor unit is to position the embryo proper deeper into the endosperm which is suspected to provide a nutritiously more favorable environment. Bhojwani and Bhatnagar (1986) indicate the endosperm is the primary source of nutritients for the embryo early in embryogenesis; however, they fail to provide conclusive evidence demonstrating a mechanism of nutrient transport from the free nuclear endosperm to the embryo. The transport of nutrients from the FNE appears possible in many species; however, in *Diplotaxis* , Pacini *et al.* (1975), indicate that the cuticular layer surrounding the proembryo prevents nutrient movement from surrounding tissues.

Symplastic transport involves the movement of material from one cell to another cell via the plasmodesmata (Brett and Waldron 1990). In

this investigation, plasmodesmata were shown linking all the proembryo cells in *Brassica napus*; however, plasmodesmata shown earlier between the egg and the synergid cells (Fig 25) were no longer evident after fertilization has occured. Similar symplastic connections were observed in *Capsella* (Schulz and Jensen 1969), *Stellaria* (Newcomb and Fowke 1974), *Beta* (Bruun 1987, 1988) and *Arabidopsis* (Mansfield *et al.* 1991b); however, in *Beta*, plasmodesmata were persistent during early embryogenesis. Bruun (1987, 1988) suggests that the plasmodesmata linking the synergids and the embryo provide nutrients important during the early stages of embryogenesis. Since plasmodesmata are absent between the synergids and the embryo of *Brassica napus* and other species, an alternative method of nutrient uptake to the embryo must exist.

The most accepted mechanism of translocation proposed in the literature is the apoplastic movement of nutrients from the surrounding integument cells into the specialized suspensor basal cell (Schulz and Jensen 1969, Simoncioli 1974, Tykarska 1976, Mansfield *et al.* 1991b). Key investigations by Yeung (1980) and Brady and Combs (1988) in *Phaseolus* clearly demonstrated the suspensor as the favoured site for nutrient uptake from surrounding somatic cells destined for the developing embryo proper.

5.5 Nutrient Transport

5.5.1 Wall Projections

Ultrastructurally the proximal end of the *ci* cell wall has a convoluted appearance characteristic of the transfer type projections described by Gunning and Pate (1969) and Pate and Gunning (1972). When stained with calcofluor, the walls of the suspensor cells appear even in thickness with the exception of the proximal end of the *ci* cell. The

proximal end of the *ci* cell wall fluoresces intensely showing the approximate distribution of wall projections which develop after fertilization in *Brassica napus*. Similar wall projections have been observed in *Capsella, Brassica napus, Diplotaxis, Arabidopsis* and other crucifers. (Schulz and Jensen 1968bc, Simoncioli 1974, Tykarska 1976, Mansfield *et al.* 1991b). These authors suggested that these wall projections at the proximal end of the basal cell during embryogenesis are involved in short distance apoplastic translocation. Apoplastic translocation involves the movement of materials through the cell wall and plasma membranes from the apoplast of a cell to the apoplast of a neighboring cell (Brett and Waldron 1990). In *Brassica napus* the cytoplasm at the proximal end of the basal cell shows accumulations of mitochondria and endoplasmic reticulum near the plasma membranes of the cell wall ingrowths (Figs 81, 82). Similar observations were made by Davis *et al.* (1990) of the transfer cell region of *Maize* caryopsis. In *Capsella, Phaseolus* and *Alisma*, the role of endoplasmic reticulum near the plasma membrane of the wall ingrowths is thought to be involved in intracellular transport (Schulz and Jensen 1969, Yeung and Clutter 1979, Bohdanowicz 1990). Evidence from investigations by Bohdanowicz (1990) shows long cisternae of endoplasmic reticulum extending from the proximal to the distal end of the basal cell. The numerous mitochondria near the plasma membrane may be involved in providing the energy needed for the active transport of material through the plasma membrane (Schulz and Jensen 1969, Yeung and Clutter 1979, Bohdanowicz 1990).

During embryogenesis, these may be alternate routes of nutrient flow. Mansfield *et al.* (1991b) suggested that large embryos require nutrients in addition to those provided via the suspensor. They indicate

that nutrients could be obtained apoplastically from free nuclear endosperm; however, there is no evidence to support this theory.

The appearance of convoluted wall ingrowths during seed development suggests an increased requirement for nutrient transport in a desired region. In *Brassica napus* the wall projections present in the ovule appear to designate the megagametophyte as the sink early in development since they are present prior to anthesis (Figs 21, 22, 26). During seed development, wall projections in the proembryo basal cell signals the possible establishment of a new sink. The initiation of wall projections in the proembryo appears to be triggered by fertilization (Figs 81, 82). Concurrent with prembryo wall projection development is the increase in number and size of the central cell wall projections. At early stages of embryogenesis it is unknown whether the embryo or the free nuclear endosperm is the most significant sink; however, the depletion of insoluble carbohydrates of the inner integument adjacent the micropyle region of the megagametophyte provides circumstantial evidence supporting the apoplastic route of nutrient transport via the basal and central cell wall projections. In contrast to post-anthesis ovule which shows large quantities of starch grains surrounding the megagametophyte (Fig 5), the more advanced stage of *Brassica napus* embryogenesis shows a majority of PAS-positive starch grains located in the inner integument basal body region of the seed (Fig 65). It is unknown if the starch formation is caused by the translocation of sugars into plastids or if the plastids themselves are photosynthetically active. Starch reserves in the basal body appear to be deposited in close proximity to the free nuclear endosperm and the enlarging embryo proper. Because nutrient deposition at the micropyle end only precedes embryo development, it appears that

this is a function of normal unfertilized ovule development and independent of embryo or endosperm requirements. *Brassica napus* that which megagametophytes, but are otherwise normal, there was an accumulation of starch in the basal body region (Fig 113) similar to that in fertilized ovules (Fig. 59). This supports the suggestion that starch deposition occurs independently of fertilization and embryo development.

Ultrastructurally the integument tissue near the megagametophyte of *Brassica napus* contains insoluble carbohydrates which appear as electron-transparent starch grains. The cells also contain cisternae of endoplasmic reticulum plastids, dictyosomes, mitochondria and numerous ribosomes which pepper the cytoplasm. Some of the integument cells, however, show an unusual structure which appears to be an expanded region of rough endoplasmic reticulum containing striated inclusions (Figs 105, 106, 107). Similar structures have previously been identified by Grant *et al.* (1986) and Polowick and Sawhney (1990) in *Brassica napus* tapetum cells of cytoplasmic male sterile anthers. Grant *et al.* (1986) indicates the dilated endoplasmic reticulum did not appear to affect male sterility and speculates the cisternae is involved with organelle lysis. In fungi, a structure of similar appearance has also been reported in the pre-cleavage sporangium of *Saprolegnia ferax* and identified as "Flimmer Hairs" in a ribosome studded cisternae by Beckett *et al.* (1974); however, no explanation of their function is provided.

5.5.2 Vasculature of the Seed

Evidence from the literature suggests that most nutritional requirements by the embryo prior to autotrophic development is provided from the somatic cells within the seed (Schulz and Jensen 1969, Nagl 1974, Tykarska 1976, Yeung and Clutter 1979, Yeung and Sussex 1979, Yeung

1980, Folsom and Cass 1986, Bohdanowicz 1987, Dute *et al* 1989, Nagl 1990, Mansfield *et al.* 1991b). Little attention, however, is given to the importance of vascularization. Corner's (1976) diagrammatic representation of the crucifers showed a single vascular bundle terminating at the chalaza of the developing seed (Fig 13). Other diagrammatic representations by Kallarackal and Bhathagar (1981), suggest the nutritional material provided via the single vascular trace is translocated from the chalaza to the micropyle through somatic cells surrounding the megagametophyte. Observations using fresh *Brassica napus* seeds showed a more complex vasculature than previously documented (Fig 14). In *Brassica napus* a "net-like" distribution of vascular tissue extends from the raphe region and surrounds a large portion of the chalazal end of the seed(Figs 11, 14).

At the site of funicular attachment, some of the phloem elements in *Brassica napus* are observed in close proximity to the micropyle end of the megagametophyte suggesting a possible direct route for nutrition of the egg apparatus and proembryo (Fig 59). From the vascular trace the first possible path of transport from the vascular tissue could occur as nutrients are unloaded into the surrounding somatic tissue which subsequently transport the nutrients symplastically to the megagametophyte. The second possible transport pathway could occur entirely through the apoplastic movement of nutrients from the vascular trace to the megagametophyte; however, cells involved in apoplastic transport must be close together. Although evidence proposed by Brady and Combs (1988) in *Phaseolus* implicates the vascular tissue in the transport of metabolites during embryogenesis, no conclusive evidence exists describing a precise transport mechanism.

5.6 Aberrant Ovules

Occasionally poorly developed or abortive ovules were examined during the course of this study. Such ovules were shown to contain an intact megagametophyte surrounded by an underdeveloped inner and outer integument with fewer cell layers than an normal ovule at the same stage of development. The synergid cells filiform apparatus of the micropyle of the megagametophyte appears well-developed. Fertilization of these ovules has never been observed. In the study nutrient uptake by the megagametophyte is suggested to occur at the micropyle. The absence of integument cells of the micropyle suggests the lack of nutrition may cause ovule demise, since underdeveloped ovules were not shown to persist longer than 22 hours after anthesis (Figs 110-112).

Ovules lacking megagametophytes were occasionally observed during the course of this study. Sectioned longitudinally, an aberrant ovule harvested 10.5 hours after pollination shows normal integument development, starch accumulation and distribution (Fig 113) relative to the normally developed ovule of the same age. This suggests integument and starch development are not influenced by megagametophyte development or fertilization since the ovules were not fertilized. The aborted megagametophyte is typically lined with a single layer of nucellar epidermal cells and contains nucellar tissue throughout (Figs 113, 114). These observations suggest an alteration to the normal sequence of early development during megasporogenesis or early megagametogenesis since the micropylar nucellar epidermis would normally be crushed during the post-four nucleate stage of development in *Brassica campestris* (Sumner 1986).

The ovule lacking proper integument development is smaller relative to a normally developed ovule of the same age. This difference in size could possibly serve as a method to cull viable from underdeveloped smaller sized ovules; however, ovules with aborted megagametophytes have a similar external morphology to the normally developed seed of the same age making them difficult to detect.

Evidence showing these two types of aberant ovules in *Brassica campestris* by Hotz (1991) reinforces observations in *Brassica napus* which suggest the sporophytic (integuments) and gametophytic (megagametophyte) tissues are capable of a normal development, independent from one another.

6.0 Conclusion

In this study the developmental phases characterized in the *Brassica napus* "Regent" proembryo were similar to those described in other cultivars of *Brassica napus* by Tykarska (1976) and in other crucifers such as *Capsella* (Schulz and Jensen 1968a,b,c 1969) and *Arabidopsis* (Mansfield et al. 1991a,b). The similarities between these crucifers lies mainly in the sequence and origin of the proembryo cells; however, dissimilarities were shown to exist. Evidence gathered during this study indicates much of the *Brassica napus* proembryo length is acquired prior to basal cell division at which time the apical cell is produced (250-350 μm). This conflicts with a report by Tykarska (1976) of *Brassica napus* indicating the post-cytokinetic proembryo including the apical cell occurs at the young zygote stage (45-55 μm) after which extensive basal cell elongation occurs.

Although the later stages of *Brassica napus* embryogenesis have not been examined, they are suspected to be similar to other crucifers. Future studies could involve comparative light and electron microscopy the stages of embryogenesis subsequent to the stages of proembryo development observed in this study.

Gradients in cell wall chemistry and the dynamic nature of the zygote vacuolation appears highly regulated during early embryogenesis. These factors probably affect greatly cell polarity and elongation; however, the stimulus that controls polarity and elongation during embryogenesis has not been clearly defined. The cellulose gradient revealed in the zygote cell walls varies in cell wall rigidity and is not typical of the normal somatic plant cell. The variation in zygote cell wall chemistry is thought to influence important physiological processes, mainly cell elongation,

direction and termination. The above cytochemical observation of the developing egg and the young *Brassica napus* zygote are similar to those by Sumner (1992) in *Brassica campestris.*

Invaluable information could be derived from future studies, involving radioactive isotopes to determine the precise location of metabolites. This information would clarify the importance of the nutrient partitioning and, if experiments are conducted during embryogenesis, it may indicate the possible change of sinks. This type of study could also show the time needed for metabolite incorporation and determine if metabolite transport pathways change over time. The apoplastic movement of material in the seed is speculated to be most important during embryogenesis; however, conclusive evidence showing active transport from somatic tissue and central cell into the embryo is lacking. ATPase experimentation using whole seeds of *Brassica napus* was unsuccessful. However, the use of megagametophyte digestion techniques (Huang *et al.* 1990) wonld provide renewed interest in ATPase localization studies, since the impeding integument layers would be removed.

The occasional observation of the aberrant *Brassica napus* ovule with poorly formed integuments or aborted megagametophytes during this study suggested possible agronomic ramifications. This topic area could be the focus of future research because of the obvious lack of literature clearly describing the detection and the frequency of this phenomenon.

7.0 Literature Cited

Ag Canada 1991. Grains 2000: Report of the Canola Marketing Task Force. Agriculture Canada's National Grains Bureau under the Grains 2000 program. pp 1-15.

Alpi A., Tagoni F.,and D'Amoto F. 1975. Growth regulator levels in the embryo and suspensor of *phaseolus coccineus* at two stages of development. Planta, **127:** 153-162.

Baskin T.I. and Candle W.Z. 1991. The structure and function of the mitotic spindle in the flowering plants. Annu. Rev. Plant Physiol. **41:** 277-315.

Beckett A., Heath I.B. and McLaughlin D.J. 1974. Anatomy of fungal ultrastructure. Longman Group LTD. London. pp 33.

Berger C.H. and Erdelska O. 1973. Ultrastructure aspects of the embryo sac of *Jasione Montana* cell walls. Caryolagia, **25:** 109-120

Bhojwani S.S. and Bhotnagar S.P. 1986. The female Gametophyte. *In*: The Embryology of Angiosperms (1988 edition). *Edited by* S.S.Bhojwani and S.P Bhotnagar. Vikos Publishing House PVT, Ltd. New Dehli. pp 66-86.

Bohdanowicz J. 1990. *Alisma* embryogenesis: The development and the ultrastructure of the suspensor. Protoplasma, **137:** 71-83.

Boller T. and Wiemken A. 1986. Dynamics of vacuolar compartmentation. Ann. Rev. Plant Physiol. **37:** 173-164.

Brady T., and Combs S.H. 1988. The suspensor is a major route of nutrients into proembryo, globular and heart stage *Phasiolus vulgaris* embryos. *In*: Sexual reproduction in higher plants. *Edited by* M. Cresti, P. Gori and E. Pacini. Springer-Verlag. New York. pp 419-424.

Brett C. and Waldron K. 1990. Physiology and biochemistry of plant cell walls. Unvin Hyman, London.

Brewbaker J.L. and Kwack B.H. 1964. The calcium-ion and substances influencing pollen growth. *In*: Pollen physiology and fertilization. *Edited by* H.F. Linskens. North-Holland Amsterdam. pp 143-151.

Bruun L. and Olesen P. 1989. A structural investigation of the ovule in Sugar Beet, *Beta vulgaris* : The micropylar nucellus Nord. J. Bot. **9(1):** 81-87.

Bruun L. and Olesen P. 1988. A structural investigation of the ovule in Sugar Beet, *Beta vulgaris* : the degenerated synergid and the micropylar nucellus (Abstr). *In*: Sexual reproduction in higher plants. *Edited by* M. Cresti, P. Gori and E. Pacini. Springer-Verlag. New York. pp 462.

Bruun L. 1987. The mature embryo sac of the sugar beet, *Beta vulgaris*: A structural investigation. Nord. J. Bot. **7:** 543-551.

Burgess J. and Linsted P.J. 1982. Cell wall differentiation during growth of electrically polarized protoplasts of *Physcomitrella*. Planta, **156:** 241-248.

Casgrove D.J. 1986. Biophysical control of plant cell growth. Ann. Rev. Physiol. **37:** 377-405.

Cass D.D. 1972a. Occurance and development of a filliform apparatus in the egg of *Plumbago capensis*. Am. J. Bot., **59:** 279-283.

Cass D.D. 1972b. Ultrastructure of the egg of *Plumbago zeylanica*. (Abstr) Am. J. Bot. **59:** 648.

Cass D.D. and Fabi G.C. 1990. Early ovule development in *Papaver rhoeas*. Can. J. Bot. **68:** 258-265.

Cass D.D. and Karas I. 1974. Ultrastructural organization of the egg of *Plumbago Zeylanica*.. Protoplasma, **81:** 49-62.

Chao C.Y. 1971. A periodic acid-schiff's substance related to the directonal growth of pollen tube into embryo sac in *Paspalum* ovules. Am. J. Bot. **58:** 649-645.

Chao C.Y. 1977. Further cytological studies of a periodic acid-schiff's substance in the ovules of *Paspalum orbiculare* and *P langifolium*.. Am. J. Bot. **64:** 922-930.

Chaubal R. and Reger B.J. 1990. Relatively high calcium is localized in the synergid cells of wheat ovaries (Abstract). Sex. Plant. Repro. **3(2):** 98-102.

Cionini P.G., Bennici A., Alpi A. and D'Amato F. 1976. Suspensor, gibberellin and in vitro development of *Phaseolus coccineus* embryos. Planta, **131:** 115-117.

Cocucci A. and Jensen W.A. 1969. Orchid embryology: Megagametophyte of *Epidendrum scutella* following fertilization. Am. J. Bot. **56:** 629-640.

Corner J.J.H. 1976. The seeds of dicotyledons. 1st edn. 2vols. Cambridge University Press, Cambridge, London, NY, Melbourne. pp 19-119.

Cosgrove D.J. 1987. Wall relaxation and the driving force for cell expansive growth. Plant Physiol. **84:** 561-564.

Davis W.R., Smith J.D. and Cobb G.B. 1990. A light microscope investigation of the transfer cell region of *maize* caryopsis. Can. J. Bot., **68:** 471-479.

Diball A.G. 1968. Fine structure development of the megagametophyte of *Zea mays* following fertilization. Am. J. Bot. **55:** 787-806.

Diball A.G. and Larson D.A. 1966. An electron microscopic study of the mature megagametophyte *Zea mays*. Am. J. Bot. **53:** 391-402.

Dong J. and Yang H.Y. 1990. An ultrasructural study of the emmbryo sac in *Oryza sativa* L.(Abstract). Acta Botanica Sinica. **31(2)**: 81-88.

Dute R.R., Peterson C.M. and Rushing A.E. 1989. Ultrasrtuctural change of the egg apparatus associated with fertilization and proembryo development of Soyabean Glycine max (fabceae). Annals of Botany, **64:** 123-135.

Engell K. 1989. Embryology of barley: Time course and analysis of controlled fertilization and early embryo formation based on serial sections. Nord. J. Bot. **9:** 265-280.

Erdelská and Klasovà 1978. La region micropylaire du sac embryonaire de Jasione maotana L. avant et après la fecondation. Actual. Bot. **125**: 249-252.

Esau K. 1977. Anatomy of seed plants. 2nd edition. John Wiley and Sons, Inc., New York.

Fisher D.B. 1968. Protein staining of ribboned epon sections for light microscopy. Histochemie, **16:** 92-96.

Folsom M.W. and Peterson C.M. 1984. Ultrastructural aspects of the mature embryo sac of soyabean, *Glycine max* L. Merr. Bot. Gaz. **145:** 1-10.

Folsom M.W. and Cass D.D. 1986. Changes in transfer cell distribution in the ovule of soyabean after fertilization. Can. J. Bot. **64:** 965-972.

Folsom M.W. and Cass D.D. 1989. Embryo sac development in soyabean: ultrastructure of megasporogenesis and early megegametogenesis. Can. J. Bot. **67:** 2841-2849.

Fougère - Rifot M. 1975. L'edification de l'appareil filiform et l'evolution cytoplasmique des synergides du sac embryonnaire *d'Aquilegia Vulgaris*. C.R. Acad. Sci. Paris, **280(D):** 2445-2447.

Fougère - Rifot M. 1978. Sa cellule central du sac embryonnaire *d'Aquilegia vulgaris*: Des noyaux polaires aux noyaux d'albumen laiteux. Bull. Soc. Bot. Fr. **125:** 207-213.

Fulcher R.D. and Wong S.I. 1980. A fluorescence microscopical view. *In* Cereals for food and beverages, Recent progress in cereal chemistry. *Edited by* G.E. Inglett and L. Munch. Academic Press, Inc. New york. pp 1-26.

Gartner P.J. and Nagl W. 1980. Acid phosphatase activity in plastids (plastolysomes) of senescing embryo suspensor cells. Planta, **149:** 341-349.

Gerhardt P., Murray R.G.E, Castilow R.W., Wood W.A., Krieg N.R., Phillips G.B. 1981. Manual of methods for general bacteriology. American society for microbiology Washington D.C. pp 26.

Grant I., Beversdorf W.D., Peterson R.L. 1986. A comparative light and electron microscopic study of microspore and tapetal development in male fertile and cytoplasmic male sterile oilseed rape (*Bassica napus*). Can. J. Bot. **64:** 1055-1068.

Gunning B.E.S. and Pate J.S. 1969. "Transfer cells" plant cells with wall ingrowth specialized in relation to short distance transport of solutes: Their occurance structure and development. Protoplasma, **68:** 107-133.

Hayat M.A. 1970. Principles and techniques of electron microscopy: Biological applicatons. Van Nostrand Reinhold Company, Toronto. Volume 1, pp 5-107.

Hayat M.A. 1975. Positive staining for electron microscopy. Van Nostrand Reinhold Co. New York.

Hendrix D.L. 1990. Carbohydrates and carbohydrate enzyme in the developing Cotton ovules (Abstract). Physiol. Plant. **78(1):** 85-92.

Hepler P.K. 1980. Membranes in the mitotic apparatus of barley cells. J. Cell. Biol. **21**: 490-499.

Hepler P.K. 1981. The structure of the endoplasmic reticulum revealed by osmium tetroxide-potassium ferricyanide staining. Eur. J. Biol. **26:** 102-110.

Herth W. 1985. Plant cell formation. *In* Botanical microscopy. *Edited by* A.W. Robards. Oxford University Press, Oxford. pp 285-310.

Hotz C. 1991. The development of the synrgids of *Brassica campestris* L. Honours Thesis. Dept. Botany ,University of Manitoba, Canada.

Huang B.Q., Russell S.D., Strout G.W. and Mao L.J. 1990. Organisation of isolated embryo sacs and eggs of *Plumbago zeylanica* (Plumbaginaceae) before and after fertilization. Am. J. Bot. **77:** 1401-1410.

Jensen W.A. 1962. Botanical histochemistry. *Edited by* G.W. Beadle, R. Emerson, and D.M. Whitaker. W.H. Freeman and Company. London. pp 199.

Jensen W.A. 1963. Cell development during plant embryogenesis *In*: Meristems and differentiation. Brookhanen Symp.Biol. **16:** 179-202.

Jensen W.A. 1964. Observations on the fusion of nuclei in plants. J. Cell. Biol. **23:** 669-672.

Jensen W.A. 1965a. The ultrastructure and histochemistry of the synergids of cotton. Am. J. Bot. **52:** 238-256.

Jensen W.A. 1965b. The ultrastructure and composition of the egg and the central cell of cotton. Am. J. Bot. **52:** 781-797.

Jensen W.A. 1965c. The composition and ultrastructure of the nucellus in cotton. J. Ultrastruct. Res. **13:** 112-128.

Jensen W.A. 1968a. Cotton embryogenesis: The zygote. Planta, **79:** 346-366.

Jensen W.A. 1968b. Cotton embryogenesis: Polysome formation in the zygote. J. Cell. Biol. **36:** 403-406.

Jensen W.A. 1972. The embryo sac and fertilization in angiosperms. Harold L Lyon Arbor Lect, **3:** 1-32.

Jensen W.A. 1974. Reproduction in flowering plants. *In* Dynamic aspects of plant ultrasrtucture. *Edited by* A.W.Robarts. McGraw-Hill, London. pp 481-503.

Jensen W.A. and Fisher D.B. 1968. Cotton embryogenesis: The entrance and discharge of the pollen tube in the embryo sac. Planta, **78:** 158-183.

Johansen D.A. 1950. Plant embryology. Chronoca Botanica, Waltham, Ma.

Jones T.J. and Rost T.L. 1989. Histochemistry and ultrastructure of rice (*Oryza sativa*) zygotic embryogenesis. Am. J. Bot. **76 (4)**: 504-520.

Kallarockal J. and Bhatnagar S.P. 1981. Cytochemical studies on the integument and integumentary tapetum in *Lanaria bepartita* (Vent) Willd. Caryologia, **34:** 447-455.

Kutschera U. , Bergfeld R. and Schopfer P. 1987..Cooperation of epidermis and inner tissues in auxin-mediated growth of maize coleoptiles. Planta, **170:** 168-180.

Lammeren A.A.M. Van 1981. Early events during embryogenesis in *Zea mays* L. Acta. Soc. Bot. Pol. **50:** 289-290.

Lane B.P. and Europa D.L. 1965. Differential staining of ultrathin sections of epon-embedded tissues for light microscopy. J. Histochem. Cytochem. **13:** 579-582.

Lorenzi R., Bennici A., Cionini P.G., Alpi A. and D'Amato F.1978. Embryo suspensor relations in *Phaseolus cocccineus* : Cytokinins during seed development. Planta, **143:** 59-62.

Maheshwari P. 1950. An introduction to the Embryology of Angiosperms 1st (ed) McGraw-Hill Book Co Inc..

Malik C.P.and Vermani S. 1975. Physiology of sexual reproduction I A histochemical study of the embryo sac development in *Zephyranthes rosea* and *Lagenaria vulgaris*. Acta. Histochem. **53:** 244-280.

Mansfield S.G. , Briarty L.G. and Erni S. 1991a. Early embryogenesis in *Arabidopsis thaliana*. I. The mature embryo sac. Can. J. Bot. **69**: 447-460.

Mansfield S.G.and Briarty L.G. 1991b. Early embryogenesis in *Arabidopsis thaliana*. II. The developing embryo. Can. J. Bot. **69**: 461-476.

Marsden M.P.F. and Meinke D.W. 1985. Abnormal development of the suspensor in an embryo-lethal mutant of *Arabidopsis Thaliana*. Am. J. Bot. **72(11)**: 1801-1812.

Mattoo A.K. and Aharoni N 1988. Ethylene and plant senescence. *In* Senescence and Aging in plants. *Edited by* L.D.Noodén and A.C.Leopold. Academic Press Inc., Toronto. pp 241-280.

Maze J., Bohm L.R. and Meklenbacker L.E. Jr. 1970. Embryo sac and early ovule development in *Oryzopsis miliacea* and *Stipa tortilis*. Can. J. Bot. **48**: 27-41.

Maze J. and Lin S.C. 1975. A study of the mature magagametophyte of *Stipa elmeri*. Can. J. Bot. **53**: 2958-2977.

Mizuta S. and Brown R.M. Jr. 1992. High resolution analysis of the formation of cellulose synthesizing complexes in *Vaucheria hamata*. Protoplasma, **166**: 187-199.

Mogensen H.L. 1972. Fine structure and composition of the egg apparatus before and after fertilization in *Quercus gambelii* The functional ovule. Am. J. Bot. **59**: 931-941.

Mogensen H.L. 1981. Translocation of uranin within the living ovules of selected species. Am. J. Bot.. **68(2)**: 195-199.

Mogensen H.L. and Suthor H.K. 1979. Ultrastructure of the egg apparatus of *Nicatiana tobacum* (*Solanaceae*) before and after fertilization. Bot. Gaz., **140**: 168-179.

Nagl W. 1974. The *Phaseolus* suspensor and its polytene chromosomes. ZPflanzenphysiol. **73**: 1-44.

Nagl W. 1990. Translocation of Putrescine in the ovule, suspensor and embryo of *Phaseolus coccineus*. J. Plant Physiol. **136**: 587-591.

Natesh S. and Rau M.A. 1984. The embryo. *In*: Embryology of Angiosperms. *Edited by* B.M. Johri. Springer-Verlog Berlin, Heidilberg. pp 377-434.

Newcomb W. 1973a. The development of the embryo sac of the sunflower *Helianthus annus* before fertilization. Can. J. Bot. **51:** 863-878.

Newcomb W. 1973b. The development of the embryo sac of the sunflower *Helianthus annus* after fertilization. Can. J. Bot. **51:** 879-890.

Newcomb W. and Fowke L.C. 1974. *Stellaria media* embryogenesis: The development and ultrastucture of the suspensor. Can. J. Bot. **52:** 607-614.

Newcomb W. and Steeves T.A. 1971. *Helianthus annus* embryogenesis: Embryo sac wall projections before and after fertilization. Bot. Gaz. **132:** 367-371.

Norstog K. 1972. Early development of barley embryo: Fine structure. Am. J. Bot. **59:** 123-132.

O'Brien T. P. and McCully M. E. 1981. The study of plant structure principles and selected methods. Termarcarphi Pty Ltd. Melbourne Australia.

Olson A.R. and Cass D.D. 1981. Changes in megagametophyte structure in *Papaver nudicaule* L. (Papaveraceae) following in vitro placental pollination. Am. J. Bot. **68:** 1333-1341.

Orr A.R. 1978. Influorescence development in *Brassica campestris* L. Am. J. Bot. **65:** 466-470.

Pacini E., Simoncioli C. and Cresti M. 1975. Ultrastructure of nucellus and endosperm of *Diplotaxis erucoides* during embryogenesis. Caryologia, **28:** 525-538.

Pate J.S. and Gunning B.E.S. 1972. Transfer cells. Annu. Rev. Plant. Physiol. **23:** 173-196.

Picciarelli P., Alpi A., Pistelli L. and Scalet M. 1984. Gibberellin-like activity in the suspensor of *Tropaeolumm majus* L. and *Cytisus laburnum* L. Planta, **162:** 566-568.

Picciarelli P., Piaggesi A. and Alpi A. 1991. Gibberellins in suspensor, embryo, and endosperm of developing seeds of *Cytisus laburnum.* Phytochem. **30(6):** 1789-1792.

Pollock E.G. and Jensen W.A. 1964. Cell development during early embryogenesis in Capsella and Gossypium. Am. J. Bot. **51:** 915-921.

Polowick P.L. and Sawhney 1990. Microsporogenesis in a normal line and in the *ogu* cytoplasmic male-sterile line of *Brassica napus* I. The influence of high temperatures. Sex. Plant Reprod. **3:** 263-276.

Przybyllock T. and Nagl W. 1977. Auxin concentration in the embryo and suspensor of *Tropaeolum majus* as determined by mass fragmentation (single ion detection). ZPflanzenphysiol. **84:** 463-465.

Ray P.M. 1987. Principals of plant cell growth. *In* Physiology of cell expansion during plant growth. *Edited by* D.J. Cosgrove and D.P. Knievel. American Society of Plant Physiologists, Rockvill,Md. pp 1-17.

Reiss H.D., Schnepf E. and Herth W 1984. The plasmamembrane of *Funaria* caulonema tip cell: morphology and distribution of particle rosettes and the kinetics of cellulose synthesis. Planta, **160:** 428-435.

Reynold E.S. 1963. The use of lead citrate at high pH as an electron opaque stain in electron microscopy. J. Cell. Biol. **17:** 208.

Russell S.D. 1980. Participation of male cytoplasm during gamete fusion in an angiosperm *Plumbago zeylanica*. Science (Wash DC), **210:** 200-201.

Russell S.D. 1983. Fertilization in *Plumbago zeylanica*:. Gametic fusion and fate of the male cytoplasm. Am. J. Bot. **70:** 416-434.

Russell S.D. 1989. Preferential fertilization in the synergid-lacking angiosperm Plumbago zeylanica. Phytomorphology, **39(1):** 1-20.

Russell S.D. and Mao L.J. 1990. Patterns of embryo-sac organisation, synergig degeneration and cotyledon orientation in *Linum usitatissium* L. Planta, **182:** 52-57.

Russell S.D., Rougier M. and Dumas C. 1990. Organization of the aerly post-fertilization megagametophyte of *Populus deltoides*. Ultrastructure and implications for male cytoplasmic transmission. Protoplasma, **155:** 153-165.

Salisbury F.B. and Ross C.W. 1991. Plant physiology, 4th ed. Wadsworth Publishing Co.

Schnepf E. 1986. Cell polarity. Ann. Rev. Plant Physiol. **37:** 23-47.

Schulz P. and Jensen W.A. 1973. *Capsella* embryogenesis: The central cell. J. Cell. Sci. **12:** 741-763.

Schulz P.and Jensen W.A. 1969. *Capsella* embryogenesis: The suspensor and the basal cell. Protoplasma, **67:** 139-163.

Schulz P. and Jensen W.A. 1971. *Capsella* embryogenesis: The chalazal proliferating tissue. J. Cell. Sci. **8:** 201-227.

Schulz P. and Jensen W.A. 1974. *Capsella* embryogenesis: The development of the free-nuclear endosperm. Protoplasma, **80:** 183-205.

Schulz S.R. and Jensen W.A. 1968a. *Capsella* embryogenesis: The synergids before and after fertilization. Am. J. Bot. **55:** 541-552.

Schulz S.R. and Jensen W.A. 1968b. *Capsella* embryogenesis: The egg zygote and young embryo. Am. J. Bot. **55:** 807-819.

Schulz S.R. and Jensen W.A. 1968c. *Capsella* embryogenesis: The early embryo. J. Ultrastruure Res. **22:** 376-392.

Simoncioli C. 1974. Ultrastructural characteristic of Diplotaxis erucoides (L.) DC suspensor. Giorn. Bot. Ital., **108:** 175-189.

Singh A.P.,and Mogensen H.L. 1975. Fine structure of the zygote and early embryo in *Quercus gambelii.* Am. J. Bot., **62:** 105-115.

Smith M.M. and McCully M.E. 1978. A critical evaluation of the specificity of aniline blue induced fluorescence. Protoplsma, **95:** 229-254.

Smith P. 1977. Vascular plant families. Mad River Press, INC. Eureka, Ca. pp 130.

Spurr A. R. 1969. A low viscosity epoxy resin embedding medium for electron microscopy. J. Ultra. Res. **26:** 31-43.

Sumner M.J. 1986. Ovule development and zygote formation in *Brassica campestris* L.cv. Candle. Ph.D. Thesis. Botany Department, University of Manitoba, Canada.

Sumner M.J. 1992. Embryology of *Brassica campestris*: the entrance and discharge of the pollen tube in the synergid and the formation of the zygote. Can. J. Bot. in press.

Sumner M.J. and Van Caeseele L. 1988. Ovule development in *Brassica campestris*: a light microscope study. Can. J. Bot. **66:** 2459-2469.

Sumner M.J. and Van Caeseele L. 1989. The ultrastructuere and cytochemistry of the egg apparatus of *Brassica campestris*. Can. J. Bot. **67:** 177-190.

Sumner M.J. and Van Caeseele L. 1990. The development of the central cell of *Brassica campestris* prior to fertilization. Can. J. Bot. **68:** 2553-2563.

Thiery J. P. 1967. Mise en évidence des polysaccharides sur coupes fines en microscopie electronique. Journal de microscopie, **6:** 987-1018.

Thompson R. 1933. A morphological study of flower and seed development in cabbage. J. Agr. Res. **47:** 215-232.

Tykarska T. 1976. Rape embryogenesis. I. The proembryo development. Acta. Soc. Bot. Pol. **XLV(1-2):** 1-16.

Tykarska T. 1979. Rape embryogenesis. II. Development of embryo proper. Acta. Soc. Bot. Pol. **XLVIII(3):** 391-421.

Tykarska T. 1980. Rape embryogenesis. III. Embryo development in time. Acta. Soc. Bot. Pol. **49(4):** 369-385.

Tykarska T. 1982. Rape embryogenesis. IV. Appearance and disappearance of starch during embryo development. Acta. Soc. Bot. Pol. **51(3-4):** 381-387.

Tykarska T. 1987a. Rape embryogenesis. V. Accumulation of lipid bodies. Acta. Soc. Bot. Pol. **56(4):** 573-584.

Tykarska T. 1987b. Rape embryogenesis. VI. Formation of protein bodies. Acta. Soc. Bot. Pol. **56(4):** 585-597.

Verneulen C.A. and Wessels J.G.H. 1984. Ultrastructural differences between wall apices of growing and non-growing hyphae of *Schizophyllum commune*. Protoplasma, **120:** 123-131.

Wardlaw C.W. 1950. Embryogenesis in plants. Methuen, London.

Webb M.C. and Gunning E.S. 1991. The microtubular cytoskeleton during development of the zygote, proembryo and free-nuclear endosperm in *Arabidopsis thaliana* (L.) Heynh. Planta, **184:** 187-195.

Went J.L. Van. 1970a. The ultrastructure of the synergids of *Petunia*. Acta. Bot. Neerl., **19:** 121-132.

Went J.L. Van. 1970b. The ultrastructure of the egg and central cell of *Petunia*. Acta. Bot. Neerl., **19:** 313-322.

Willemse M.T.M. and Went J.L. Van 1984. The female gametophyte. *In* : Embryology of Angiosperms. *Edited by* B.M. Johri. Springer-Verlog Berlin,Heidelberg. pp 170-190.

Wilms H.J. 1980a. Ultrastructure of the developing embryo sac of spinach. Acta. Bot. Neerl., **29:** 243-260.

Wilms H.J. 1980b. Ultrastructure of the stigma and style of spinach in relation to pollen germination and pollen tube growth. Acta. Bot. Neerl. **29:** 33-47.

Wilms H.J. 1981a. Ultrastructure of the developing embryo sac of spinach. Acta. Bot. Neerl. **30:** 75-99.

Wilms H.J. 1981b. Pollen tube penetration and fertilization in spinach. Acta. Bot. Neerl. **30:** 101-122.

XI XY 1991. Development and structure of pollen and embryo sac in peanut (*Arachis hypogeal* L.). Bot. Gaz. **152:** 164-172.

Yan H., Yang H.Y. and Jensen W.A. 1991. Ultrastructure of the developing embryo sac of sunflower (*Helianthus annus*) before and after fertilization. Can. J. Bot. **69:** 191-202.

Yeung E.C. 1980. Embryogeny of *Phaseolus*: The role of the suspensor. ZPflanzenphysiol, **96:** 17-28.

Yeung E.C.and Clutter M.F. 1979. Embryogeny of *Phaseolus coccineus* : Growth and microanatomy. Protoplasma, **94:** 19-40.

Yeung E.C. and Sussex I.M. 1979. Embryogeny of *Phaseolus coccineus* : The suspensor and the growth of the embryo proper in vitro. ZPflanzenphysiol, **91:** 423-433.

Yu S.H. and Chao C.Y. 1979. Histochemical studies of ovary tissues during the embryo sac development in *Paspalum longifolium* Roxe. Caryolagia, **32:** 147-160.

Zaki M.A.M. and Dickinson H.G. (1990). Structural changes during the first division of embryos resulting from anther and free microspore culture in *Bassica napus*. Protoplasma, **156:** 149-162.